eLife

Reviewed Preprint
v2 • June 9, 2025
Revised by authors

Reviewed Preprint
v1 • November 22, 2024

Developmental Biology

Identification and characterization of early human photoreceptor states and cell-state-specific retinoblastoma-related features

Dominic WH Shayler, Kevin Stachelek, Linda Cambier, Sunhye Lee, Jinlun Bai, Bhavana Bhat, Mark W Reid, Daniel J Weisenberger, Jennifer G Aparicio, Yeha Kim, Mitali Singh, Maxwell Bay, Matthew E Thornton, Eamon K Doyle, Zachary Fouladian, Stephan G Erberich, Brendan H Grubbs, Michael A Bonaguidi, Cheryl Mae Craft, Hardeep P Singh, David Cobrinik

The Vision Center, Department of Surgery, and Saban Research Institute, Children's Hospital Los Angeles, Los Angeles, United States • Development, Stem Cell, and Regenerative Medicine Program, Keck School of Medicine, University of Southern California, Los Angeles, United States • Cancer Biology and Genomics Program, Keck School of Medicine, University of Southern California, Los Angeles, United States • Department of Cancer Biology, Keck School of Medicine, University of Southern California, Los Angeles, United States • Norris Comprehensive Cancer Center, Keck School of Medicine, University of Southern California, Los Angeles, United States • Maternal-Fetal Medicine Division of the Department of Obstetrics and Gynecology, Keck School of Medicine, University of Southern California, Los Angeles, United States • Department of Radiology and The Saban Research Institute, Children's Hospital Los Angeles, Los Angeles, United States • Department of Radiology, Keck School of Medicine, University of Southern California, Los Angeles, United States • Department of Development, Stem Cell, and Regenerative Medicine, Keck School of Medicine, University of Southern California, Los Angeles, United States • Department of Integrative Anatomical Sciences, Keck School of Medicine, University of Southern California, Los Angeles, United States • USC Roski Eye Institute, Department of Ophthalmology, Keck School of Medicine, University of Southern California, Los Angeles, United States

eLife Assessment

In this **important** paper, the authors use single-cell RNA sequencing to understand post-mitotic cone and rod developmental states and identify cone-specific features that contribute to retinoblastoma genesis. The authors report findings that have practical implications for retinal development, gene expression, and cell fate specification. The evidence is **compelling** as the experimental design and analysis are exceptionally rigorous.

https://doi.org/10.7554/eLife.101918.2.sa4

Abstract

Human cone photoreceptors differ from rods and serve as the retinoblastoma cell-of-origin, yet the developmental basis for their distinct behaviors is poorly understood. Here, we used deep full-length single-cell RNA-sequencing (scRNA-seq) to distinguish post-mitotic cone and

rod developmental states and identify cone-specific features that contribute to retinoblastomagenesis. The analyses revealed nascent, immediately post-mitotic cone- and rod precursor populations characterized by higher THRB or NRL regulon activities, immature and maturing cone and rod precursors with concurrent cone- and rod-related gene and regulon expression, and distinct early and late cone and rod maturation states distinguished by maturation-associated declines in RAX regulon activity. Cell-state-specific gene expression features inferred based on full-length scRNA-seq were consistent with past single nucleus 3' RNA-seq analyses. Beyond the cell state characterizations, full-length scRNAseq revealed that both L/M cone and rod precursors co-expressed *NRL* and *THRB* RNAs, yet they differentially expressed functionally antagonistic *NRL* and *THRB* isoforms and prematurely terminated *THRB* transcripts. Moreover, early L/M cone precursors exhibited successive expression of several lncRNAs along with *MYCN*, which composed the seventh most L/M-cone-specific regulon, and *SYK*, which was implicated in the cone precursors' proliferative response to *RB1* loss. These findings reveal previously unresolved photoreceptor precursor states and suggest a role for early cone-precursor-intrinsic *SYK* expression in retinoblastoma initiation.

Impact Statement

Features acquired by early post-mitotic retinal cells underlie the distinct behaviors of rods and the cone cells of origin of retinoblastoma tumors.

Introduction

Vertebrate photoreceptors develop from optic vesicle retinal progenitor cells (RPCs) through progressive RPC lineage restriction, fate determination, and post-mitotic maturation[1,2]. While several transcription factors that govern these events have been identified, important aspects of photoreceptor fate determination and maturation remain unclear. For example, it is unclear if fate is determined in RPCs, where OTX2 and ONECUT1 are thought to control the post-mitotic expression of long- or medium-wavelength (L/M) cone determinant TRβ2 and rod determinant NRL[3], or is determined in post-mitotic photoreceptor precursors with concurrent TRβ2 and NRL expression [4]. Following fate commitment, post-mitotic developmental stages have been defined based on morphologic features and phototransduction-related gene or protein expression[5,6], but it is unclear if progression through such stages is subdivided into distinct cell states governed by unique transcription factor combinations or represents a developmental continuum.

An improved understanding of photoreceptor development may provide insight into the pathogenesis of retinal dystrophies, retinal degenerations, and the retinal cone precursor cancer, retinoblastoma[7,8]. In the latter case, L/M cone precursors lacking the retinoblastoma protein (pRB) were shown to proliferate in a manner dependent on the L/M-cone lineage factors RXRγ and TRβ2 and the intrinsically highly expressed MDM2 and MYCN oncoproteins, likely representing the first step of retinoblastoma tumorigenesis[8–11]. Similarly, retinoblastoma cell proliferation depends on RXRγ, TRβ2, MDM2, and MYCN[9], implying that intrinsic L/M-cone factors contribute to the oncogenic state. However, retinoblastoma cells also express rod lineage factor *NRL* RNAs, which – along with other evidence – suggested a heretofore unexplained connection between rod gene expression and retinoblastoma development[12,13]. Improved discrimination of early photoreceptor states is needed to determine if co-expression of rod- and cone-related genes is adopted during tumorigenesis or reflects the co-expression of such genes in the retinoblastoma cell of origin.

The cone precursors' propensity to form retinoblastoma is a human-specific feature whose study requires analysis of developing human retina[8]. Single-cell RNA-sequencing (scRNA-seq) is well suited to such analyses as it enables discrimination of cell type-specific fate determination and maturation features. scRNA-seq studies employing 3' end-counting have defined age-related post-mitotic transition populations, fate-determining features of post-mitotic photoreceptor precursors, and gene expression changes associated with the cone fate decision and early development[14–20]. However, 3' end-counting cannot be used to interrogate transcript isoforms, and the relatively low number of genes detected per cell limits the ability to distinguish closely related states in individual cells.

In this study, we sought to further define the transcriptomic underpinnings of human photoreceptor development and their relationship to retinoblastoma tumorigenesis. We generated deep, full-length single-cell transcriptomes of human retinal progenitor cells (RPCs) and developing photoreceptors from fetal week (FW) 13-19 retinae, with enrichment of rare cone precursor populations, and applied long-read cDNA sequencing, RNA velocity, pseudotemporal trajectory reconstruction, and single-cell regulatory network inference and clustering (SCENIC) to interrogate individual cell states. These analyses discriminated previously unresolved photoreceptor developmental states, identified photoreceptor precursor states with cone and rod-related RNA co-expression, uncovered cell type-specific expression of RNA isoforms of photoreceptor fate-determining genes, elucidated post-mitotic photoreceptor developmental trajectories, and revealed retinoblastoma cell-of-origin features that may contribute to retinoblastoma genesis.

Results

Regulon-defined RPC and photoreceptor precursor states

To interrogate transcriptomic changes during human photoreceptor development, dissociated RPCs and photoreceptor precursors were FACS-enriched from 18 retinae, ages FW13-19 (**Figure S1A**), and isolated using microfluidics or direct sorting into microliter droplets, followed by full-length cDNA synthesis, paired-end sequencing, and alignment to Ensembl transcript isoforms (**Figure 1A**). The FACS enrichment was based on a prior cone isolation method[10] but with wider gating to include rods and RPCs. After sequencing, we excluded all cells with <100,000 read counts and 18 cells expressing one or more markers of retinal ganglion, amacrine, and/or horizontal cells (*POU4F1*, *POU4F2*, *POU4F3*, *TFAP2A*, *TFAP2B*, *ISL1*) and concurrently lacking photoreceptor lineage marker *OTX2*. This yielded 794 single cells with averages of 3,750,417 uniquely aligned reads, 8,278 genes detected, and 20,343 Ensembl transcripts inferred (**Figure S1A-C**). Sequencing batches were normalized and transcriptomes clustered and visualized in uniform manifold approximation and projection (UMAP) plots that integrated cells across different retinae, ages, isolation methods, and sequencing runs (**Figures 1B,C**, S1D-F).

Low resolution Louvain clustering (level 0.4) generated six clusters that segregated into mostly distinct UMAP domains (**Figure 1B**). One cluster was comprised of RPCs and Müller glia (MG), with specific expression of *LHX2*, *VSX2*, *SOX2*, and *SLC1A3*, while five clusters were comprised of cells with photoreceptor features, with wide expression of *OTX2* and *CRX* and cluster-specific rod- and cone gene expression (**Figures 1D**, S2). In UMAP space, the cluster designated immature photoreceptor precursors (iPRPs) intermixed with the RPC/MG population, extended towards early L/M cone precursors, and was predominantly comprised of cells expressing the L/M cone determinant *THRB* (**Figure 1B,D**).

Two clusters highly expressing the rod determinant *NR2E3* were designated early-maturing rod (ER) and late-maturing rod (LR) (**Figure 1B**), based on the latter's increased expression of rod phototransduction genes *GNAT1*, *CNGB1*, *PDE6G*, *GNGT1* and *RHO* (**Figures 1D**, S2C). Few rods

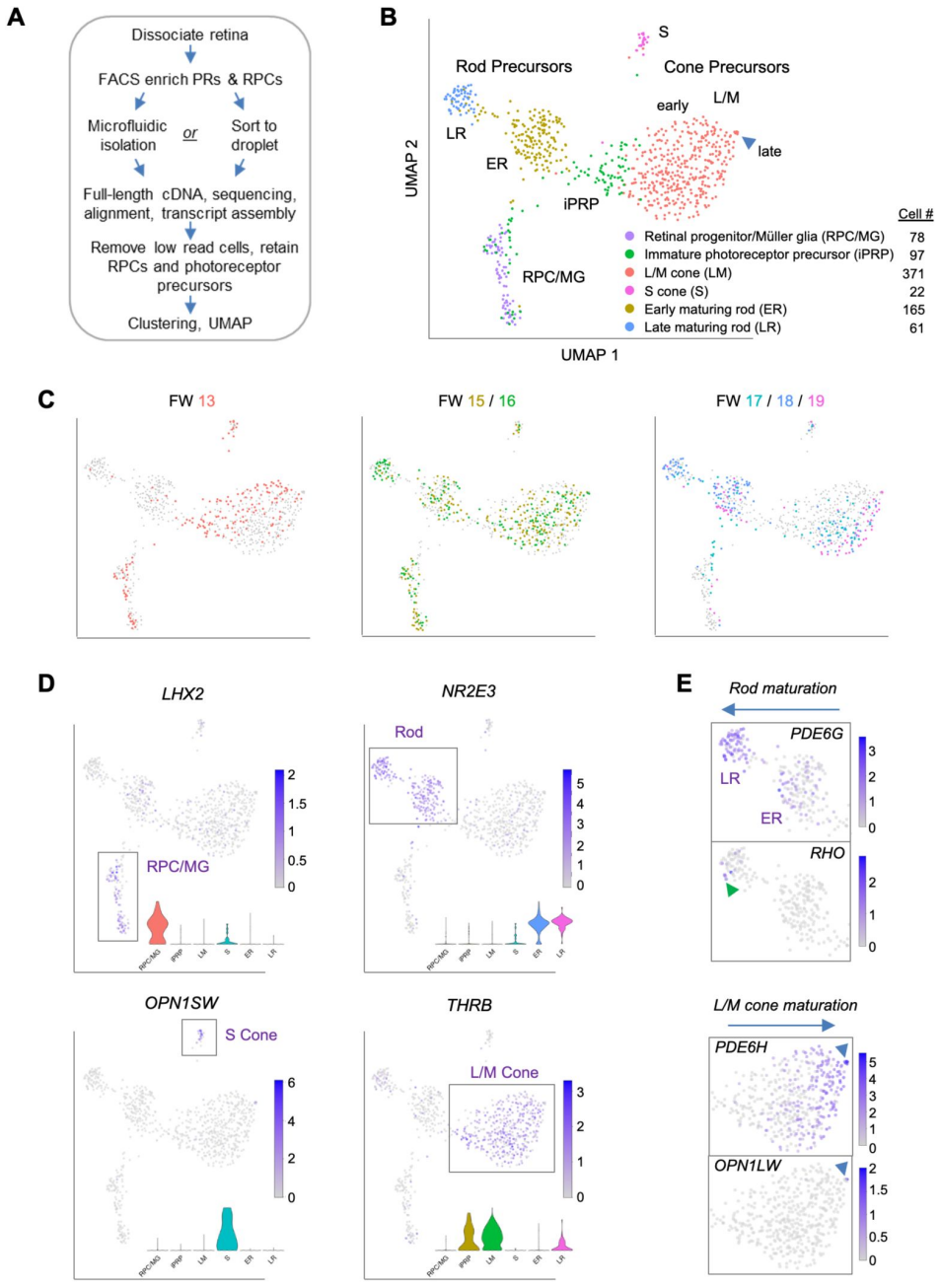

Figure 1

Photoreceptor-enriched full-length scRNA-seq of developing human retina.

A. Overview of sample collection and sequencing. **B, C.** UMAP plots showing low-resolution cell type clusters (B) and ages (C). **D.** Expression of marker genes for RPC/MGs (*LHX2)*, rods (*NR2E3)*, S cones (*OPN1SW)*, L/M cones (*THRB*). *Insets*: Gene expression violin plots (from *left* to *right*): RPC/MG (red), iPRP (brown), LM cone (green), S cone (teal), early rod (blue), late rod (pink). **E.** Expression of markers of rod maturation (*PDE6G*, *RHO*) and cone maturation (*PDE6H*, *OPN1LW*). Arrowheads: Late-maturing *RHO*+ rods (*top*), late-maturing *OPN1LW*+ cones (*bottom*). See **Figure S2** for additional examples. UMAP and violin plots for any gene or transcript isoform can be produced at *https://docker.saban.chla.usc.edu/cobrinik/app/seuratApp/*.

were detected at FW13, whereas both early and late rods were detected from FW15-19 (**Figure 1C**), corroborating prior reports[15,20]. Differential expression analysis revealed other genes upregulated in late rods (*GNB1*, *SAMD7*, *NT5E*)[21,22] as well as the downregulated *CRABP2*, *DCT*, and *FABP7* (**Figure S3A**, Table S1). Genes upregulated in the LR cluster were enriched for photoreceptor and light sensing gene ontologies (**Figure S3B**) including spectrin binding, likely relating to proteins that control photoreceptor polarity and synapse formation[23,24], and purine biosynthesis and ribonucleotide metabolic processes, potentially related to the developing photoreceptors' high NAD+ requirements[25].

Cones segregated into distinct S- and L/M-cone clusters, with differential expression of cone subtype markers (*OPN1SW*, *THRB*), previously identified S-cone enriched genes (*CCDC136*, *UPB1*)[26–28], novel S cone enriched genes (*MEGF10*, *NRXN3*, *ACKR3*), and the L/M cone transcription factor *ISL2*[15], among others (**Figure 1B,D**, S3C, Table S2). Gene ontology analysis did not reveal relevant terms enriched in S cones, whereas L/M cones were enriched for protein translation related ontologies (**Figure S3D**) due to increased expression of ribosomal protein genes *RPL23A*, *RPLP0*, *RPS19*, *RPS27*, *RPS27A*, *RPS29*, *RPS3A* (Table S2).

In UMAP space, the *THRB*+ L/M-cone cluster segregated into a large 366-cell proximal population and a 5-cell distal population inferred to represent early-maturing and late-maturing stages, respectively, based on the latter's increased expression of cone phototransduction genes *OPN1LW* (encoding L-opsin), *PDE6H*, and *GUCA1C* (**Figure 1E**, S3E,F), analogous to *RHO*, *PDE6G*, and *GNGT1* upregulation in late rods. L/M cone precursors from different age retinae occupied different UMAP regions, suggesting age-related differences in L/M cone precursor maturation (**Figure 1C**). Compared to the early L/M population, late L/M cones had upregulation of three M-opsin genes, *TTR*, encoding the retinol-binding protein transthyretin, *PCP4*, a small protein that binds calmodulin previously noted in foveal cones[29], and *MYL4*, a myosin light chain gene upregulated in retinal organoid L/M cones[28], among others (**Figure S3E,F**, Table S3). The low proportions of *OPN1MW*+ and *OPN1LW*+ late-maturing L/M cones is consistent with a prior analysis of similar-age retinae and with the further upregulation of these proteins in later maturation[15].

We next asked whether similar distinctions between early-maturing and late-maturing L/M cone and rod precursors were observed in prior studies. Indeed, a 3' snRNA-seq analysis of ~ 220,000 retinal cells from post-conception week (pcw) 8 – 23 distinguished the *cone precursor* versus *ML cone* and the *rod precursor* versus *rod* subclasses (Zuo *et al.*[20]). (*N.b.*, we retain the *pcw* and *ML cone* terms of Zuo *et al.* when describing their data and the synonymous *FW* and *L/M cone* for our data to maintain continuity with past publications.) The Zuo *et al.* cone and rod precursor versus cone and rod photoreceptor comparisons were not strictly analogous to our early-maturing versus late-maturing precursor comparisons in that our early-maturing precursors excluded immature iPRP cells. Still, the comparisons revealed many of the same differentially expressed genes (**Figures S3A** versus S3G and S3E versus S3H; Tables S1, S3-S5).

To further interrogate cell identities, we used SCENIC to identify cluster-specific transcription factor regulons, which represent the overall expression of single transcription factors and their likely coregulated target genes[30]. The highest specificity regulons defined major cell populations including RPC/MG-specific E2F2, E2F3, VSX2, and PAX6; pan-photoreceptor NEUROD1, OTX2, and CRX; rod-specific NRL; and L/M cone-specific THRB and ISL2 (**Figure 2**, Table S6). SCENIC also distinguished ER and LR states via the latter's increased NRL, CRX, ATF4, and LHX3 and decreased HMX1 and RAX activities ($p < 0.0005$ for each, Dunn test). RAX activity also decreased in the 5-cell late-maturing L/M cone group (**Figure 2B**), supporting its distinct transcriptomic identity and suggesting a similar mode of late cone and late rod maturation. Additionally, iPRPs expressed their most specific regulons, LHX9 and OLIG2, at levels similar to RPC/MGs along with photoreceptor-related regulons, consistent with the transitional nature of this population (**Figure 2A**, Table S6). However, SCENIC did not identify S cone-specific regulons, in keeping with the notion that S cones

represent a default photoreceptor state induced by pan-photoreceptor factors such as OTX2, CRX, and NEUROD1 in the absence of NRL and THRB[31]. Thus, deep, full-length scRNA-seq enabled identification of regulons underlying RPC and developing photoreceptor states at the single cell level.

Differential expression of *NRL* and *THRB* isoforms in rod and cone precursors

Although cone and rod precursors segregated into distinct clusters, mRNAs encoding rod-determining factor NRL, L/M cone-determining factor TRβ, and cone marker RXRγ were co-expressed in both rod and cone precursor populations, with mean *NRL* expression only 4.3-fold higher in the ER vs LM cluster, mean *THRB* expression 5.0-fold higher in LM vs LR, and mean *RXRG* expression 4.3-fold higher in LM vs ER (**Figure S2C,D** and below). Cone *NRL* expression was unexpected given NRL's role in rod fate determination[28] and rod-specific NRL regulon activity (**Figure 2A,D**). Similarly, rod *RXRG* and *THRB* expression were unexpected given their roles in cone gene expression and fate determination[32,33] and L/M cone-specific THRB regulon activity (**Figure 2A,D**). Accordingly, we used full-length scRNA-seq data to determine if cone and rod precursors differentially express *NRL*, *THRB*, and *RXRG* transcript isoforms.

For *NRL*, three assigned transcript isoforms (*ENST00000397002*, *ENST00000561028*, and *ENST00000558280*) are predicted to encode the canonical full-length NRL protein (FL-NRL) (RefSeq NP_001341697.1), while two others (*ENST00000560550* and ENST00000396995) are previously uncharacterized transcripts predicted to use an alternative "P2" promoter and first exon, here termed exon 1T (**Figure 3A-C**). The novel transcripts are predicted to encode an N-terminally truncated NRL protein (Tr-NRL) retaining the leucine zipper DNA binding domain but lacking the minimal transactivation domain[34] (**Figure 3C**, **Figure S4A,B**). While all transcript isoforms were inferred to be more highly expressed in the ER rod cluster versus the LM cone cluster, the ratio of all FL-NRL:Tr-NRL transcripts was 2.9:1 in early rod precursors and 2.2:1 in late rod precursors, in contrast to 0.67:1 in L/M cone precursors (**Figure 3B**). Consistent with the assigned isoform ratios, mean read coverage of the Tr-NRL-specific exon 1T was higher in S and LM cones while coverage of FL-NRL-specific exon 1 was higher in rods (**Figure 3C**, red *vs*. black arrowheads). Comparing the reads mapped to each first exon relative to total reads further confirmed that the Tr-NRL exon 1T predominated in individual cones whereas the FL-NRL exon 1 predominated in rods (**Figure 3D**). The cone cells' higher proportional expression of Tr-NRL first exon sequences was validated by RNA fluorescence *in situ* hybridization (FISH) of FW16 fetal retina in which NRL immunofluorescence was used to identify rod precursors, RXRγ immunofluorescence was used to identify cone precursors, and FISH probes specific to Tr-NRL exon 1T or to FL-NRL exons 1 and 2 were used to assess Tr-NRL and FL-NRL expression (**Figure 3E,F**).

While the Tr-NRL-encoding *NRL* isoforms were not to our knowledge previously described, another *NRL* isoform that initiated within exon 2 and lacked the NRL transactivation domain due to alternative exon 2 splicing, termed DD10 (**Figure 3C**), was previously identified in adult retina[36]. Concordantly, we detected reads spanning the unique DD10 splice junction, yet at lower levels than the unique Tr-NRL junction (5,942 versus 57,048).

As transcript isoforms inferred from short-read sequencing do not necessarily reflect the original transcript structures, we further defined the *NRL* isoforms expressed in early cone and rod precursors by performing 5' rapid amplification of cDNA ends (RACE) on the already generated single cell cDNA libraries from 23 early rod (ER) and 21 early L/M cone (LM) cells, followed by nanopore long-read sequencing of the pooled RACE products. The long-read sequencing revealed isoforms consistent with FL-NRL, Tr-NRL, DD10, and several other *NRL* isoforms with alternative transcription initiation and alternative splicing within exon 2 as well as within the Tr-NRL exon 1T

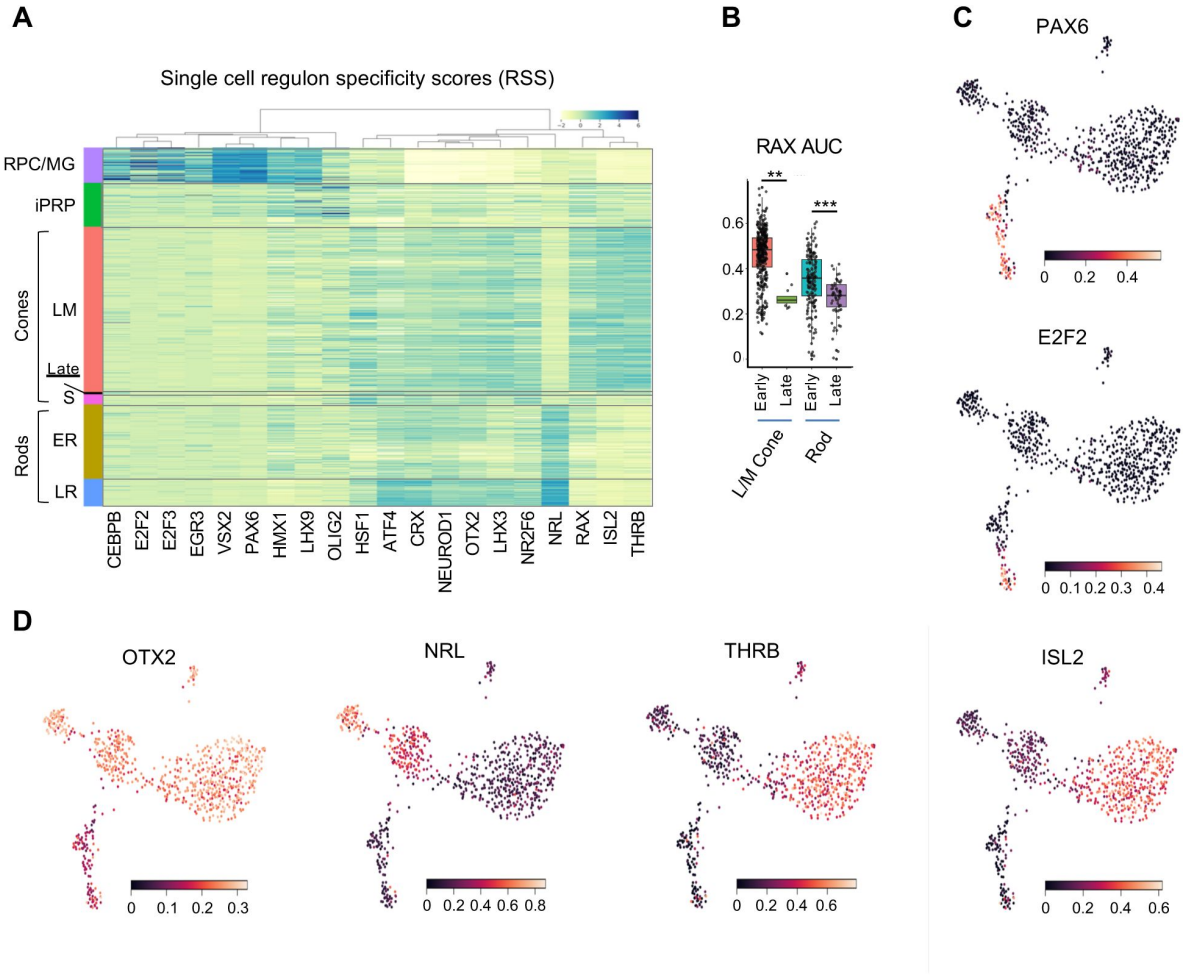

Figure 2

Regulon-defined RPC and photoreceptor precursor states

A. Ward-clustered heatmap of the highest scoring SCENIC regulons in each cluster, displaying Z-score normalized regulon activities. Late = late-maturing L/M cones. **B.** Box plot of RAX regulon area under the curve (AUC) values for early and late L/M cones and rods. *, p<0.005; ***, p<0.0005, Dunn test. **C,D.** UMAP plots of regulon AUC values for (C) PAX6 (RPC/MG) and E2F2 (RPC), and (D) OTX2 (photoreceptors and photoreceptor-committed RPCs), NRL (rod) and THRB and ISL2 (L/M cone).

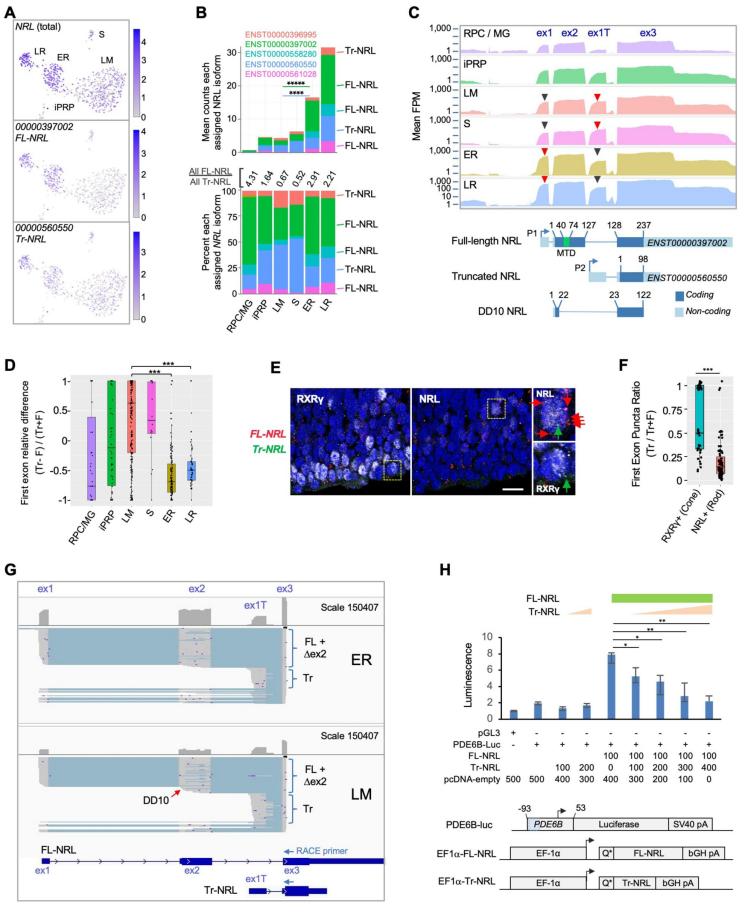

Figure 3

Differential expression of *NRL* isoforms in rod and cone precursors.

A. Expression of *NRL* gene and the most highly assigned Ensembl isoforms *ENST00000397002* (FL-NRL) and *ENST00000560550* (Tr-NRL). **B.** Mean *NRL* isoform assignments for clusters defined in **Figure 1B**, presented as total counts (*top*) and percentage of total counts (*bottom*). Significance for LM vs. ER fold change, colored by isoform. ****, p <0.0002; *****, <0.000001 (bootstrapped Welch's t-test). Ensemble transcript IDs shown in color with structures shown in **Figure S4B**. **C.** *Top*: Mean read counts (fragments per million, FPM) across Ensembl *NRL* exons for each cluster. *Bottom*: Transcript structures numbered according to amino acid positions. Minimal transactivation domain (MTD) in green. Arrowheads: Red/black: First exons where red is higher of two peaks. **D.** Relative difference box plot of raw reads mapping to truncated (Tr) and full length (F) transcript first exons in each cell, according to cluster. Relative difference is the difference in reads mapping to truncated and full-length *NRL* first exons (Tr-F) divided by the sum of both (Tr+F). Values >0 indicate more reads assigned to truncated isoform, values < 0 indicate more reads assigned to full-length isoform. ***, p <0.0001 (post-hoc Dunn test). **E.** NRL and RXRγ immunostaining and RNA FISH with probes specific to truncated Tr-NRL exon 1T (green puncta) and FL-NRL exons 1 and 2 (red puncta) in FW16 retina. Boxed regions enlarged at right show an RXRγ^{lo}, NRL^{+} rod with one Tr-NRL and six FL-NRL puncta (*top*) and an RXRγ^{hi}, NRL^{-} cone with one Tr-NRL and no FL-NRL puncta (*bottom*), indicated with same-color arrows. Scale bar: 10 µm. **F.** Ratio of fluorescent puncta observed in experiment depicted in (E) for NRL+ or RXRγ^{hi} cells where Tr puncta >0. ***; p <0.0005 (Welch's t-test). **G.** Long-read nanopore sequencing of pooled 5′ RACE reactions initiated with *NRL* exon 3 primers and performed on cDNA libraries from 23 ER cells (*top*) and 21 LM cells (*bottom*). Each schematic shows total exon coverage (*above*) and individual transcripts (*below)*, where expressed sequences are grey and introns light blue. Full-length (FL), alternatively spliced or internally initiated exon 2 (βex2), and truncated (Tr) transcripts are indicated by brackets. Red arrow: Transcripts resembling DD10, with internal exon 2 transcription initiation and premature splicing to exon 3. Ensembl FL-NRL and Tr-NRL transcript isoforms and RACE primer positions are shown below. **H.** *Top*: PDE6B-luciferase reporter activity in NIH-3T3 cells transfected with indicated amounts (ng) of pcDNA4-C-EF1α and derived FL-NRL and Tr-NRL constructs. *Bottom:* PDE6B-luc reporter and pcDNA4-C-EF1α expression constructs. Blue box = NRL response element. Error bars = standard deviation of triplicate measurements. *, p <0.05; **, <0.005 (Student's t-test). Data representative of two experiments in NIH-3T3 and one in 293T.

(**Figure 3G**, **Figure S4C**). In keeping with the computationally assigned isoforms and differential exon usage, ER libraries had a higher proportion of FL-NRL exon 1 and exon 2 reads and LM libraries had a higher proportion of Tr-NRL exon 1T reads (**Figure 3G**, **Figure S4C**). Moreover, alternative splicing within NRL exon 2 was more prevalent in LM libraries, affecting 6,788 of 29,177 (23 %) of exon 2 reads compared to 5,378 of 85,860 (6 %) in ER cells ($p<0.0001$; Chi-square with Yates correction), resulting in rarer full-length (exon 1-2-3) transcripts than inferred from short-read sequencing. Thus, long-read sequencing revealed cell type-biased *NRL* isoform expression with a preponderance of FL-NRL transcripts in early rods and disrupted FL-NRL and Tr-NRL transcript isoforms in L/M cones.

Despite our detection of L/M cone RNAs encoding Tr-NRL and FL-NRL, cone expression of NRL protein has not been reported. To assess endogenous Tr-NRL expression, we performed immunoblot analysis of CHLA-VC-RB-31 retinoblastoma cells[37], which were predicted to express FL-NRL and Tr-NRL transcripts in a cone-like 0.73:1 ratio, with an antibody that recognizes both FL-NRL and Tr-NRL proteins (**Figure S5A,B**). As in other retinoblastoma cells[13], FL-NRL increased in response to retinoic acid and proteasome inhibition, whereas Tr-NRL was not detected (**Figure S5C**). Similarly, Tr-NRL was not detected in EGFP+, RXRγ+ cones following lentiviral transduction of an explanted fetal retina with an EGFP-P2A-Tr-NRL cassette (**Figure S5D-G**). These findings suggest that Tr-NRL is poorly translated or unstable in most cone precursors.

As Tr-NRL might be expressed in contexts that were not examined in our analyses, we explored the function of the putative Tr-NRL protein. As both Tr-NRL and the previously described NRL DD10 lack the NRL transactivation domain and as DD10 interferes with FL-NRL transactivation[35], we examined if Tr-NRL similarly opposes FL-NRL transcriptional activity. Indeed, in luciferase reporter assays, Tr-NRL suppressed FL-NRL activation of a *PDE6B* promoter (**Figure 3H**).

For *THRB*, the most highly assigned transcript isoforms encoded the L/M cone-specific TRβ2 (*ENST00000280696)* and the more widely expressed TRβ1 (*ENST00000396671* and others) (**Figure 4A-C**, S6). While both TRβ1 and TRβ2 promote L/M cone fate determination[38], the isoform encoding TRβ2 predominated in L/M cones while those encoding TRβ1 predominated in early rods (**Figure 4B**). Moreover, late rods preferentially expressed *THRB* exons 1-6 and the *THRB* 3' untranslated region (UTR), implying that RNAs encoding full-length TRβ proteins were rare (**Figure 4B,C**). Notably, a higher percentage of reads extended from the exon 4 and exon 6 splice donor sequences into the subsequent introns in LR versus LM cells (**Figure 4D,E**) ($p \leq 0.001$ for both, two-tailed Chi square test), suggesting that premature transcription termination (PTT) in introns 4 and 6 preferentially limits TRβ expression in the LR population. The inferred PTT events are consistent with structures of the assigned Ensembl isoforms (**Figure 4B**, S6).

To further evaluate PTT events, we used *THRB* 3' RACE and long-read sequencing on single cell cDNA libraries from 23 L/M cone cells and five LR cells selected for high *THRB* expression. RACE reactions were performed separately with primers complementary to the TRβ1-specific exon 4 and to the TRβ2-specific first exon (**Figure 4F**). Sequencing of LM and LR RACE products corroborated pronounced PTT in introns 4 and 6, with greater intron 6 PTT in LR versus LM cells (**Figure 4F**, **Figure S7**). However, we did not corroborate the late rods' proportionately higher intron 4 PTT, likely due to the small number of LR cells examined and heterogeneity in PTT frequency in individual cells. Long read sequencing also revealed PTT following the TRβ2-specific exon and a novel transcription-terminating exon following the canonical exon 5 observed solely in TRβ2 transcripts (**Figure 4F**, S7). 3' RACE transcripts rarely extended into the 3' UTR in LM or LR cells, suggesting that reads mapping to this region do not reflect protein-coding RNAs and confound the assessment of protein-coding *THRB* mRNA expression. These analyses demonstrate that *THRB* is regulated by multiple PTT events in rod and cone precursors as well as by cell type-specific promoter utilization and independent 3' UTR RNA expression.

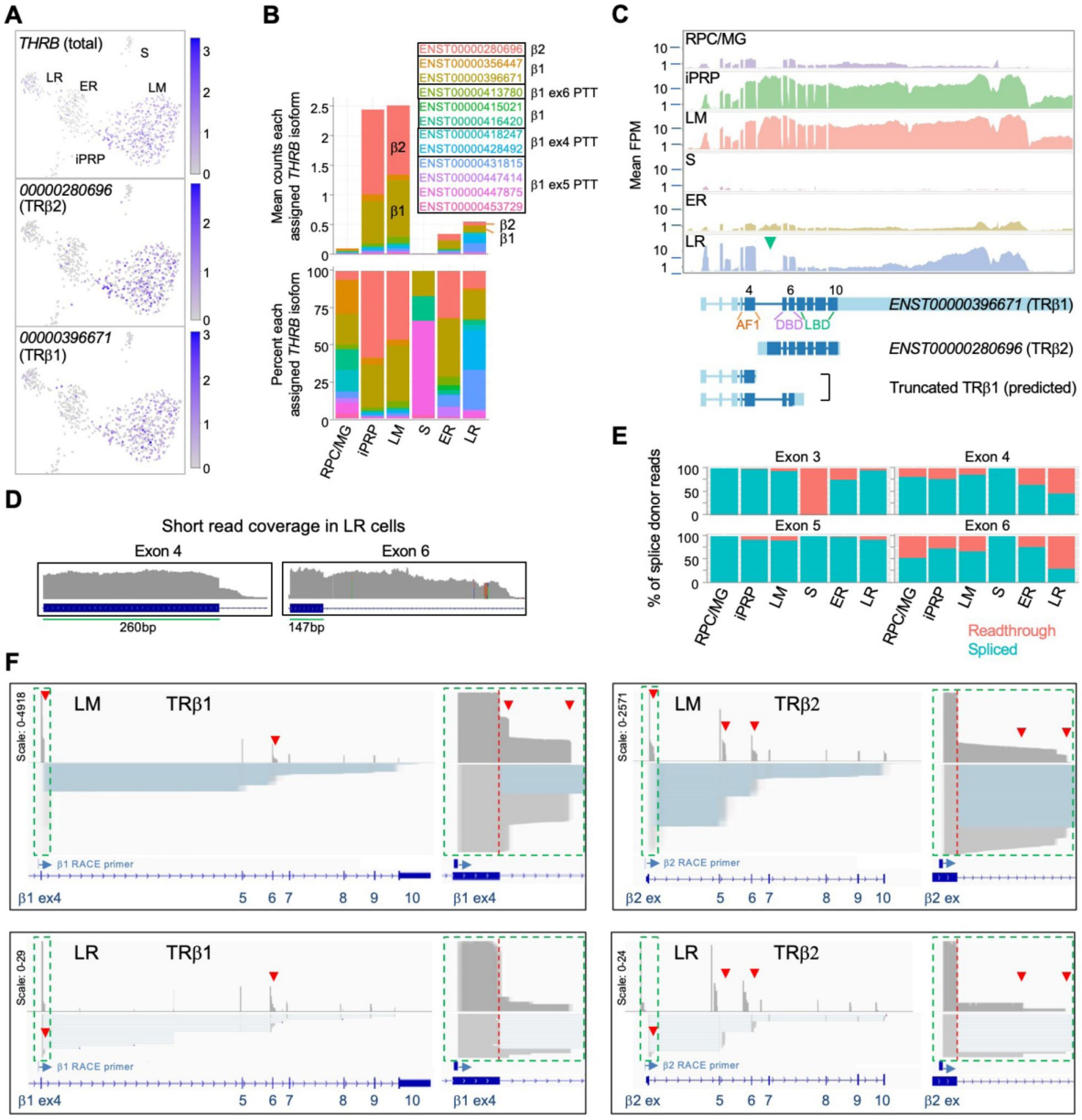

Figure 4

Differential expression of *THRB* isoforms in rod and cone precursors.

A. Expression of *THRB* and highly assigned isoforms *ENST00000280696* (encoding TRβ2) and *ENST00000396671* (TRβ1). **B.** Mean *THRB* isoform assignments for each cluster presented as counts (*top*) and percentage of counts (*bottom*); Ensemble transcript IDs shown in color with β2, β1, and β1 PTT isoform structures as in **Figure S6B**. **C.** *Top*: Mean read counts across Ensembl *THRB* exons. *Bottom*: Transcript structures for TRβ1, TRβ2, and two TRβ1 truncations. Green arrowhead: First TRβ2 exon. *ENST00000396671* exon numbers are indicated above and protein domains (AF1, DNA-binding (DBD), and ligand binding (LBD)) below. **D.** Read coverage for LR cells across *THRB* exons 4 and 6 splice donor sites. **E.** Percentage of exon splice donor reads that are spliced or readthrough to the subsequent intron. **F.** Long-read sequencing of pooled 3′ RACE reactions initiated with exon 4 (*left*) or TRβ2 exon 1 (right) performed on cDNA libraries from 21 LM cells (*top*) and 5 LR cells (*bottom*). Schematics show total coverage (*above*) and individual transcripts (*below)*. TRβ1 and TRβ2 first exons (green boxes) are enlarged at right. Red arrowheads: intronic premature transcription termination (PTT).

For *RXRG*, short read sequencing reads were assigned to several isoforms that differed in their 5' promoter position and exon utilization (**Figure S8A-C**). However, 5' RACE and long-read sequencing did not support differential isoform expression (**Figure S8D**), and quantitative imaging revealed an average ~3.5-fold higher RXRγ protein in cones compared to rods (**Figure S8E**). Thus, long-read sequencing clarified that *RXRG* expression is moderately higher in human cone versus rod precursors without evidence of cell-type specific isoforms.

Two post-mitotic immature photoreceptor precursor populations

To further define photoreceptor developmental states, we subdivided the initial six cell populations with higher resolution clustering (level 1.6), identified high resolution cluster-associated genes and regulons, and inferred each cell's rate and direction of transcriptomic change using RNA velocity[39] (**Figure 5A,B**). Increased clustering resolution divided the RPC/MG cluster into separate RPC and Müller glia (MG) groups, divided L/M cones into four subgroups (LM1 – LM4), which partially overlapped in UMAP space, and divided the iPRP cluster into two clusters here designated immature cone precursors (iCPs) and immature rod precursors (iRPs), the latter also drawing cells from the low-resolution ER cluster (**Figure 5A,C**). Similar clusters were observed at reduced k.param values that defines nearest neighbors.

The distinction between RPCs and MG was corroborated by the expression of known marker genes, with the RPC cluster having increased expression of cell cycle markers (*CCNE2*, *CCNA2*, *CCNB2*) and the cell cycle-associated *PBK* and *E2F7* (**Figure 5D**, S9A,B, Table S7).

The MG cluster was spatially segregated, lacked expression of most cell cycle genes, and expressed genes known to be expressed in both populations (*CCND1*, *SLC1A3*, *PAX6*, *LHX2*, *VSX2*) as well as the MG marker *RLBP1*[40–42] (**Figure 5C,D**, S9A). Differential gene expression analyses revealed upregulation of cell cycle-related genes and G2/M checkpoint and E2F target ontologies in the RPC cluster but no significantly upregulated ontologies in the MG population (**Figure S9B,C**), consistent with early MGs resembling quiescent RPCs[43]. In contrast to other studies, we did not distinguish primary RPCs (PRPCs) from neurogenic RPCs (NRPCs)[14,15,20], likely due to the underrepresentation of RPCs in our dataset.

The high resolution iCP and iRP clusters included 'RPC-localized' cells positioned adjacent to RPCs and 'non-RPC-localized' cells adjacent to the LM and ER clusters in UMAP space (**Figure 5C**). RNA velocity suggested that the RPC-localized cell groups flowed towards the larger early maturing L/M cones and rods, respectively (**Figure 5B,C**). Compared to RPCs and MG, RPC-localized iCP and iRP cells had minimal expression of cyclin RNAs or RPC markers *PAX6*, *LHX2*, and *VSX2*, and had increased expression of photoreceptor determinants *OTX2* and *CRX* (**Figure 5D**), consistent with their being immediately post-mitotic photoreceptor precursors. iCP cells in this region upregulated the early cone cell fate determinant *ONECUT1*[3,44], the L/M cone determinant *THRB*, and the cone differentiation marker *GNAT2*, whereas iRP cells trended towards higher expression of the rod determinant *NR2E3* (**Figures 5D**, S10A); however, such RNAs may be more highly expressed in cone- and rod-fated NRPCs than in the unspecified RPCs in our study. Notably, *THRB* and *GNAT2* expression did not significantly change while *ONECUT1* declined in the subsequent non-RPC-localized iCP and LM1 stages, whereas *NR2E3* and *NRL* dramatically increased on transitioning to the ER state (**Figure S10A**).

In the RPC-localized region, iCPs had higher *ONECUT1*, *THRB*, and *GNAT2*, whereas iRPs trended towards higher *NRL* and *NR2E3* ($p = 0.19$, $p = 0.054$, respectively; **Figure 5D**). While we detected differential expression when selectively examining these genes of interest, no genes were differentially expressed (Padj < 0.05) in a transcriptome-wide comparison, likely due to the lack of statistical power given the small number of cells examined.

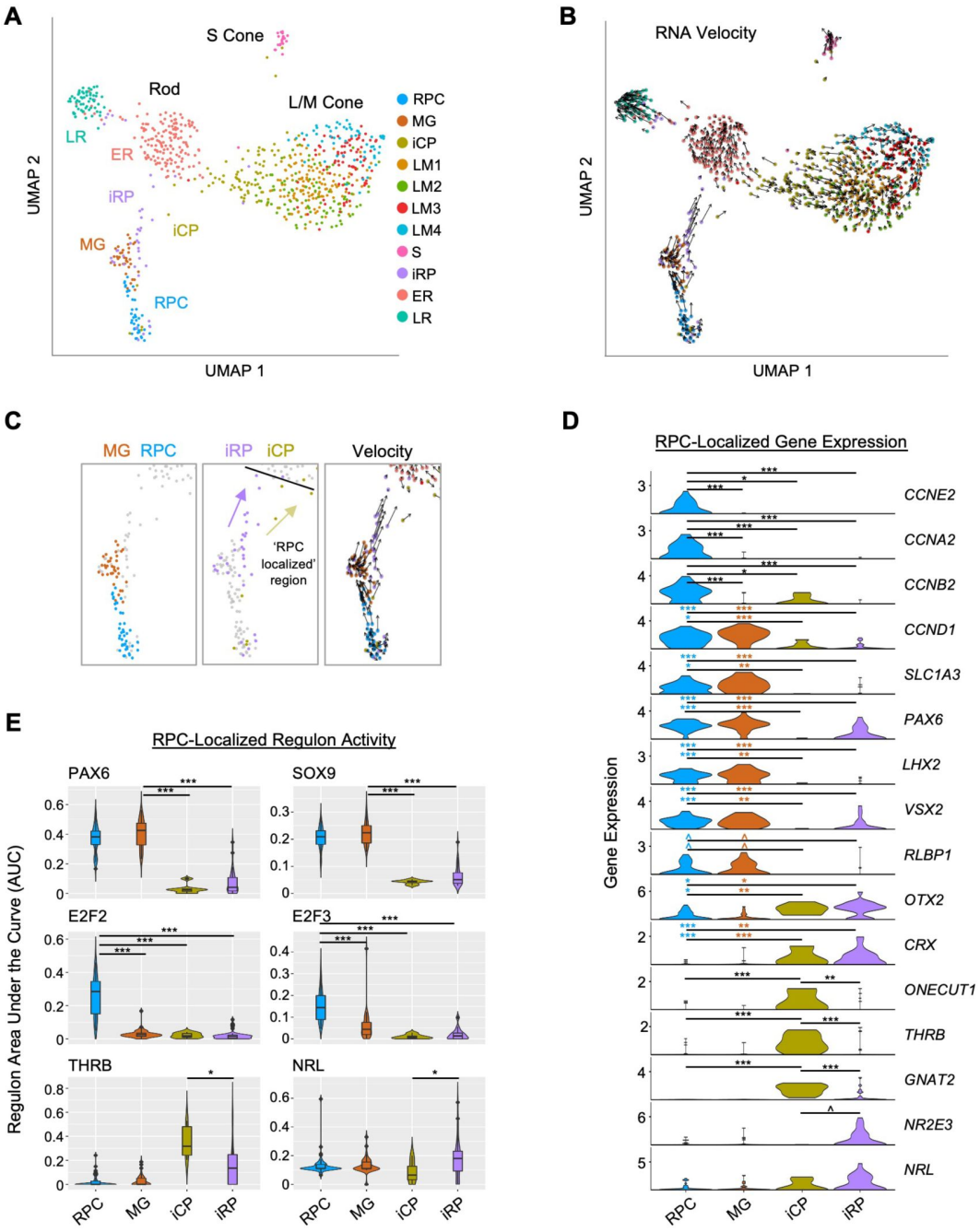

Figure 5

Two post-mitotic photoreceptor precursor populations expressing rod or cone markers.

A. UMAP plot colored by high resolution clusters. **B.** RNA velocity plots with cell clusters as in A. **C.** Enlarged view highlighting RPC and MG clusters (*left*), RPC-localized iCP and iRP clusters (*middle*), and RNA velocity (*right*). Black line: limit of RPC-localized region. Arrows depict inferred trajectories. **D.** Violin plots depict expression of selected genes in RPC, MG, and RPC-localized iCP and iRP cells. Colored asterisks compare cluster of same color to cluster at right of line. **E.** SCENIC regulon violin and box plots for RPC-localized cells in each cluster, selected from most specific regulons for MG, RPC, ER and LM clusters. ^, pAdj <0.1; *, <0.05; **, <0.005; ***, <0.0005 (post-hoc Dunn test).

To our knowledge, past studies have not distinguished immature cone and rod precursors (*i.e.*, iCPs and iRPs) from the subsequent maturing cone and rod precursor states. To explore whether early cone and rod precursors with similar properties are present in droplet-based scRNA-seq studies, we examined gene expression in spatiotemporally segregated cone and rod precursor populations as well as in cone and rod NRPCs in the Zuo *et al.* 3' snRNA-seq dataset[20]. This revealed that cone NRPCs and the earliest (pcw 8-10) cone precursors had high *ONECUT1* and *THRB* yet minimal *NR2E3* (**Figure S10B**). Similarly, rod NRPCs had high *NRL* and *NR2E3*, yet it was not possible to examine the earliest (pcw 10-13) rod precursors, as many had cone-like gene expression profiles, suggesting they may have been mis-assigned (**Figure S10B**, *grey boxes*). Further evaluation suggested misassignment of a smaller proportion of rod and cone precursors at other ages (**Figure S11**). In particular, cells potentially mis-assigned as rod precursors were located in the cone precursor UMAP region and highly expressed *THRB* (**Figure S11D**, **), while cells potentially mis-assigned as cone precursors were located in the rod precursor UMAP region and highly expressed *NR2E3* (**Figure S11E**, *). When considering only the main cone and rod precursor UMAP regions, early (pcw 8-13) cone precursors expressed *THRB* and lacked *NR2E3* (**Figure S11D,E**, blue arrows), while early (pcw 10-15) rod precursors expressed *NR2E3* and lacked *THRB* (**Figure S11D**,E, red arrows), similar to RPC-localized iCPs and iRPs in our study (**Figure 5D**). We conclude that Louvain clustering of deep full-length scRNA-seq distinguished immediately post-mitotic iCP and iRP populations with features similar to early cone and rod precursors in a large 3' snRNA-seq dataset.

In a further comparison, we noted lower detection of *GNAT2* in L/M cone precursors and lower detection *CCNE2*, *CCNA2*, and *CCNB2* in RPCs in 3' snRNA-seq versus full-length scRNA-seq datasets (**Figure S10A,B**). This suggests that deep full-length scRNA-seq enabled more sensitive detection of certain cell-type-specific RNAs along with improved discrimination of immature cone versus rod precursor states.

SCENIC regulons further clarified the identities of the four RPC-localized clusters. The MG cluster was best specified (*i.e.*, had highest regulon specificity scores) by PAX6 and SOX9, both previously described in RPCs and MGs[40,45,46], whereas RPCs were best specified by E2F2 and E2F3 (**Figure 5E**). These RPC and MG regulons were low or absent in the early post-mitotic iCPs and iRPs, suggesting they undergo an abrupt cell state change. Moreover, RPC-localized iCPs had greater THRB regulon signal than RPC-localized iRPs, while RPC-localized iRPs had higher NRL regulon signal ($p<0.05$ for both) (**Figure 5E**). Interestingly, RPC-localized and/or non-localized iCPs also had higher activity of the pan-photoreceptor regulons LHX3, OTX2, and NEUROD1 compared to their iRP counterparts (**Figure S10C,D**). Finally, activities of the cone-specific THRB and ISL2 regulons, the rod-specific NRL regulon, and the pan-photoreceptor LHX3, OTX2, CRX, and NEUROD1 regulons increased to varying extents on transitioning from immature iCP or iRP states to the early-maturing LM1 or ER states (**Figure 10C**).

Early cone and rod precursors with rod- and cone-related RNA co-expression

In addition to the immediately post-mitotic RPC-localized iCPs, the iCP cluster included cells bridging the UMAP region between early maturing cones and early maturing rods (**Figure 6A**). Many iCP and ER cells in this bridge region expressed RNAs encoding cone markers (*GNAT2*, *THRB*), rod markers (*GNAT1*, *NR2E3*), or, in many cases, both (**Figure 6B**), suggestive of a proposed hybrid cone/rod precursor state more extensive than implied by the co-expression of different *THRB* and *NRL* isoforms[4].

To determine whether the intermixed cone and rod gene expression reflects a hybrid cone-rod precursor state, we examined bridge region NRL and THRB regulon activities, which embody the overall transcriptomic effects of these factors. Indeed, in the bridge region, cells with NRL and THRB regulon signals intermixed, and some cells showed signals for both (**Figure 6C**, arrows).

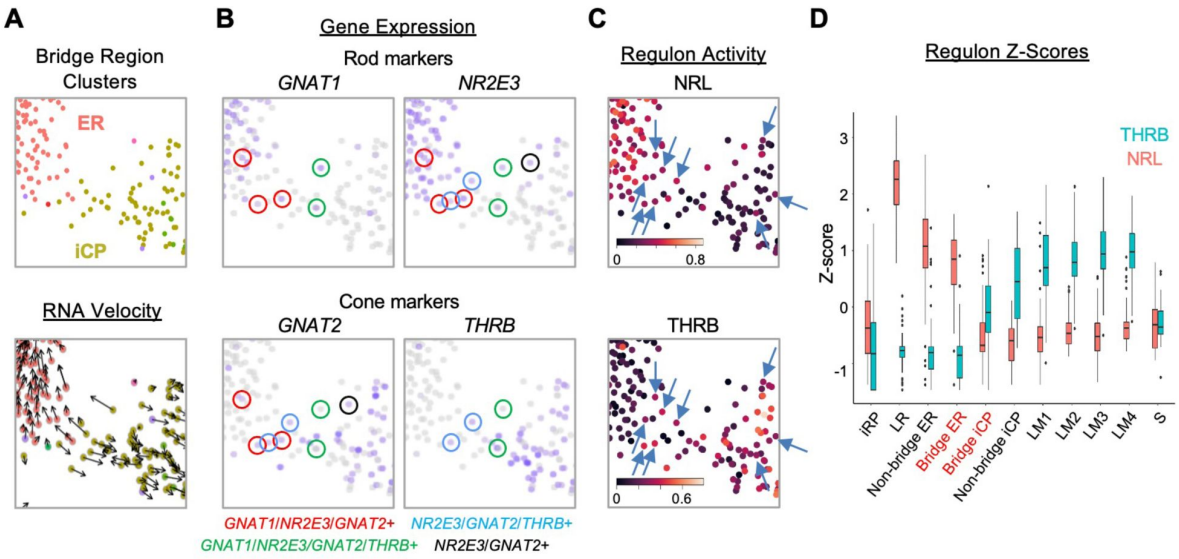

Figure 6

An iCP sub-population with cone- and rod-related RNA co-expression.

A-C. UMAP 'bridge' region cells colored by ER and iCP cluster and RNA velocity (A), rod and cone marker gene expression (B), and NRL and THRB regulon activity (C, arrows indicate cells with both regulon signals). **D**. Box plot of Z-score-normalized NRL and THRB regulon AUCs for each cluster; Bridge ER and Bridge iCP represent cells present in the UMAP region in panels A-C.

However, iCP cells had low NRL regulon z-scores similar to L/M cones and most had THRB z-scores above that of adjacent ER cells (**Figure 6D**). The difference between regulon signals increased in rod and cone clusters outside the bridge region as NRL or THRB regulons became more dominant (**Figure 6D**).

To identify cells with early cone- and rod-related RNA co-expression in the developing retina, we performed multiplex RNA FISH for early cone marker *GNAT2* and rod marker *NR2E3* combined with immunofluorescence (IF) staining for RXRγ, which has high expression in outermost neuroblastic layer (NBL) cone precursors and low expression in middle NBL rod precursors (as earlier shown in **Figure S8E**), and for NR2E3, which is detected solely in rods. To infer the spatiotemporal pattern of such expression across human retinal development, we examined *GNAT2* and *NR2E3* RNA co-expression in RXRγ+ cone precursors in the outermost NBL and in RXRγ+ rod precursors in the middle NBL across 13 regions of a FW14 retina section (**Figures 7**; see **Figure S12** for IF + FISH images). Limiting our analysis to the outer and middle NBL allowed us to disregard RXRγ+ retinal ganglion cells in the retinal ganglion cell layer or inner NBL.

The analyses revealed that most of the far peripheral (hence, nascent) outer NBL RXRγ+ cone precursors (**Figure 7A,B**, regions 2 and 13) lacked detectable *GNAT2* and *NR2E3* RNA (green bars in **Figure 7C**), whereas those in the more mature central retina (regions 3-12) were uniformly *GNAT2*+ (yellow and red bars in **Figure 7C**). However, starting with regions 3 and 11, some outermost NBL *GNAT2*+ cones were also *NR2E3*+ (red bars in **Figure 7C**). The proportion of outermost NBL cells that co-expressed *GNAT2* and *NR2E3* RNA increased in the more central retina (regions 5-10), yet all of these cells had strong RXRγ staining and lacked NR2E3 protein, consistent with their having a cone identity (illustrated in **Figure 7E**). In contrast, most middle NBL RXRγ+ cells had either a low number of *NR2E3* RNA puncta without NR2E3 protein (*NR2E3*$^{+}$ / NR2E3^{-}, magenta bars in **Figure 7D**), likely in nascent rods, or prominent *NR2E3* RNA with NR2E3 protein (*NR2E3*$^{+}$ / NR2E3^{+}, purple bars in **Figure 7D**), in maturing rods (**Figure 7D**, E). However, we did not detect *GNAT2* puncta in middle NBL RXRγ+, *NR2E3*+ cells, including the most peripheral RXRγ+ cells with low-level *NR2E3* RNA (**Figures 7E**, S12). In summary, most photoreceptor precursors with *GNAT2* and *NR2E3* RNA co-expression had high RXRγ, no detectable NR2E3 protein, and outermost NBL positions expected of cone precursors. This supports the notion that, in our scRNA-seq analyses, bridge region iCP cells with combined *GNAT2* and *NR2E3* RNA expression are likely cone-directed.

Cone and rod precursor populations that co-express cone and rod marker genes were also evident in the Zuo *et al.* 3' snRNA-seq dataset. While the earliest cone precursors were *NR2E3*-negative and the earliest rod precursors were *THRB*-negative (as described above), starting at pcw 15, later cone precursors expressed *NR2E3* (**Figure S11E**, green arrows) and later rod precursors expressed *THRB* (**Figure S11D**, purple arrows). *THRB* was highest in the most distal rod precursors (yet still lower than in cone precursors), corroborating our findings in **Figure 1D** and **Figure 4B-C**. In contrast, in the 3' snRNA-seq analysis, *GNAT2* expression was sparse in rod precursors of all ages (**Figure S11F**), consistent with the lack of *GNAT2* in rod precursors in our RNA FISH analyses and implying that different cone- and rod-related genes have different tendencies to be expressed in the other photoreceptor precursor type.

Thus, a 3' snRNA-seq analysis confirmed the initial production of immature photoreceptor precursors with either L/M cone-precursor-specific *THRB* or rod-precursor-specific *NR2E3* expression, followed by lower-level co-expression of their counterparts, *NR2E3* in cone precursors and *THRB* in rod precursors. However, in the Zuo *et al.* analyses, the co-expression was first observed in well-separated UMAP regions, as opposed to a region that bridges the early cone and early rod populations in our UMAP plots. These findings are consistent with the notion that cone- and rod-related RNA co-expression begins in already fate-determined cone and rod precursors, and that such precursors aberrantly intermixed in our UMAP 'bridge region' due to their insufficient representation in our dataset.

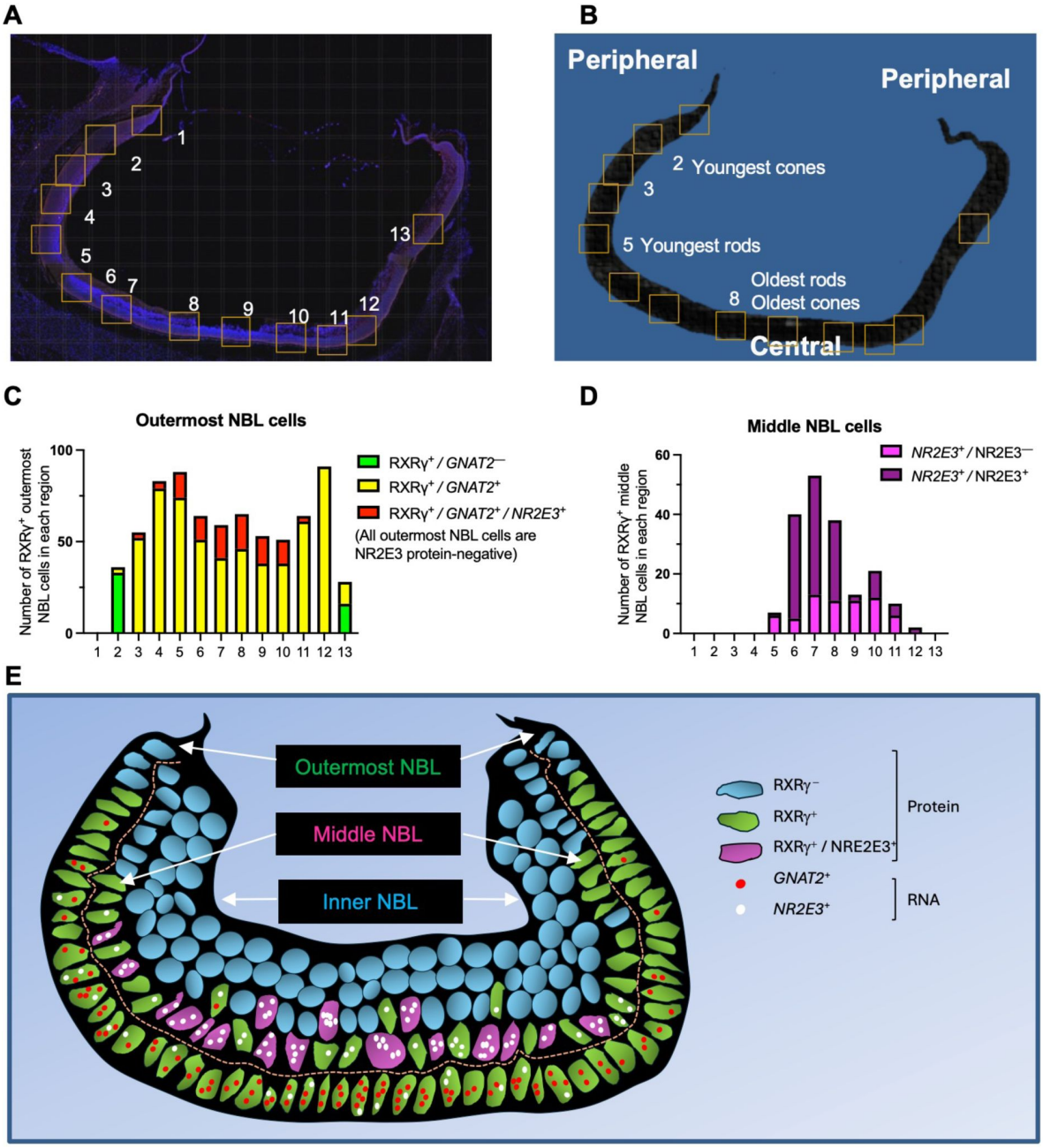

Figure 7

Cone-related *GNAT2* and rod-related *NR2E3* RNA co-expression in human cone precursors.

A,B. Tiled composite fluorescence image of FW14 retinal section after immunofluorescence staining of RXRγ and NR2E3 and RNA FISH of *GNAT2* and *NR2E3* (A) and diagram of the same section indicating the most peripheral (*i.e.*, youngest and least mature) and most central (*i.e.*, oldest and most mature) rods and cones (B). Boxes indicate regions further evaluated in Supplementary Figure S12 and quantitated in panels C and D. **C,D.** Quantitation of (C) outermost and (D) middle (*i.e.*, sub-outermost) NBL photoreceptor precursors expressing combinations of RXRγ and NR2E3 proteins and *GNAT2* and *NR2E3* RNAs (*n.b.*, italics are used for RNAs, non-italics for proteins). **E.** Patterns of *GNAT2* and *NR2E3* RNA and RXRγ and NR2E3 protein expression inferred from *in situ* hybridization and immunofluorescence staining. RXRγ is expressed in the outermost NBL starting in the far periphery, consistent with cone precursors, and in middle NBL cells, starting more centrally, consistent with rod precursors. *GNAT2* and *NR2E3* RNA co-expression in outermost NBL cells lacked NR2E3 protein, representing putative cone precursors. RXRγ+ retinal ganglion cells in the inner NBL and ganglion cell layer not shown.

Developmental expression of photoreceptor precursor markers and fate determinants

To further assess relationships between iCP subpopulations, we examined the expression and UMAP distributions of the four iCP marker genes identified in **Figure S9A**. Among these genes, *CHRNA1* was mainly expressed in bridge region iCP and ER cells, whereas *ONECUT1* was biased to cone-directed iCPs, lncRNA *CTC-378H22.2* was expressed in a narrow zone of *THRB*+, *GNAT2*+ iCPs, and *S100A6* was more widely expressed (**Figure 8A**). iCP cells also expressed *ATOH7* and *DLL3*, which were previously proposed to define transitional photoreceptor precursors and promote cone fate determination[14–16]. *ATOH7* was largely restricted to RPC-localized and bridge region iCPs whereas *DLL3* was broadly expressed similar to *S100A6* (**Figure 8A**).

A similar pattern was seen in the Zuo *et al.* 3' snRNA-seq dataset[20], where *CHRNA1*, *ONECUT1*, *S100A*, *ATOH7*, and *DLL3* were most highly expressed in the youngest and developmentally earliest ML cone and rod precursors and persisted to various extents during cone and rod maturation, whereas *CTC-378H22.2* (ENSG00000259436) had more restricted and cone-specific expression (**Figure S13A**). However, the early cone and rod precursor UMAP regions did not adjoin one another (in contrast to our UMAP bridge region), suggesting that the cone and rod precursors expressing the above markers had begun their distinct trajectories and that their juxtaposition in our UMAP analyses is spurious. Also, different iCP markers had different spatiotemporal expression: *CHRNA1* and *ATOH7* were most prominent in peripheral retina with *ATOH7* strongest at pcw 10 and *CHRNA1* strongest at pcw 13; *CTC-378H22.2* was prominently expressed from pcw 10-13 in both the macula and the periphery; and *DLL3* and *ONECUT1* showed the earliest, strongest, and broadest expression (**Figure S13B**). The distinct patterns suggest spatiotemporally distinct roles for these factors in cone precursor differentiation.

As *CHRNA1* appeared to be the most specific marker of both early cone and early rod precursors, we evaluated whether *CHRNA1* RNA marked specific cone and rod populations in the developing retina using RNA-FISH combined with RXRγ and NRL immunofluorescent staining. In a FW12 retina, we detected highest *CHRNA1* in the earliest, most peripheral NRL^+ rods and $RXR\gamma^+$ cones and fewer *CHRNA1*+ cells in more mature, central regions ($p < 0.005$ in cones) (**Figure 8B-D**), consistent with its expression in early cone and rod precursors.

To identify factors that regulate transcriptomic states during cone cell fate determination, we examined the UMAP distributions of the most iCP-specific transcription factor regulons, OLIG2 and LHX9 (**Figure S10D**, Table S8). As Olig2 was previously detected in mouse RPCs in which Onecut1 enabled *Thrb* expression and cone fate determination[3,47], the OLIG2 regulon was expected to be most active in RPCs and in early, immediately post-mitotic iCPs. While the OLIG2 and LHX9 regulons were indeed active in RPCs, both were also active in a narrow zone of *ONECUT1*+ iCPs positioned farthest from S cones and immediately preceding the upregulation of the THRB regulon, a location with sparse *OLIG2* RNA expression (**Figure S14**). These data indicate that the OLIG2 and LHX9 regulons are active in and potentially relevant to human L/M cone fate determination in a post-mitotic iCP subpopulation.

An early L/M cone trajectory marked by successive lncRNA expression

After fate commitment, L/M cones initiate a maturation process with upregulation of RNAs and proteins related to phototransduction, axonogenesis, synaptogenesis, and outer segment morphogenesis[5,6]. To evaluate whether early L/M cone maturation is comprised of distinct transcriptomic cell states, we assessed marker gene and regulon differences between high resolution clusters LM1, LM2, LM3, and LM4. While clusters LM1-4 were distinguished by sequential increasing expression of *ACOT7*, *RTN1*, *PDE6H*, *OLAH*, and *NPFF*, they showed only

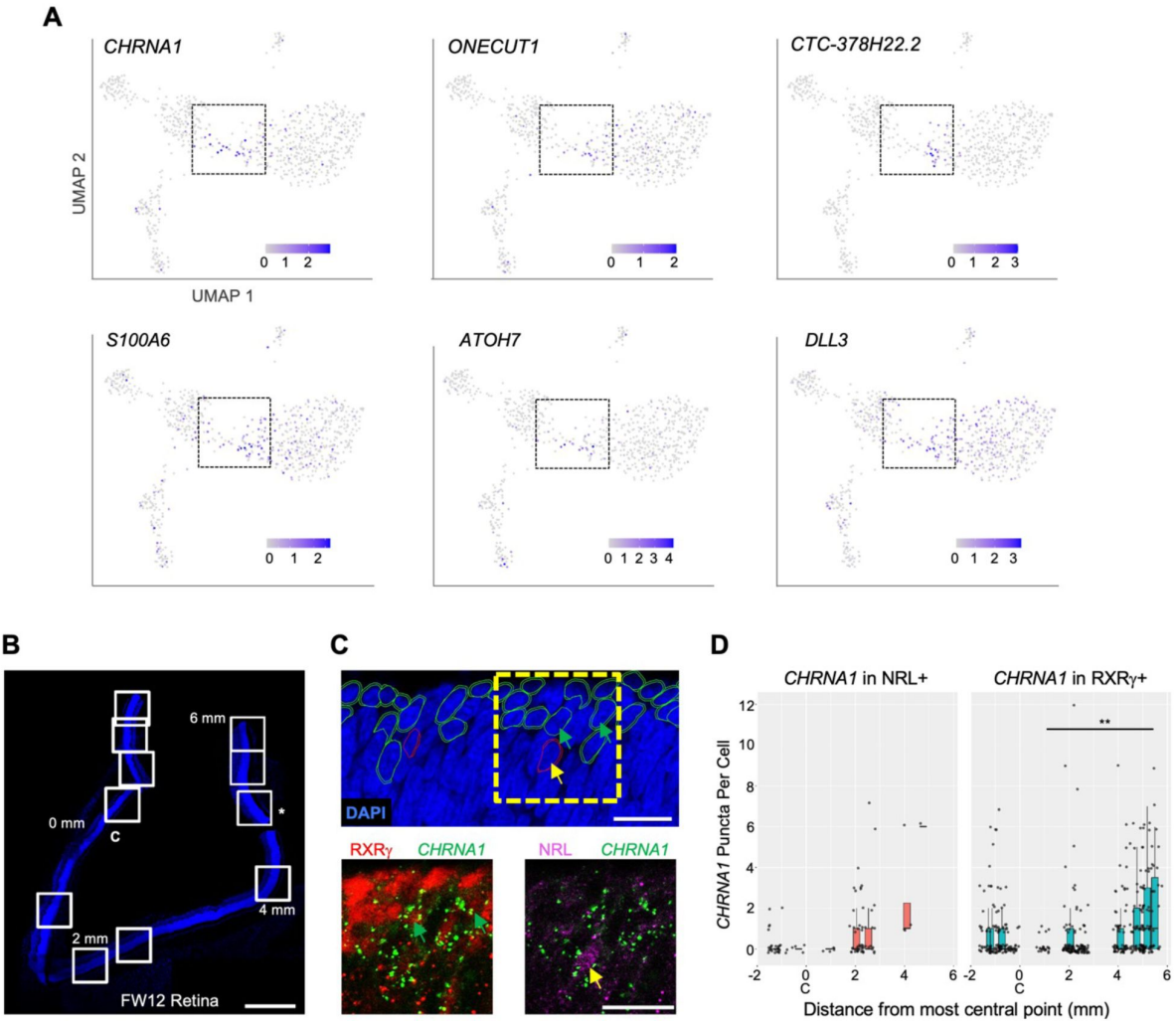

Figure 8.

Developmental expression of early cone and rod precursor markers.

A. UMAP plots of iCP marker genes *CHRNA1*, *ONECUT1*, *CTC-378H22.2*, and *S100A* (see **Figure S9A**) and previously identified photoreceptor precursor markers *ATOH7* and *DLL3*. **B-D.** Combined RXRγ/NRL immunohistochemical staining and *CHRNA1* RNA FISH of FW12 retina. **B**. Tiled images of retina section with nuclei stained with DAPI. White boxes: fields used for quantitative fluorescent imaging. Distances along apical edge of tissue marked in mm from midpoint of central image (0 mm, C). *: Imaged region shown in C. Scale bar = 500 µm. **C.** *Top:* Retinal nuclear and cellular segmentation and identification of cells as RXRγ+ (green outline) or NRL+ (red outline). Yellow box: Field shown below. *Bottom:* RXRγ or NRL immunofluorescence staining with *CHRNA1* FISH. Arrows: RXRγ+,*CHRNA1*+ (green), NRL+,*CHRNA1*+ (yellow). Scale bars = 15 µm. **D**. Quantitation of fluorescent puncta in RXRγ+ and NRL+ cells by image field. X-axis: Distance from the midpoint of each image to retina center (0 mm, C). **, p <0.005 (Wald test, images from 0-6 mm).

subtle differences among the three regulons with highest LM1-4 specificity scores, THRB, ISL2, and LHX3 (**Figure 9A,B**). The lack of cluster-specific marker genes and regulons suggest that LM1-LM4 represent different stages of a graded maturation process.

We further evaluated gene expression changes in maturing cones by pseudotemporally ordering iCP and L/M cone precursors (**Figure 9C**). This identified 967 pseudotime-correlated genes (q-value < 0.05, expression > 0.05 in >5% of cells; Table S9) in seven gene modules (**Figure S15**). Among the top 20 pseudotime-correlated genes in each module, we identified four lncRNAs that were sequentially expressed (**Figure 9D**). To determine if these lncRNAs distinguish developmentally distinct maturing cones *in vivo*, we probed their expression via multiplex RNA FISH in co-stained RXRγ+ cone precursors across a FW16 retina (**Figure 9E,F**). Quantitation of FISH puncta defined four cone maturation zones based on expression peaks and significant count differences for each lncRNA as color-coded in **Figure 9G**: the most peripheral cones with high *CTC-378H22.2* and *HOTAIRM1* (blue), peripheral cones with high *HOTAIRM1* only (green), cones with low expression of all four lncRNAs (red), and parafoveal/foveal cones with upregulated *RP13143G15.4*, *CTD-2034I21.2*, and *CTC-378H22.2* (purple) (**Figure 9G**). The detection of foveal *CTC-378H22* by ISH but not in late LM transcriptomes may relate to a lack of the most mature cones in our scRNA-seq analyses. These data support the concept that maturing L/M cones sequentially express specific lncRNAs as they develop.

Cone-intrinsic SYK expression associated with the proliferative response to pRB loss

We next assessed whether early-maturing cone transcriptomic features are conducive to the proliferative response to pRB loss[10,11]. Given the high transcriptomic similarity across the L/M cone population, we compared gene expression between all early-maturing L/M cones and early-maturing rods. This identified 422 genes upregulated and 119 downregulated in cones ($p<0.05$, $log2FC>|0.4|$) (**Figure S16A**, Table S10). Among cone-enriched genes, the top three enriched ontologies related to translation initiation, protein localization to membrane, and MYC targets (**Figure S16B**). The upregulation of MYC target genes was of interest given that many MYC target genes are also targets of MYCN, that MYCN protein is highly expressed in maturing (ARR3+) cone precursors but not in NRL+ rods (**Figure 10A**), and that MYCN is critical to the cone precursor proliferative response to pRB loss[8–10]. Indeed, whereas *MYC* RNA was not detected, the LM cone cluster had increased *MYCN* RNA (log2FC = 0.54) and MYCN regulon activity, representing the seventh highest LM cluster regulon specificity score (**Figure 10B,C**, Table S6).

Among other differentially expressed genes, we noted the L/M cone-specific upregulation of *SYK* (**Figure 10D**, Table S10), which encodes a non-receptor tyrosine kinase. Whereas SYK was previously implicated in retinoblastoma genesis and proposed to be induced in response to pRB loss[48], its expression was not previously reported in developing fetal retina. Indeed, our scRNA-seq analyses revealed that *SYK* RNA expression increased from the iCP stage through cluster LM4, in contrast to its minimal expression in rods (**Figure 10E**). Moreover, *SYK* expression was abolished in the five-cell group with properties of late-maturing cones (characterized in **Figure 1E**), here displayed separately from the other LM4 cells and designated LM5 (**Figure 10E**). Similarly, immunohistochemical staining revealed high SYK protein expression in immature (ARR3-) and early-maturing (ARR3+) cones from the retinal periphery to the maturing foveal cones at FW16, while SYK was not detected in the most mature foveal cones at FW18 (**Figure 10F**). The loss of SYK protein and RNA expression with cone maturation is consistent with the lack of SYK in cones of normal retina adjacent to a retinoblastoma tumors[48] and implies that SYK is a defining feature of the human early cone precursor state.

While *MYCN* RNA was also preferentially expressed in early cones, it did not increase as much relative to RPCs nor decline as much in late-maturing cone precursors when compared to *SYK* RNA dynamics (**Figure 10E**).

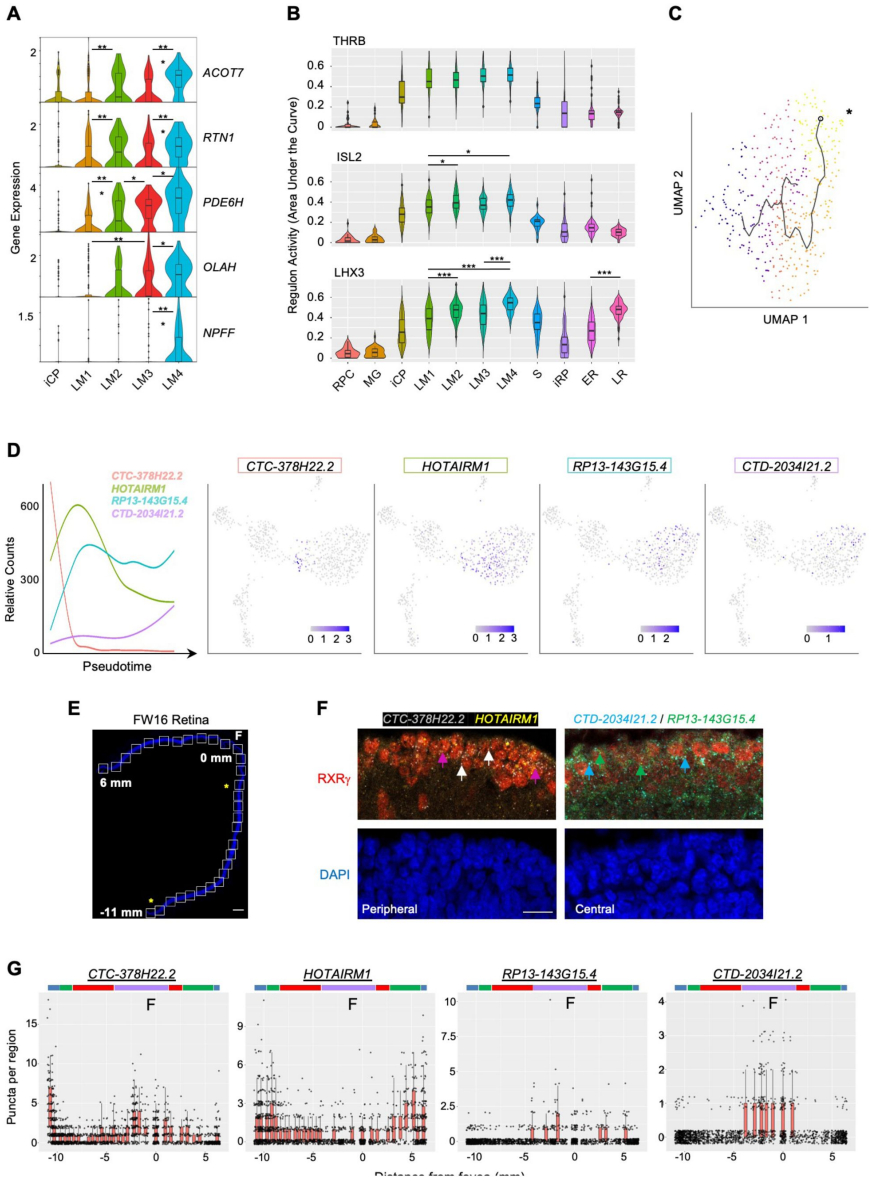

Figure 9

L/M cone subcluster marker genes, regulons, and pseudotemporal trajectory with successive lncRNA gene expression.

A. Violin plots of high-resolution cone cluster marker genes with increasing maturation-associated expression. All significant differences between adjacent clusters are indicated. **B.** Violin plots of regulons with highest LM1-4 cone cluster specificity scores. *, p <0.05; **, <0.005; ***, <0.0005 (post-hoc Dunn test). **C.** Pseudotemporal trajectory through the L/M cone population derived with Monocle 3. *: Root cell used to define endpoint. The pseudotime trajectory may be related to LM1-LM4 subcluster distributions in **Figure 5A**. **D.** Trendlines of relative count expression (*left*) and UMAP plots for lncRNAs correlating with early or late-upregulating modules. Line color matched to labels. **E, F.** Combined RXRγ immunohistochemical staining and FISH of lncRNAs on FW16 retina. **E**. Tiled images of retina with nuclei stained with DAPI. White boxes: fields used for quantitative fluorescent imaging. Distances along apical edge of tissue marked in mm from fovea to ciliary margins. Scale bar = 500 µm. Asterisks identify fields shown in F. **F.** Combined RXRγ immunostaining and multiplex FISH for four lncRNAs, of which two are shown in peripheral and central retina regions. Arrows: White: RXRγ/*CTC-378H22.2*+. Magenta: RXRγ/*HOTAIRM1*+. Blue: RXRγ/*CTD-2034I21.2*+. Green: RXRγ/*RP13-143G15.4*+. Scale bar = 15 µm. **G.** Quantitation of lncRNA fluorescent puncta assigned to RXRγ+ cells after segmentation. Colored bars mark lncRNA expression regions as described in the text. Arrows indicate significant count differences between images (p <0.05, Wald test).

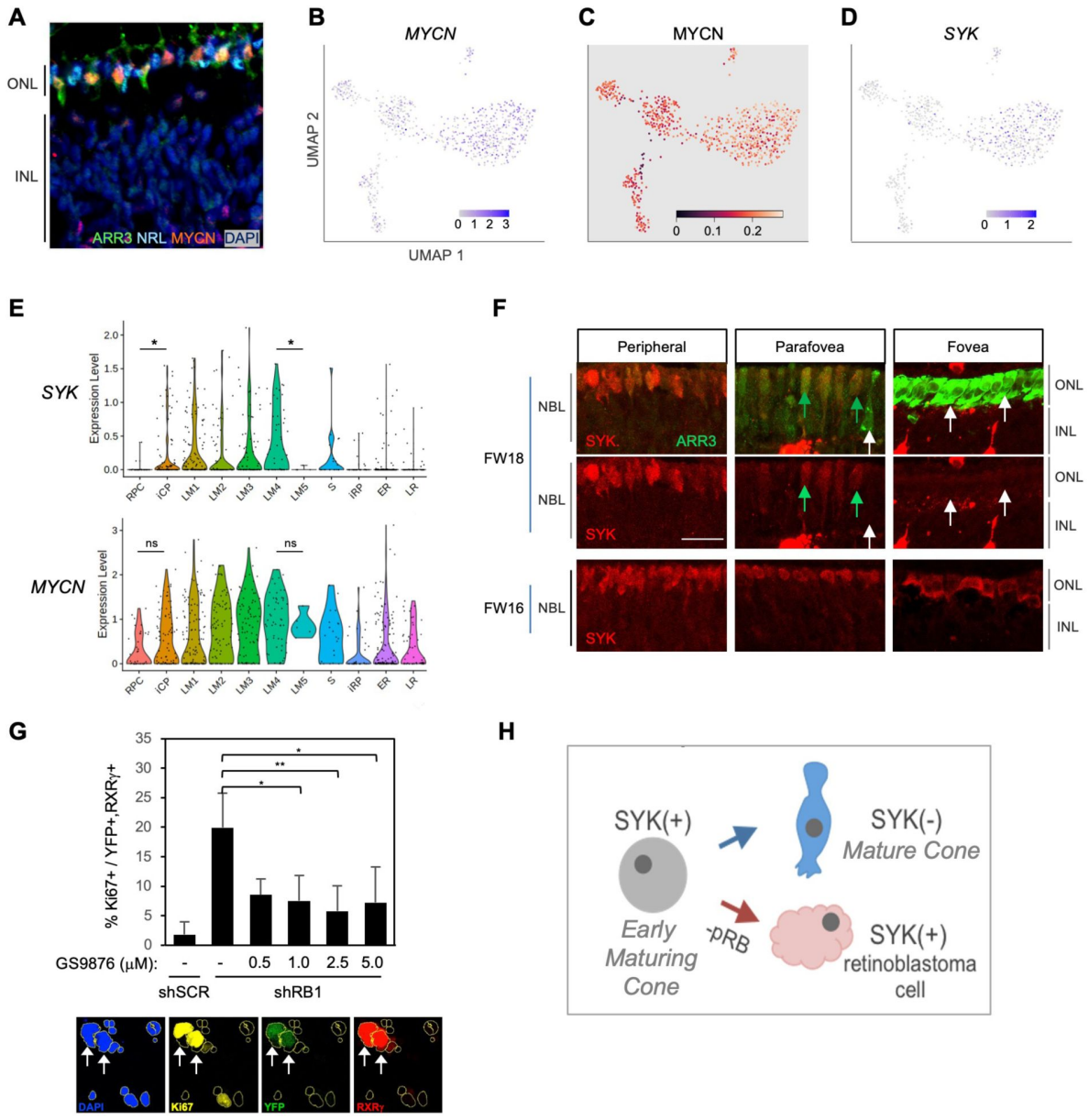

Figure 10

Cone intrinsic MYCN and SYK associated with proliferative response to pRB loss.

A. Immunofluorescent staining shows high MYCN in ARR3+ cones but not in NRL+ rods in FW18 retina. **B-D.** UMAP plots of *MYCN* expression (B), MYCN regulon activity (C), and *SYK* expression (D). **E.** *SYK* and *MYCN* gene expression violin plots by cluster. *, p <0.05; ns = not significant (t-test). **F.** Immunohistochemical staining of SYK and cone arrestin (ARR3) in FW18 and FW16 retinae. Green arrow: ARR3+, SYK+. White arrow: ARR3+, SYK–. Scale bar = 25 μm. **G.** *Top:* Effect of SYK inhibitor GS-9876 on Ki67 expression in RXRγ+ cones from FW16.5 retina co-transduced with YFP and shRB1- or control shSCR-shRNA. Values represent means of three analyses from two treatment replicates. Error bars: standard deviation. *, p <0.05; **, <0.005 (Student's T-test with equal variance, 2-tailed). RXRγ+ cells: Experiment 1, n=1,340. Experiment 2, n=804. Range 107 – 366 cells per condition. *Bottom:* Example of Ki67, YFP, and RXRγ co-immunostaining with DAPI+ nuclei (yellow outlines). Arrows: Ki67+, YFP+, RXRγ+ nuclei. **H.** Model of SYK expression in cone maturation and retinoblastoma development.

To determine if SYK might contribute to retinoblastoma initiation, dissociated fetal retinal cells were transduced with an *RB1*-directed shRNA (shRB1-733) known to induce cone precursor proliferation[10], treated with the selective SYK inhibitor GS-9876[49] for 12 days, and examined for cone precursor cell cycle entry by co-staining for RXRγ and Ki67. GS-9876 treatment suppressed the proliferative response to pRB knockdown at all concentrations from 1.0 – 5.0 μM (**Figure 10G**), consistent with the notion that cone precursor intrinsic SYK activity contributes to the proliferative response to pRB loss and is retained in retinoblastoma cells (**Figure 10H**). However, given potential SYK inhibitor off-target effects, validation of the role of SYK in retinoblastoma initiation will require gene ablation studies.

Discussion

This study evaluated cell state changes associated with human cone and rod photoreceptor development using deep full-length scRNA-seq. Whereas prior scRNA-seq studies provided insights into RPC fate determination and trajectories using 3' end counting[14–18,20,26], deep full-length sequencing enabled more precise resolution of cell states and identification of cell type-specific regulon activities and transcript isoforms. Additionally, our cell enrichment strategy provided insight into the transcriptomic profiles and potential cancer-predisposing features of developing cones, a rare population with unique cancer cell-of-origin properties[8,10,11].

One advantage of full-length scRNA-seq is that it enables the detection of differential transcript isoform expression. Here, we show that the rod determinant *NRL*, the L/M-cone determinant *THRB*, and the cone marker *RXRG* are all co-expressed in cone and rod precursors at the RNA level yet use distinct cell type-specific mechanisms to enable appropriate differential protein expression. Long-read cDNA sequencing revealed that L/M cones preferentially express novel *NRL* transcript isoforms predicted to encode a truncated NRL protein (Tr-NRL) lacking a transactivation domain as well as *NRL* isoforms with intra-exon-2 transcription initiation and alternative splicing. As with DD10[35], Tr-NRL opposed transactivation by full-length NRL and thus may suppress rod-related transcription. However, our inability to detect intrinsic Tr-NRL or to overexpress Tr-NRL in cone precursors suggests there are additional layers of regulation, possible effects of untranslated Tr-NRL RNA, and alternative contexts in which these isoforms act. A similar assortment of *NRL* isoforms were expressed in rods, yet a far higher proportion of rod *NRL* transcripts encoded full-length (FL-) NRL protein. Thus, the L/M cone precursors' greater use of the Tr-NRL first exon and *NRL* exon 2 disruptions reveal a multipronged approach to suppress FL-NRL function while downregulating overall *NRL* RNA by only ~ 4-fold.

Similarly, we uncovered cell type-specific differences in *THRB* transcript isoforms, albeit generated through premature transcription termination (PTT) and 3' UTR expression in late rod precursors. PTT is widely used to govern expression of transcription regulators[50], and while PTT-shortened *THRB* transcripts had been identified[51], their retinal cell specificity was not previously recognized. In contrast, the expression of *THRB* 3' UTR sequences independent of *THRB* protein-coding sequences was not previously reported and may enable additional regulation[52]. As a general matter, the expression of 3' UTR transcripts that are detached from protein-coding sequences may be inferred from full-length scRNA-seq but may be misinterpreted to represent protein-coding transcripts and thus confound the interpretation of scRNA-seq performed with 3' end-counting. To address this issue, our publicly available Shiny app displays exon coverage for all genes expressed in the RPC and photoreceptor clusters in this study.

One limitation of these studies is that individual cells may express a small and varying spectrum of transcript isoforms. While this variability was mitigated by combining cDNAs of cells deemed to be in similar states based on short-read sequencing, analysis of more cells might better reveal the spectrum of isoforms expressed by specific cell populations

Understanding human photoreceptor development requires the identification of photoreceptor lineage developmental states and elucidation of mechanisms underlying their transitions. While cell states may be defined in various ways, at the transcriptome level they are perhaps best defined by unique combinations of transcription factor regulon activities[30]. Our deep sequencing approach uncovered discrete cell states distinguished by gene expression as well as by regulon activities. For example, early- and late-maturing rod populations were distinguished by the latter's increased expression of phototransduction genes together with increased activity of the NRL, ATF4, CRX, and LHX3 regulons and decreased HMX1 and RAX regulons (**Figure 2**). Similarly, L/M cones formed an early-maturing cone cluster characterized by high THRB and ISL2 regulons, consistent with THRB and ISL2 driving L/M cone identity[4,15,53], and a late-maturing cone group with decreased RAX activity. Downregulation of the RAX regulon in late-maturing rod and cone precursors is consistent with decreasing RAX protein during photoreceptor maturation and with RAX-mediated suppression of the cone opsin and rhodopsin promoters[54,55].

Increased clustering resolution further divided the L/M cone cluster into four subgroups with subtle maturation-associated changes in marker gene expression and regulon activity, consistent with LM1-4 comprising different stages of a graded maturation process (**Figure 9**). However, trajectory analyses revealed successive expression of lncRNAs that was validated in developing retinal tissue. Three of these lncRNAs (*HOTAIRM1*, *CTD-2034I21.1* (neighbor gene to *CTD-2034I21.2*), and the mouse ortholog of *CTC-378H22.2* (D930028M14Rik)) were previously observed in cone scRNA-seq[15,17,56]. Their sequential expression in the absence of discrete regulon changes suggests that they demarcate early L/M cone precursor substates.

High resolution clustering also segregated immature cone precursor (iCP) and immature rod precursor (iRP) populations, which were further partitioned according to their UMAP positions. *RPC-localized* iCP and iRP cells (those positioned adjacent to RPCs and MG in UMAP plots) lacked cell cycle-related gene expression, showed higher L/M cone-like (THRB) or rod-like (NRL) gene expression and regulon activities, respectively, and had RNA velocities directed toward distinct cone and rod populations (**Figure 5**). iCPs also upregulated core photoreceptor regulons OTX2 and NEUROD1 to a greater extent than iRPs (**Figure S10C**), supporting their distinct trajectories. Prior droplet-based scRNA-seq analyses have not to our knowledge distinguished immediately post-mitotic immature cone and rod precursors from the subsequent early-maturing cone and rod precursor stages.

Whereas deep full-length scRNA-seq enabled discrimination of immature cone and rod precursors, 3' scRNA-seq and snRNAs-seq enabled discrimination of the PRPC and cone- and rod-fated NRPCs [14,15,19,20] (**Figure S17A**). Combining these observations supports a model in which cone- and rod-fated NRPCs give rise to immediately post-mitotic (*i.e.*, *nascent*) and subsequent immature cone and rod precursors (iCPs and iRPs), which transition to early-maturing and then late-maturing L/M cone and rod precursors, with each state having unique gene expression and regulon properties (**Figure S17B,C**). It will be important to corroborate this model with lineage tracing, to extend the model to S cones, and to determine whether late-maturing cone and rod states in fetal retina are distinct from mature post-natal cone and rod photoreceptors at the transcription factor regulon level.

Although not identified as a distinct cluster, our analyses also revealed cone and rod precursor subpopulations that co-express rod and cone genes and regulons (**Figure 6**, 7, S11, S12, S17C). In both the current full-length scRNA-seq and a recent 3' snRNA-seq analysis[20], the earliest cone and rod precursors lacked such co-expression, implying that this property is acquired after cone versus rod fate-determination. In support of this notion, *NR2E3* RNA was detected in more mature central retina cone precursors but not in nascent peripheral cone precursors in fetal retina tissue (**Figure 7**). However, more information is needed to assess whether such co-expression serves a developmental purpose. For example, it is unknown if cone precursor *NR2E3* RNA ever produces

NR2E3 protein, as in zebrafish retina, which could suppress cone-related gene expression[57] and delay terminal differentiation. Similarly, it is unclear if the *THRB* RNA expressed in rod precursors – which is largely truncated or comprised of non-coding 3' UTR sequences (**Figure 4**) – has direct RNA effects[52].

Our characterization of cone and rod-related RNA co-expression may help resolve questions about the retinoblastoma cell of origin. Past studies suggested that retinoblastoma cells co-express RNAs associated with rods, cones, or other retinal cells due to a loss of lineage fidelity[12]. However, the early L/M cone precursors' expression of *NR2E3* and *NRL* RNAs suggest that their presence in retinoblastomas[12,13] reflects their normal expression in the L/M cone precursor cells of origin. This idea is further supported by the retinoblastoma cells' preferential expression of cone-enriched *NRL* transcript isoforms (**Figure S5B**).

Our analyses also refine understanding of gene expression in the earliest cone and rod precursors. Early cone and rod precursors shared expression of neurogenic precursor markers *ATOH7*, *DLL3*, and the new marker *CHRNA1*, albeit with higher expression of each in the cone lineage and preferential expression of *ATOH7* and *CHRNA1* in the retinal periphery (**Figures 8**, S13). *ATOH7*, *DLL3*, and *CHRNA1* RNAs persist in some maturing cone and rod precursors, whereas *CTC-378H22.2* more precisely marks iCPs. iCPs with velocity directed towards early-maturing L/M cones expressed *THRB* and *ONECUT1* RNAs and had OLIG2 regulon activity (**Figure S14**); as these elements were proposed to promote cone fate in lineage-restricted RPCs[3], their expression in iCPs suggests a similar role, such as in L/M cone fate determination, in post-mitotic cells.

We also mined gene expression differences in early cone versus rod photoreceptors to identify factors that impact human cone sensitivity to *RB1* loss[10,11]. We detected upregulation of genes targeted by MYC, some of which are similar to those targeted by MYCN[58], along with upregulated *MYCN* RNA, MYCN protein, and MYCN regulon activity. As MYCN is required for the proliferative response to pRB loss[10] and triggers retinoblastoma when amplified and overexpressed[8], these findings suggest that increased *MYCN* RNA expression and regulon activity contribute to pRB-deficient cone precursor proliferation and retinoblastoma genesis. We further found that cone precursors highly express SYK, an oncoprotein previously detected in human retinoblastomas and *RB1*-null retinal organoids but not in healthy tumor-associated retina[48,59]. The high SYK expression preceding early cone precursor maturation and its loss during late maturation implies that high-level SYK expression is a retinoblastoma cell-of-origin-specific feature. Moreover, the pRB-depleted cone precursors' sensitivity to a SYK inhibitor suggests that native SYK expression rather than *de novo* induction contributes to the cone precursors' initial proliferation (**Figure 10H**), although genetic ablation of *SYK* is needed to confirm this notion.

In summary, through deep, full-length RNA sequencing, we identified photoreceptor cell type-specific differences in transcript isoform expression and post-mitotic photoreceptor precursor states with distinctive gene expression and regulon activities. The discrimination of these states enabled the identification of developmental stage-specific cone precursor features associated with the cone precursors' predisposition to form retinoblastoma tumors.

Materials and Methods

Primary human tissue

Human fetal samples were provided by Advanced Bioscience Resources, Inc., Alameda, CA, or collected under Institutional Review Board approval at the University of Southern California (protocol HS-13-00399), and Children's Hospital Los Angeles (protocol CHLA-14-00122). Following the patient decision for pregnancy termination, patients were offered the option of donation of the products of conception for research purposes, and those that agreed signed an informed consent. This did not alter the choice of termination procedure, and the products of conception from those who declined participation were disposed of in a standard fashion. Fetal age was determined according to the American College of Obstetrics and Gynecology guidelines[60]. Each retina subjected to sequencing was from a different donor.

Retinal dissociation and RNA-sequencing

Single cell isolation

Retinae were dissected while submerged in ice-cold phosphate-buffered saline (PBS) and dissociated as described[10]. Briefly, retina was removed and placed in 200 µl Earle's balanced salt solution (EBSS) in a 6-well plate on ice. 2 ml of 10 u/ml papain (Worthington LK003176) solution was added and then incubated at 37°C for 10 min, followed by pipetting with a 1000 µl pipet tip to break up large pieces and additional 5 min incubations until cells were dissociated to single cell level. An additional 1-2 ml papain was added after 20 min if dissociation was insufficient (~40 min total). Retina culture media [Iscove's Modified Dulbecco's Medium with glutamine (Corning, #12440046), 10% fetal bovine serum (FBS, FB-01, Omega Scientific), 0.28 U/mL insulin (Eli Lilly NDC 0002-0213-01), 55 µM β-mercaptoethanol (Fisher Scientific, # 21985023), penicillin and streptomycin] (Fisher Scientific, # MT30002CI) was used to stop enzyme activity and cells were centrifuged in 14 ml round bottom tubes at 300 x g, 4°C for 10 min. Supernatants were centrifuged at 1100 x g for an additional 3 min. After resuspension in Hank's balanced salt solution (Fisher Scientific, 14025092), a 10 µl volume of cells was combined with 10 µl trypan blue and counted using a hemocytometer.

FACS isolation of single cells and cDNA synthesis

Single cells were FACS-isolated as described[10] with differences as follows. Dissociated cells were centrifuged and resuspended in a 5% fetal bovine serum in PBS (FBS/PBS) with CD133-PE (Miltenyi Biotec 130-113-108), CD44-FITC (BD Pharmingen 555478) and CD49b-FITC antibodies (BD Pharmingen 555498) to a final concentration of 10,000 cells/µl. After incubation at room temperature (RT) for 1 h, samples were diluted in 5% FBS/PBS, centrifuged as above, and resuspended in 300-400 µl 1% FBS/PBS containing 10 µg/ml 4',6-diamidino-2-phenylindole (DAPI). Single cells were sorted on a BD FACSAria I at 4°C using 100 µm nozzle in single-cell mode into each of eight 1.2 µl lysis buffer droplets on parafilm-covered glass slides, with droplets positioned over pre-defined marks (S. Lee et al., *in preparation*). Gating removed low forward- and side-scatter cells before collecting a CD133-high, CD44/49b-low population. Upon collection of eight cells per slide, droplets were transferred to individual low-retention PCR tubes (eight tubes per strip) (Bioplastics K69901, B57801) pre-cooled on ice to minimize evaporation. The process was repeated with a fresh piece of parafilm for up to 12 rounds to collect 96 cells. cDNA was prepared and amplified using the SMART-Seq V4 Ultra Low Input RNA Kit (Takara Bio 634891) in 10x reduced volume reactions using a Mantis liquid handling system (S. Lee et al., *in preparation*). Samples

were stored at -20°C until quantitation and library preparation. All RNA/cDNA volumes during FACS and processing were handled using low retention siliconized pipette tips (VWR 53503-800, 535093-794).

C1 isolation of single cells and cDNA synthesis

Dissociated cells were FACS isolated as above and collected into a single 1.5 ml tube. Cells were centrifuged and resuspended at 400-800 cells/µl, combined with C1 suspension reagent, and loaded onto the C1 chip and imaged at each site to define cell number in each well. cDNA was synthesized using SMARTer chemistry (SMARTer Ultra Low RNA Kit for the Fluidigm C1 System, Clontech 634835/634935) (three retinae, Seq 1, FW17 and FW13-1), or SMART-Seq V4 (all others). Final cDNA was harvested into low-retention tube strips and stored at -20°C.

Quality control, library preparation and sequencing

DNA was quantitated using Quant-iT PicoGreen dsDNA assay (Life Technologies, P11496) and quality checked by Bioanalyzer. Libraries > 0.05 ng/µl were prepared using the Nextera XT DNA Library Preparation Kit (Illumina, FC-131-1096) and sequenced on the Illumina NextSeq 500 (2x75) (Seq 1) or on Illumina HiSeq 4000 (2x75) (all others).

5’ and 3’ RACE and nanopore sequencing

1 µl of amplified single cell cDNAs libraries produced as above (23 ER cells, 21 LM cells, and 5 LR cells) were re-amplified using the 5’ PCR Primer II A (described for Clontech SmartSeq V4 and purchased from Integrated DNA Technologies) and using CloneAmp HiFi PCR Premix (Clontech Laboratories, Inc. Takara Bio #639298) (Table S9) by heating to 98°C x 2 min followed by 20 cycles of 98°C x 10 s, 65 °C x 15 s, and 72 °C x 35 s, followed by 72 °C x 5 min. Re-amplified cDNAs were quantified using Qubit^{TM} Flex Fluorometer (InVitrogen) and 50 pg of each re-amplified library was used for separate RACE PCR reactions with gene-specific *NRL, RXRγ, TRβ1 and TRβ2* primers and universal 5’ RACE and 3’RACE primers (Table S9) using CloneAmp HiFi PCR Premix by heating to 98°C x 2 min followed by 30 cycles of 98°C x 10 s, 60 °C x 15 s, and 72 °C x 35 s, followed by 72 °C x 5 min. The “5’ RACE primer for SmartSeq cDNA” sequence (5’–AAGCAGTGGTATCAACGCAGAGTACGGG–3’) was based on the SMART-Seq V4 SMARTer II A oligonucleotide (5’– AAGCAGTGGTATCAACGCAGAGTACXXXXX–3’) after library sequencing revealed that AAGCAGTGGTATCAACGCAGAGTAC was most often followed by GGGNN. The “3’ RACE primer for SmartSeq cDNA” sequence (5’- AAGCAGTGGTATCAACGCAGAGTACTTTT-3’ was based on the SMART-Seq V4 3’ SMART CDS Primer II A (5’– AAGCAGTGGTATCAACGCAGAGTACT(30)(N-1)N–3’) but with only four Ts at the 3’ end. Equal volumes of RACE PCR products were pooled according to cell type, and DNA concentrations of LM (32.8 ng/µl), ER (22.6 ng/µl), and LR (16.5ng/µl) samples determined using Qubit fluorometer. Long read sequencing libraries were prepared and samples barcoded using Oxford Nanopore Technology (ONT) Native Barcoding Kit 24 V14 as specified by the manufacturer for average DNA fragment lengths of ~ 2kb. 200-300ng of each DNA pool was subjected to repair/dA-tailing (End-Prep) with NEB Ultra II End-Prep Enzyme Mix (New England Biolabs, Ipswich, MA) followed by Native Barcode Ligation as specified by ONT with NB01 assigned to the ER pool, NB02 assigned to the LM pool, and NB03 assigned to the LR pool. Ligation reactions were quenched by addition of 4 µl EDTA and each reaction mixture (24 µl) pooled for a 72 µl volume. The final pool was incubated with Native Adapter (NA) and NEB Quick T4 ligase. The adapter-ligated pool was recovered by AMPure XP magnetic beads and then loaded onto a PromethION flow cell (R10.4.1) as specified by the manufacturer. Sequencing was performed on a PromethION 24 system using MinKNOW software for 72 hours. Raw FAST5 data files were converted to FASTQ files using ONT MinKNOW base calling software.

Computational Methods

Software packages used in this study are described in Table S10.

Read processing and dimensionality reduction

Adapter sequences were removed using the *trimgalore* wrapper for *Cutadapt*[61]. Trimmed FASTQ files were used as input for *HISAT2*[62] with a non-canonical splice penalty of 20, maximum and minimum penalties for mismatch of 0 and 1, and maximum and minimum penalties for soft-clipping set to 3 and 1. Aligned bam files were quantified with *StringTie*[63] and *Tximport*[64], yielding cell-by-transcript and cell-by-gene count matrices annotated according to Ensembl build 87. All analyses can be reproduced using a custom snakemake[65] workflow accessible at *https://github.com/whtns/ARMOR*.

For analysis of short-read sequencing of full-length scRNA-seq, dimensionality reduction and data visualization were performed using the Seurat (V3) toolset[66,67]. Expression counts from all sequencing datasets were integrated using Seurat's standard integration workflow. Seven sample sequencing batches were integrated after default normalization and scaling using the top 2000 most variable features in each set to identify anchor features. Normalized read counts for gene expression are reported as raw feature read counts divided by total cell read counts, then multiplied by a scaling factor of 10,000 and natural log transformed. These features of the integrated dataset were used to calculate principal component analysis (PCA) and UMAP embeddings[68,69]. A nearest-neighbors graph was constructed from the PCA embedding and clusters were identified using a Louvain algorithm at low and high resolutions (0.4 and 1.6)[70]. Read coverage plots for genes of interest were generated using *wiggleplotr*[71] to visualize BigWig files with ENSEMBL isoforms. Individual exon counts were identified using *DEXseq*[72], which takes exons from available isoforms and bins them into intervals before assigning any read counts that overlap a bin to that same bin. These counts were normalized for length for calculation of fold change or relative difference of exon use. Reads crossing target splice donor sites were evaluated as spliced or unspliced from BAM files to determine intron readthrough.

For analysis of 3' snRNA-seq, processed data provided with Zuo *et al*[20] (CZ CELLxGENE Discover with accession code 5900dda8-2dc3-4770-b604084eac1c2c82) was downloaded as a Seurat Object. A pre-processed AnnData object containing inferred NRPC fate annotations was generously provided by Dr. Rui Chen, cone and rod fated NRPC annotations were transferred to the primary Seurat Object, and data visualization was performed using the Seurat (V5) toolset[66,67].

Analysis of long-read sequencing data was performed with the nf-core nanoseq version 3.1.0 pipeline[73] (*https://nf-co.re/nanoseq/3.1.0*). Quality control on raw reads was conducted using FastQC. Reads were aligned using minimap2[74]. SAM files were converted to coordinate-sorted BAM files and mapping metrics were obtained using SAMtools. bigWig coverage tracks were created for visualization using BEDTools and bedGraphToBigWig. bigBed coverage tracks were created using BEDTools and bedToBigBed. Transcripts were reconstructed and quantified using bambu. Quality control results for raw reads and alignment results were presented using MultiQC. All reads whose ends overlapped gene-specific RACE primers were displayed and quantitated using the Integrated Genome Browser (IGV). For *THRB* 3' RACE reactions, reads inferred to initiate through exonic internal oligo(dT) priming were removed based on the following features adjacent to the 3' end of the alignments: six continuous adenines (As), more than seven As in a 10 nucleotide window, AG-runs of six or more nucleotides, eight or more As or Gs in a 10 nucleotide window, eight or more As or high A/T content (27 out of 30 bases), or 12 or more adenines present in an 18 nt window[75]. The proportion of alternative *NRL* exon 2 splicing was calculated based on the maximum read coverage between the exon 2 splice acceptor and the first splice donor and the minimum coverage after the internal splice donor as reported in IGV.

Differential expression and overrepresentation analyses

Marker features for each cluster were identified using the Wilcoxon-rank sum tests and specificity scores were computed using the *genesorteR*[76] R package. Only genes with an adjusted p-value (pAdj) <0.05 were considered for further analyses. Differential expression analysis of full-length scRNA-seq was performed using the Seurat FindMarkers function with the Wilcoxon-rank sum test on log-normalized counts. Results were displayed as volcano plots made with *EnhancedVolcano*[77]. Differential expression analysis of a 3' snRNA-seq was performed using the Seurat FindMarkers function with the Wilcoxon-rank sum test on log-normalized counts. Results were displayed as volcano plots made with *EnhancedVolcano*[77].

Overrepresentation analyses were performed with WebGestalt[78]. Analyses were run with the default settings (5-2000 genes per category, Benjamini-Hochberg multiple-testing correction), gene list enrichment was compared to the genome reference set and ontologies were displayed with a false discovery rate (FDR) <0.05 and 'weighted set cover' redundancy reduction. All gene sets evaluated were provided within WebGestalt and the same three were used unless otherwise indicated: GO – Biological Process, KEGG, and Hallmark50.

Transcription factor regulons

Transcription factor regulons were identified using pySCENIC, the python-based implementation of Single-Cell Regulatory Network Inference and Clustering (SCENIC)[30,79]. The tool was run using the basic settings as shown (*https://pyscenic.readthedocs.io/en/latest/tutorial.html*). Initial filtering required a gene to have a minimum of 3 raw counts in 1% of cells to be considered for inclusion in a regulon. AUC scores were z-score normalized for comparison between regulons.

Trajectory analysis

RNA velocity analysis was performed with R package *velocyto*[39]. Spliced and unspliced count matrices were assembled using the run_smartseq2 subcommand with repeat-masked ENSEMBL build 87. RNA velocity was calculated using cell kNN pooling with a gamma fit based on a 95% quantile and velocities were overlaid on integrated UMAP visualizations using *velocyto*. Pseudotemporal trajectories were calculated using Monocle 3[80]. The SeuratWrappers package provided integration between Seurat's final integrated dimensional reduction and Monocle. The data was subset to include only cone-directed iCPs and L/M cones, then a principal graph was fit across the UMAP plot and a 'root cell' chosen to represent the latest maturation point in the *OPN1LW*+ late-maturing cone group. After assigning pseudotime values to each cell, genes that significantly changed as a function of pseudotime were identified and those with a correlation q-value of <0.05 with expression > 0.5 in at least 5% of the cells present in the pseudotime were grouped into modules of co-regulation by performing UMAP and Louvain community analysis.

Histology

Fixation and cryosectioning of fetal retina

Retinae were procured and dissected in cold 1x PBS. The cornea and lens were removed with a cut around the limbus of the iris leaving the front of the eye open. The tissue was submerged in ~25 ml of 4% paraformaldehyde (PFA) in 1x TBS and placed at 4°C on a rocker at low speed for ~16-18 hrs. The tissue was washed 3 times with 1x PBS before incubation in 30% sucrose [sucrose + 1x PBS] overnight at 4°C. A mold was made by cutting off the top 5 ml of a 50 ml conical tube and placed on dry ice. A solution of 1:2 OCT Compound:30% sucrose was mixed and centrifuged to remove bubbles. The mold was partially filled before adding the dissected eye and then covering fully. 10 µm frozen sections were cut at ~-24°C with the front of the eye facing side on to the blade.

Explanted retinae were fixed for 15 min in 4% PFA, washed with 1x PBS, incubated in 30% sucrose for 15 min, after which the membrane was cut from its frame and transferred to a mold containing 1:2 OCT:30% sucrose and frozen.

Immunohistochemical staining

For SYK and ARR3 co-staining, tissue sections were warmed at RT until dry and then washed in Coplin jars twice with 1x PBS for 5 min at RT. Samples were permeabilized in 1x PBS-T for 5 min, washed again in 1x PBS twice for 5 min, blocked for 1 hr in blocking solution [1x PBS, 0.1% Triton X-100, 5% normal donkey serum, 5% normal horse serum]. Primary mouse anti-SYK and rabbit anti-ARR3 (LUMIF-hCAR) antibodies were mixed in blocking solution and applied to samples overnight (16-18 h) at 4°C. Slides were washed three times with 1x PBS for 10 min each, probed with secondary antibodies (Key Resources Table) in blocking solution for 1 hr at RT, washed twice 1x PBS for 15 min each, incubated in1x PBS containing 10 µg/ml DAPI for 10 min, and mounted with Mowiol solution. Additional immunohistological staining of tissue sections and cells on coverslips was performed as described[11] but without initial EDTA wash.

Combined in situ hybridization and immunohistological staining

Human retinal sections were prepared as above but using RNase-free reagents for all stages (PBS, TBS) and ultrapure sucrose (JT Baker, 4097-04) and cryostats cleaned with ELIMINase (Decon Labs, Inc) and 70% ethanol prior to use. RNA FISH hybridization chain reaction probes were designed by and obtained from Molecular Instruments, Inc, with 20 20-bp single strand DNA probes per target RNA sequence except Tr-NRL exon 1 (4 probes), FL-NRL exons 1 and (8 probes), and *HOTAIRM1* (14 probes). The accession numbers for target sequences are shown in Table S11, except for *RP13-143G15.4* which included regions of several isoforms for maximum gene coverage. The *in situ* protocol was performed with fluorescent hairpins and buffers from Molecular Instruments using the manufacturer's instructions for mammalian cells on a slide (*https://files.molecularinstruments.com/MI-Protocol-RNAFISH-MammalianCellSlide-Rev7.pdf*), beginning with a 4% PFA treatment after thawing and drying slides at RT for 10 min, with the following changes: samples were incubated in 70% ethanol overnight in a Coplin jar, probes were added to the final hybridization volume at 4x the recommended concentration for tissue sections (2.4 pmol in 150 µl of hybridization buffer), tissues were pre-hybridized at 42°C and then lowered to 37°C once probes were added, and hairpins were used at a volume of 1 µl (6 pmol) in 50 µl amplification buffer per section. After removing amplification solution and washing, samples were directly used in the immunofluorescence protocol. Briefly, samples were blocked in a basic RNase-free solution (1% BSA, 0.1% Triton X-100, 0.05% Tween-20 in PBS) for 1 hr and primary antibodies mixed in blocking solution and applied to samples overnight at 4°C. Samples were washed three times for 10 min with 1x PBS, then incubated with secondary antibodies in blocking solution for 40 min at RT. Samples were washed as above with DAPI in the third and final wash, and mounted with Mowiol before imaging using a Leica STELLARIS 5 inverted confocal microscope. For *GNAT2* and *NR2E3* FISH, samples were washed with DAPI in the third and final wash, mounted and then imaged as above. After this first imaging, coverslips were removed, and slides were washed in PBS and then used in the immunofluorescence protocol with an alternate blocking solution) (2.5% Horse, donkey, human sera, 1% BSA, 0.1% Triton X-100, 0.05% Tween-20 in TBS).

Quantitation of FISH

For *NRL*, *CHRNA1*, and lncRNAs, QuPath[81] was used to identify nuclei, predict cell expansion, classify cells, and count FISH puncta. Apical retina regions containing RXRγ+ and/or NRL+ cells were visually selected for evaluation. The StarDist extension[82] was used to outline nuclei and cell expansion zones with deep learning model '*dsb2018_heavy_augment.pb*' on the DAPI image channel (threshold = 0.6, pixelSize = 0.15). Model results were reviewed and cells with partial, multiple, or overlapping nuclei removed from consideration. FISH puncta were thresholded then output, using the subcellular detection function (expected spot size = 0.5 µm^2, min spot size = 0.2

μm^2, max spot size = 0.7 μm^2 (*NRL* isoforms) or 1 μm^2 (*CHRNA1* and lncRNAs) to capture the most puncta above background. Image positions were determined by tracing the retina apical edge with line segments in FIJI, identifying the closest point on the line to the midpoint of each image, then measuring the distance from the line starting position. For *GNAT2* and *NR2E3* FISH, images were analyzed in FIJI. The outer layer of cells was delimited manually based on the RXRγ+ cells and the number of RXRγ+ and/or *GNAT2*+ and/or *NR2E3*+ cells were manually counted, examining each color channel separately. For the inner layer, the number of *NR2E3* RNA positive cells and NR2E3 protein positive cells were counted.

NRL isoform analyses

Proteasome inhibition of CHLA-VC-RB-31

10^6 CHLA-VC-RB-31 cells[37] were cultured in 2 ml retina culture medium in a 24-well plate with or without 10 μM retinoic acid (Cayman Chemical 11017) and incubated at 37°C in 5% CO2. MG132 (Sigma-Aldrich 474790) was added at 23 h to a final concentration of 10 μM and cells incubated for 4 h. Cells were collected and centrifuged at 300 x g for 4 min, resuspended in 60 μl cold 1x RIPA buffer (Millipore 20-188), 10% sodium dodecyl sulfate (SDS), protease and phosphatase inhibitors diluted per manufacturer instructions (Sigma-Aldrich 5892970001, 4906837001)], incubated on ice for 30 min, then centrifuged at 4°C for 20 min at 14,000 RPM. 15 μl of supernatant were mixed with 3 μl 6X sample buffer (300 mM Tris, 60% glycerol,12% SDS, 86 mM B-mercaptoethanol, 0.6 mg/ml bromophenol blue), heated to 95°C for 5 min, and separated on a 4-12% Bis-Tris gel (Invitrogen, NP0321) using 1xMOPS running buffer (Life Technologies NP0001). Protein was wet transferred to a PVDF membrane in Towbin transfer buffer (25 mM Tris, 192 mM glycine pH 8.3,10% methanol) at 20 V ON at RT. The membrane was blocked in 1xTBS-T containing 5% w/v nonfat dry milk for 1 hr, washed with TBS-T three times for 5 min, incubated overnight in 0.1% dry milk TBS-T solution containing primary antibody at 4°C with slow rocking, washed three times for 15 min in TBS-T, incubated with HRP-conjugated secondary antibody for 1 hr at RT in the 0.1% milk solution, washed six times for 15 min, incubated in chemiluminescent substrate (Thermo Fisher, 34094) and imaged.

NRL isoform and reporter constructs

The pcDNA4-His-Max-C-Nrl[83] (gift of A. Swaroop) CMV promoter was replaced with EF1α promoter to produce pcDNA4-His-Max-C-EF1α-FL-NRL. Using In-Fusion (Takara Bio) the His-Max tag was removed to produce full-length NRL expression plasmid pCDNA4-C-EF1α-FL-NRL (primers #1,2). The His-Max tag plus first 417 bp of NRL N-terminal coding sequence were removed to produce truncated NRL expression plasmid pCDNA4-C-EF1α-Tr-NRL (primers #1,2,3,4). pcDNA4-C-EF1α-empty transfection carrier plasmid was made by removing NRL coding sequence from pCDNA4-C-EF1α-Fl-NRL (primers #5,6). pGL3-PDE6B-146-luc was produced by amplifying a 146 bp promoter region of *PDE6B*[84] from H9 hESC genomic DNA and inserting into a pGL3-SV40 (Promega, primers #7,8), then removing the SV40 promoter (primers #9,10) to generate pGL3-PDE6B-146. The promoter-less pGL3-empty was produced by removing SV40 sequences from pGL3-SV40 (primers #9,11). pUltra-EGFP-P2A-Tr-NRL was produced by amplification of NRL coding sequence from pcDNA4-C-EF1α-FL-NRL and inserting into BamHI digested pUltra-EGFP (Addgene 24129) (primers #12, 13). All primers are listed in the Key Resources Table.

3NRL expression and analysis

pcDNA4-C-EF1α-NRL constructs were transfected into HEK293T cells. 4 μg plasmid in 1 ml DMEM (Life Technologies, 10313039) was combined with 1 ml DMEM + 12 μg polyethylenimine (PEI MAX) (MW 40,000, Polysciences 24765-1) and combined with 10^6 trypsinized HEK293T cells, plated into two wells of a 6-well plate with an additional 1 ml of DMEM + 10% FBS, then cultured overnight in a 37°C incubator. Media was replaced with fresh 293T media the next day and after two additional

days cells were collected, lysed, and protein quantitated via BCA assay (Thermo Scientific PI23227). 30 µg of each well was used for western blot as above, with membranes probed with antibody raised against the NRL N-terminus (Santa Cruz SC-374277) or against full-length NRL (R&D AF2945).

Luciferase assays

575 ng of total DNA (50 ng reporter, 100ng FL-NRL and/or 100-300 ng Tr-NRL expression vector, and the remainder pcDNA4-C-EF1α empty vector) in 5 µl DMEM was mixed with 2.3 µg PEI in another 5 µl DMEM (per condition, in triplicate) and then plated into one well of a white bottom 96-well cell culture plate with 50,000 NIH3T3 cells in 100 µl 293T media. The luciferase assay was carried out 48 h after transfection with the Nano-Glo Dual-Luciferase Reporter Assay System (Promega N1610) per manufacturer instructions. Luminescence was recorded using the Promega Glomax Multi+ Detection System.

Truncated NRL overexpression in fetal retina

Concentrated pUltra-EGFP-NRL-205 and control pUltra-EGFP lentivirus were produced as described[85]. At 16-24 h after 293T transfection in 15 cm dishes, media was exchanged for 20 ml UltraCULTURE (Lonza Inc., BP12-725F) containing 1% HEPES (Sigma, 0887), 1% GlutaMax (Life Technologies 35050061), and 1% Penicillin-Streptomycin (Fisher Scientific, MT30002CI). After 60-64 h, media was harvested, centrifuged at 3000 x g for 10 min at 4°C, filtered through 0.45 µm PVDF flask filter, concentrated via tangential flow filtration using a MidiKros 20 cm 500 KD 0.5 mm column (D02-5500-05-S), with both input and final supernatant containers kept in ice. The concentrate was re-filtered using a 0.45 µm PVDF syringe filter (Millipore), stored in aliquots at -80°C, and titered using a p24 ELISA kit (ZeptoMetrix 801002).

As described[11], fetal eyes were washed in 70% ethanol, washed three times in 1x sterile PBS, and dissected in cold 1x PBS. The cornea was removed and tissue cut ~one-third of the distance towards the posterior pole along 4 lines approximately equidistant and between attached tendons. The retina was removed in this flattened state after cutting the optic nerve, transferred to a polytetrafluoroethylene culture insert (Millipore, PICM0RG50) with photoreceptor side down, and placed in a 6-well plate with 1,200 µl retinal culture medium. Retinae were infected as described, cultured for 7 days with half media changes every other day, then fixed in 4% PFA for 15 min, washed three times in 1x PBS, equilibrated in sucrose (30% in PBS) for 15 min, and embedded and sectioned as above. Immunostaining and imaging were performed as above.

RB1 knockdown and SYK inhibitor treatment

FW18.5 retina was partially dissociated with papain, cultured overnight in retinal culture media at 37°C in a 6-well plate, then frozen in 10% DMSO solution and stored in liquid nitrogen. Samples were thawed and revived in retinal culture media overnight and infected with lentivirus carrying shRNAs targeting *RB1* (sh*RB1-733*)[10] or a scrambled control (sh*SCR*) and diluted β-mercaptoethanol, insulin, glutamine, penicillin, and streptomycin to the final retina culture medium concentrations along with 5 µg/ml Polybrene, for 24 hrs. After replacing 2/3 of media in each well with fresh media, cells were treated with GS-9876 (MedChemExpress, HY-109091) in DMSO at or with the same volume of DMSO vehicle control. After 12 d, cells were attached to poly-L-Lysine-coated coverslips for 3 h, fixed in 4% PFA for 10 min, washed in 1x PBS three times, and stored at -20°C until immunocytological staining with antibodies to Ki67, RXRγ, and GFP (for YFP staining) as described[10].

Statistical Analysis

Statistical methods and packages are cited in the Methods text and figure legends. Statistical comparison between more than two groups of cells for gene expression, regulon activity, or exon count proportions used the non-parametric Kruskal-Wallis test followed by pairwise post-hoc Dunn tests with Benjamini-Hochberg correction. Mean expression levels of *NRL* and *RXRG* isoforms across cell clusters were evaluated by Welch's t-tests for groups with unequal variance; p-values for these tests were estimated using bootstrapping with 1,000,000 replications per comparison. Changes in FISH puncta counts were examined within each channel individually using zero-inflated negative binomial regression models with robust standard error terms. Distance across the sample tissue was used to model degenerate zero inflation. P values reported in the manuscript text and legends are Wald Chi-Squared tests that evaluate differences in count between inflection points. Analyses were performed using Microsoft Excel, the R statistical language in RStudio, or Stata SE v14.2.

Supplementary Materials

Supplementary Figures

Figure S1

scRNA-seq sample and sequencing summary.

A. Retinae and cell numbers examined at each age. **B.** Histogram of total read counts for each cell, colored by sequencing run. Seq 1 cells were isolated by C1, Seq 2 cells by FACS or C1 as indicated, and all others by FACS. Dotted line: 100,000 read cutoff for cell exclusion. **C.** Box plots of read counts, genes detected, and Ensembl transcript isoforms detected per cell ordered by fetal age and specimen number. **D-F.** UMAP plots colored by sequencing run (D), isolation method (E), or retina ID (F).

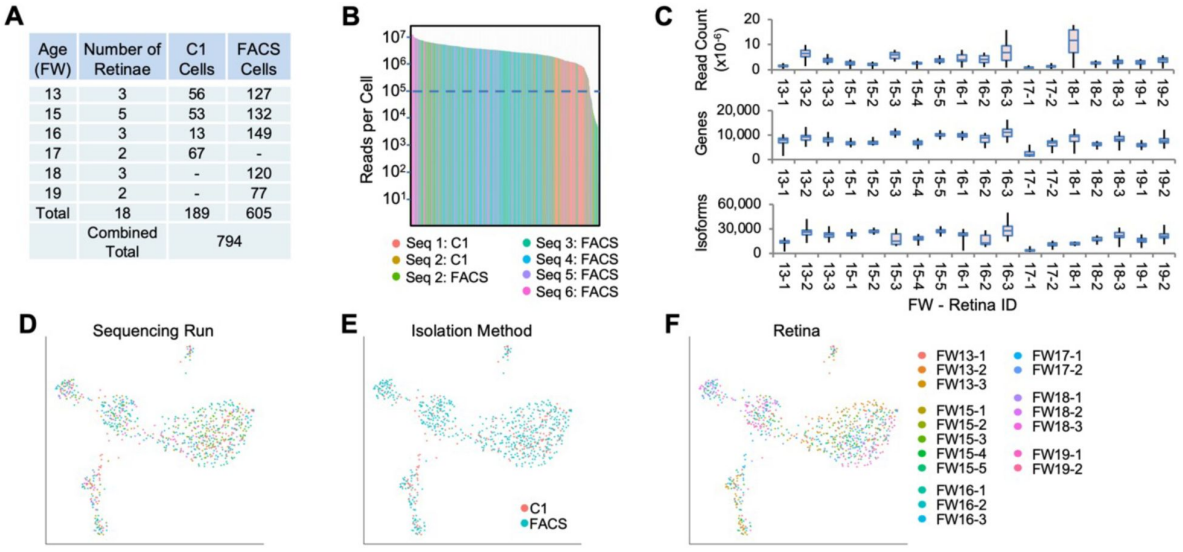

Age (FW)	Number of Retinae	C1 Cells	FACS Cells
13	3	56	127
15	5	53	132
16	3	13	149
17	2	67	-
18	3	-	120
19	2	-	77
Total	18	189	605
	Combined Total	794	

Figure S2

Expression of marker genes of RPCs and Müller glia (A), photoreceptors (B), rods (C), and cones (D).

Insets: Gene expression violin plots (from *left* to *right*): RPC/MG (red), iPRP (brown), LM cone (green), S cone (teal), early rod (blue), late rod (pink). UMAP and violin plots for any gene or Ensembl transcript can be produced at *https://docker.saban.chla.usc.edu/cobrinik/app/seuratApp/*.

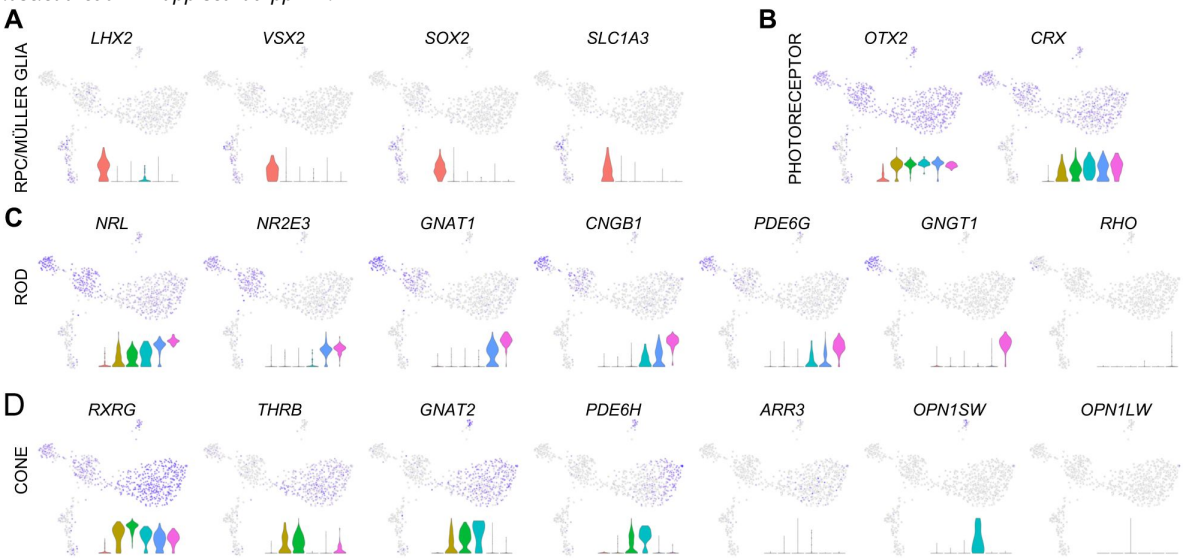

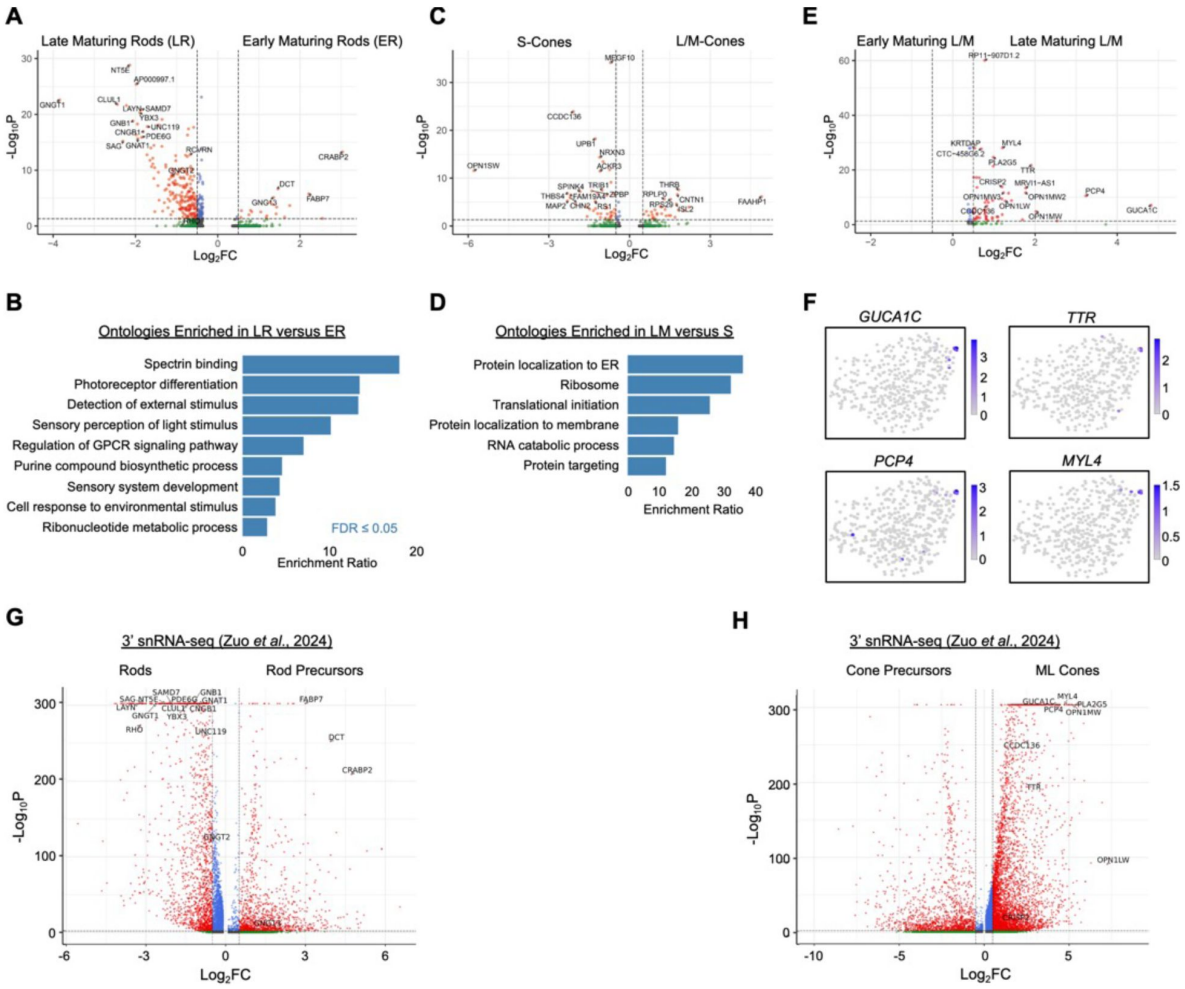

Figure S3.

Differential expression between rod and cone maturation states.

A, C, E. Volcano plots of differential expression (pAdj <0.05, log2FC >|0.5|) between ER and LR (A), LM and S (C), and spatially separated late-maturing L/M cones and remaining LM cluster (E). Labels indicate genes with highest significance and fold change. **B,D.** Overrepresentation of molecular function ontologies for genes upregulated in LR over ER (B) or upregulated in LM over S (D). **F.** UMAP plots of upregulated genes in the late-maturing L/M cone group. **G, H.** Volcano plots of differential expression (pAdj <0.01, log2FC >|0.5|) between Rod and Rod Precursor (G) and ML Cone and Cone Precursor (H) subclasses as defined **Figure S3** of Zuo *et al*[20]. Late rod- and late cone-enriched genes labeled in (A) and (E) are also labeled when present in (G) and (H).

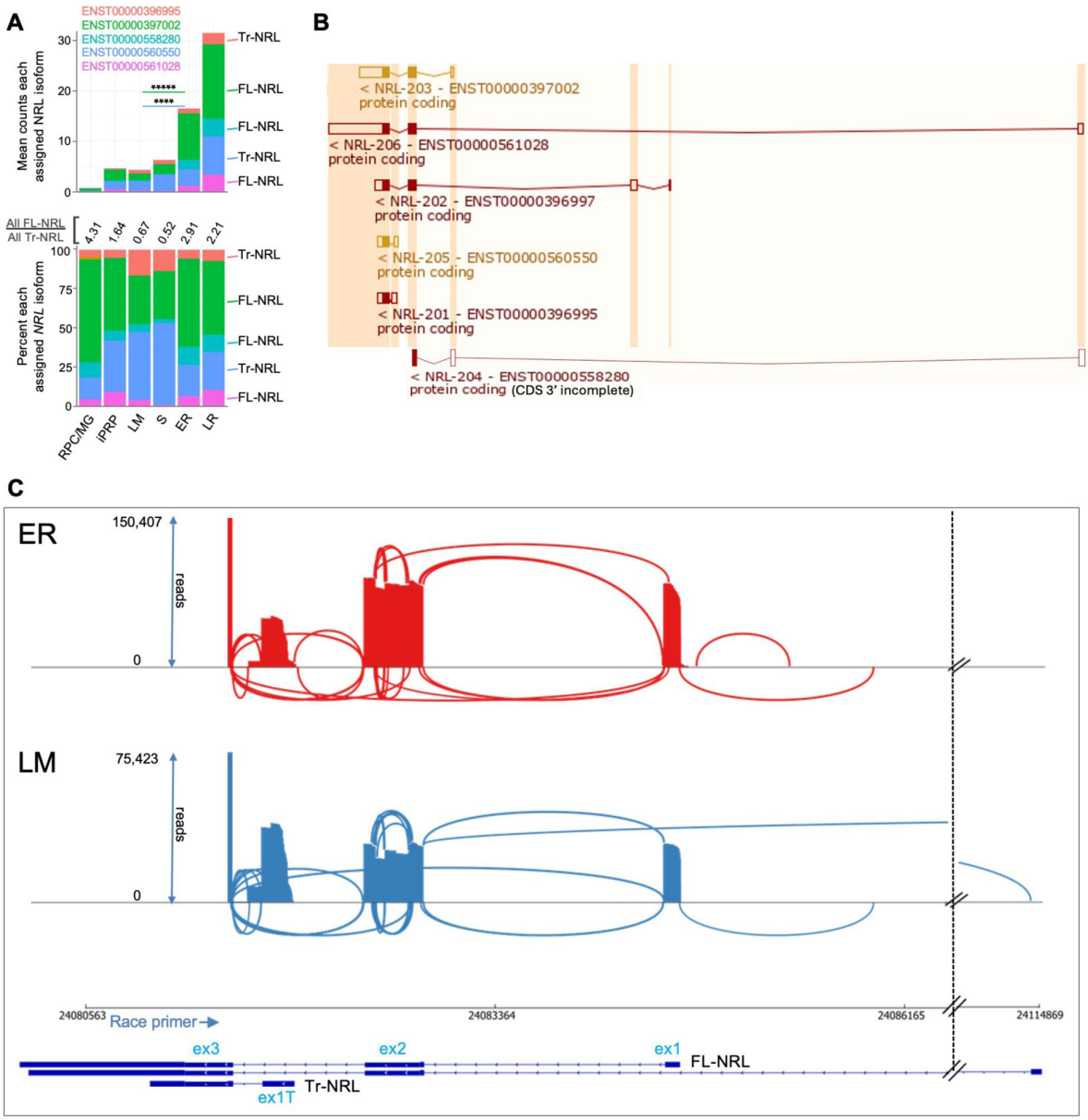

Figure S4

Differential *NRL* transcript isoform expression in early rod and cone precursors.

A. Mean *NRL* isoform counts for each cluster based on short-read full-length cDNA sequencing (*top*) and percentage of total counts (*bottom*), as in **Figure 3B**. **B.** *NRL* Ensemble isoforms. **C.** *Top:* Sashimi plots of *NRL* transcript splicing based on nanopore long read sequencing of 5' RACE reactions from 23 ER cells and 21 LM cells. The minimum number of reads required to display transcript isoforms was set at 20 for ER cells and at 10 for LM cells, proportional to the total NRL reads in each sample. *Bottom*: Exon structures of FL-NRL (*ENST00000397002*) and Tr-NRL (*ENST00000560550*) isoforms and RACE primer location. The *NRL* gene is oriented relative to chromosome 14 coordinates. Hash marks indicate sequences preceding a rarely used far upstream first exon in *ENST00000561028*. Note increased intra-exon 2 splicing and ex1T use in the LM population.

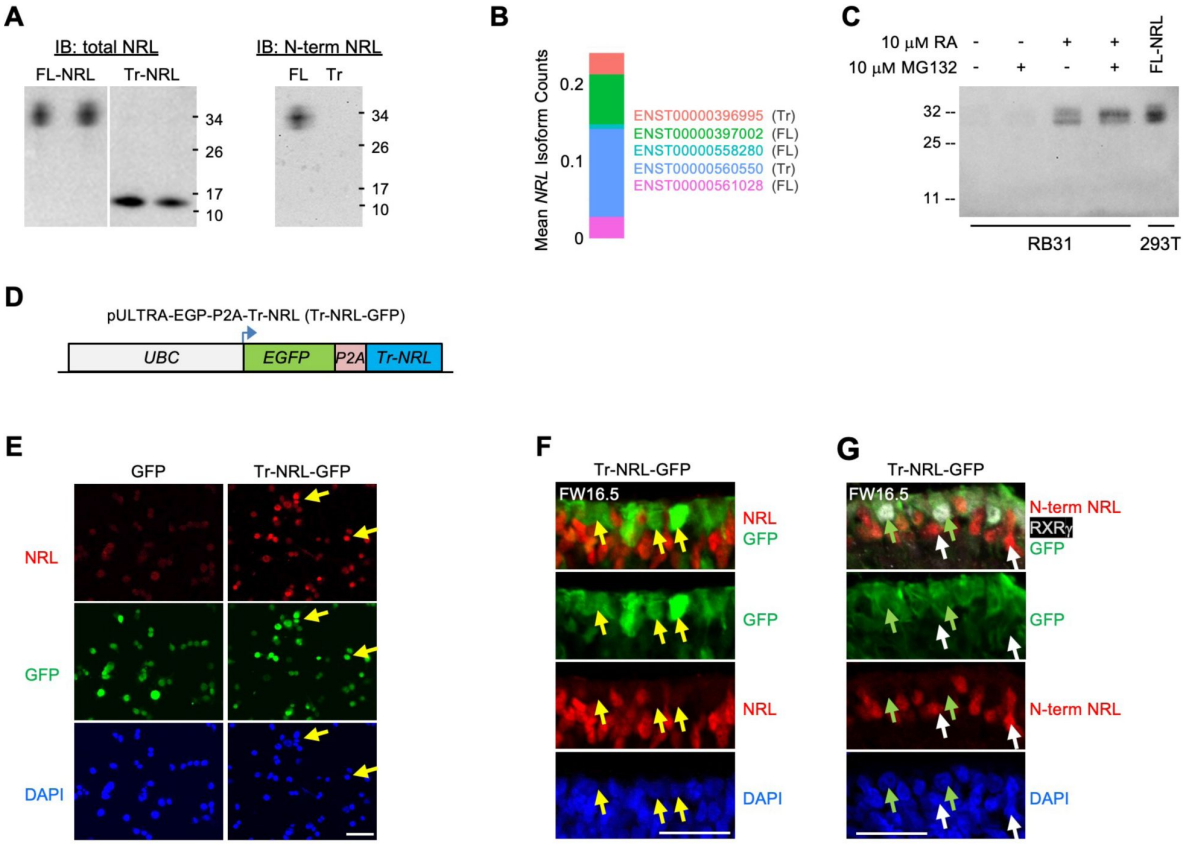

Figure S5

Cell type-specific NRL protein expression.

A. NRL antibody validation by immunoblot (IB) of ectopic FL-NRL and Tr-NRL in HEK293T. *Left:* anti-total NRL. *Right:* anti-N-terminal NRL specific to FL-NRL. **B.** Average assigned *NRL* isoform expression in scRNA-seq of RB31 retinoblastoma cell line. **C.** Immunoblot of endogenous total NRL in RB31 cells treated with or without 10 μM retinoic acid (RA) and 10 μM proteasome inhibitor MG132 and in FL-NRL transfected HEK293T. **D.** pULTRA-EGFP-P2A-Tr-NRL lentiviral vector used for explanted retina transduction. **E.** NRL Immunofluorescent staining of HEK293T cells 48 h after lentiviral transduction of Tr-NRL-GFP. Scale bar = 50 μm. **F,G.** Immunostaining of total NRL (F) or N-terminal-NRL (G) in explanted FW16.5 fetal retina 7 d after lentiviral transduction of Tr-NRL-GFP. Arrows: Yellow = GFP+, NRL-. Green = GFP+,RXRγ+. White = GFP-,FL-NRL+. Scale bar, 25 μm.

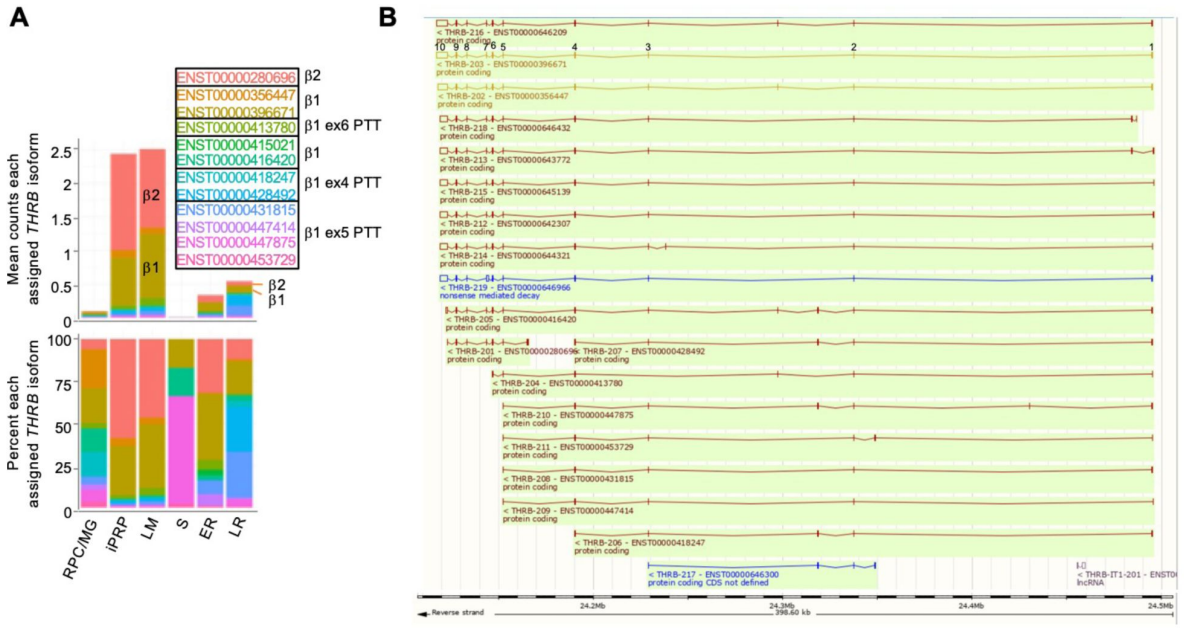

Figure S6

Differential *THRB* isoform assignments in rod and cone precursors.

A. Mean *THRB* isoform assignments for each cluster presented as total transcript counts (*top*) and percentage of total counts (*bottom*) as in **Figure 4B**, with isoforms grouped according to capacity to encode full-length canonical TRβ1 or TRβ2 or to have PTT following ex4, ex5, or ex6 (exons numbered as for *ENST00000396671*) regardless of differences in 5′ noncoding exons and 3′ poly(A) sites. **B**. *THRB* Ensemble isoforms identified in panel A with *ENST00000396671* exon numbers indicated, accessed June 22, 2024, at: *http://useast.ensembl.org/Homo_sapiens/Gene/Summary?g=ENSG00000151090;r=3:24117153-24495756*.

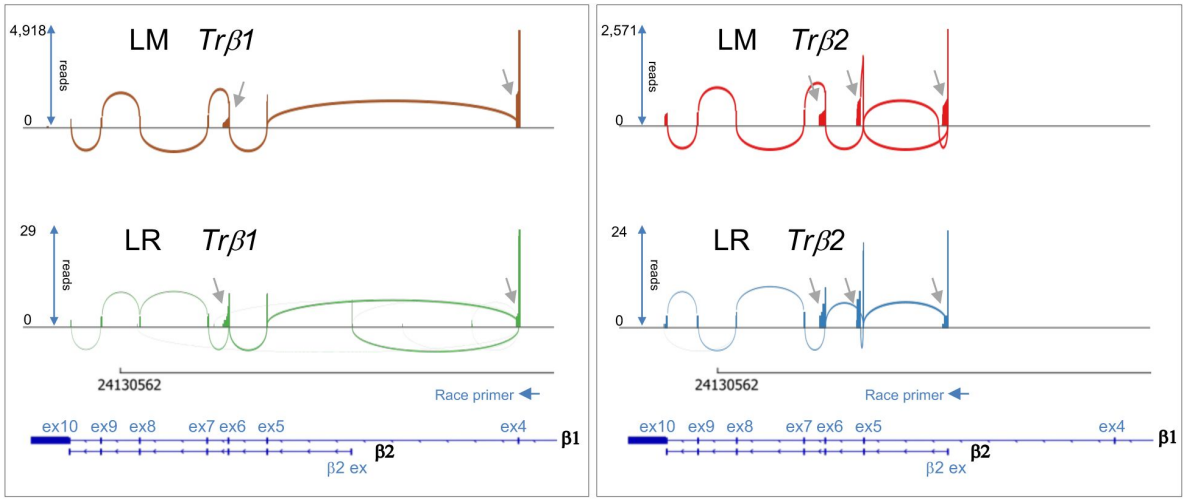

Figure S7

THRB isoforms and premature transcription termination in cone and rod precursors.

Top: Sashimi plots of *THRB* transcript splicing based on long read nanopore sequencing of 3' RACE reactions from 23 LM cells and 5 LR cells. RACE reactions were initiated from primers specific to TRβ1 exon 4 (*left*) or specific to the unique TRβ2 exon (*right*). Gray arrows: premature transcription termination following TRβ1 exon 4, the TRβ2 first exon, the shared exon 6, and a novel exon used solely in TRβ2 transcripts. *Bottom*: TRβ1 and TRβ2 exon structures and RACE primer positions. The *THRB* gene is oriented relative to chromosome 3 coordinates.

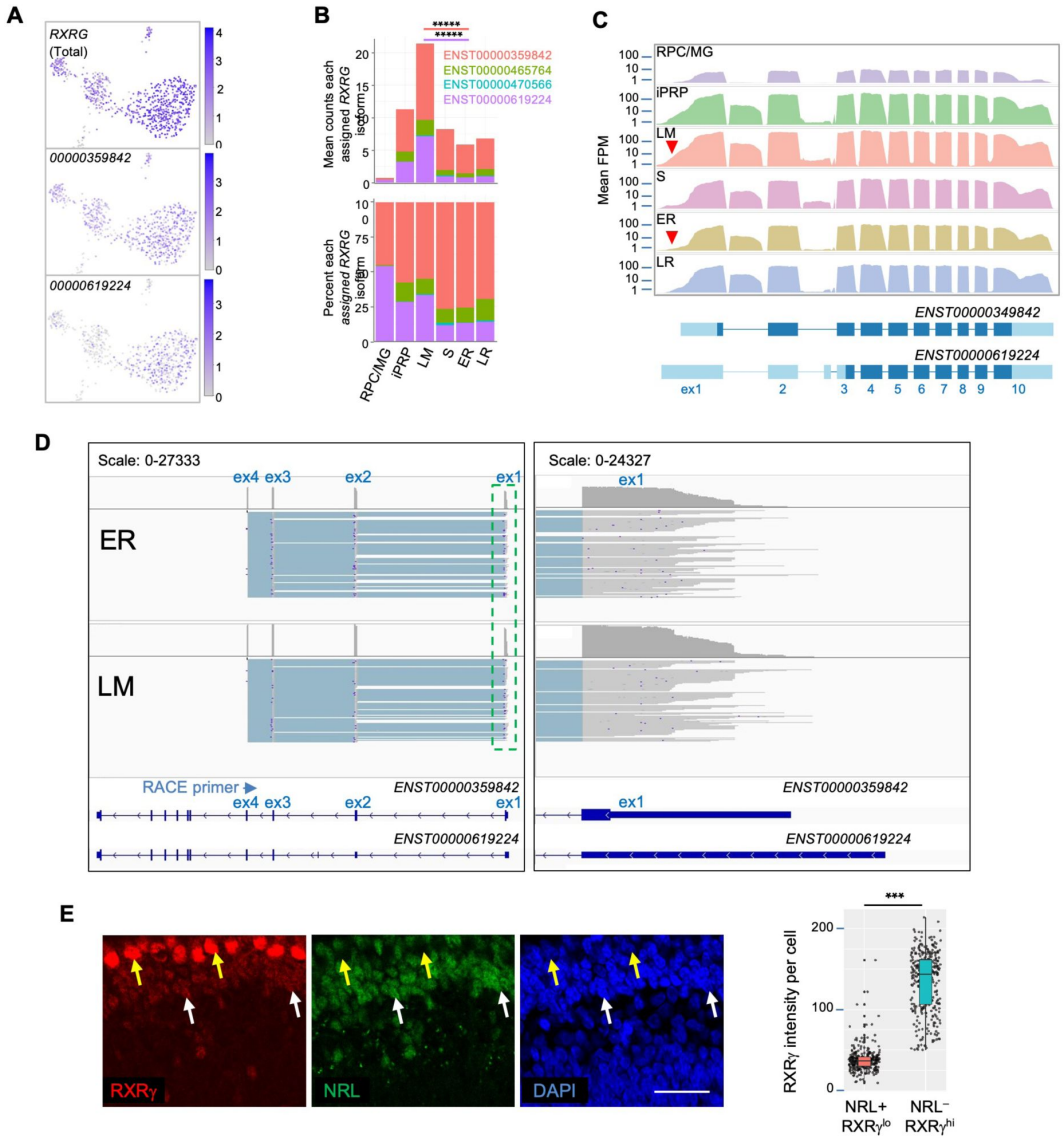

Figure S8

RXRG isoform expression in rod and cone precursors.

A. Expression of *RXRG* and the two most highly assigned *RXRG* isoforms (*ENST00000359842* and *ENST00000619224*). **B.** Mean *RXRG* isoform assignments for each cluster presented as total counts (*top*) and as a percentage of total counts (*bottom*). Lines indicate significant LM vs. ER fold change, colored by isoform. *****, p <0.000001 (bootstrapped Welch's t-test). **C.** *Top*: Mean read counts across Ensembl *RXRG* exons. *Bottom*: Structures for *ENST00000359842* and *ENST00000619224.* Red arrowheads: Extended *RXRG* 5′ UTR. **D.** Long-read nanopore sequencing of pooled 5′ RACE initiated with *RXRG* exon 4 primers from 23 ER cells (*top*) and 21 LM cells (*bottom*). Schematic shows total exon coverage (*above*) and individual transcripts (*below*). Panels at *left* show *RXRG* locus with exon 1 in green box enlarged at right, revealing a similar range of RNA 5′ ends in ER and LM populations. **E.** Immunohistochemical analysis of RXRγ and NRL in FW16 retina. Arrows: Yellow = RXRγ-high cone. White = NRL+ rod with weak RXRγ. Scale bar = 25 μm. *Right*: Boxplot of RXRγ mean grey values in NRL^{+},$RXR\gamma^{lo}$ and NRL^{-},$RXR\gamma^{hi}$ cells. ***, p<0.0001 (Welch's T-test).

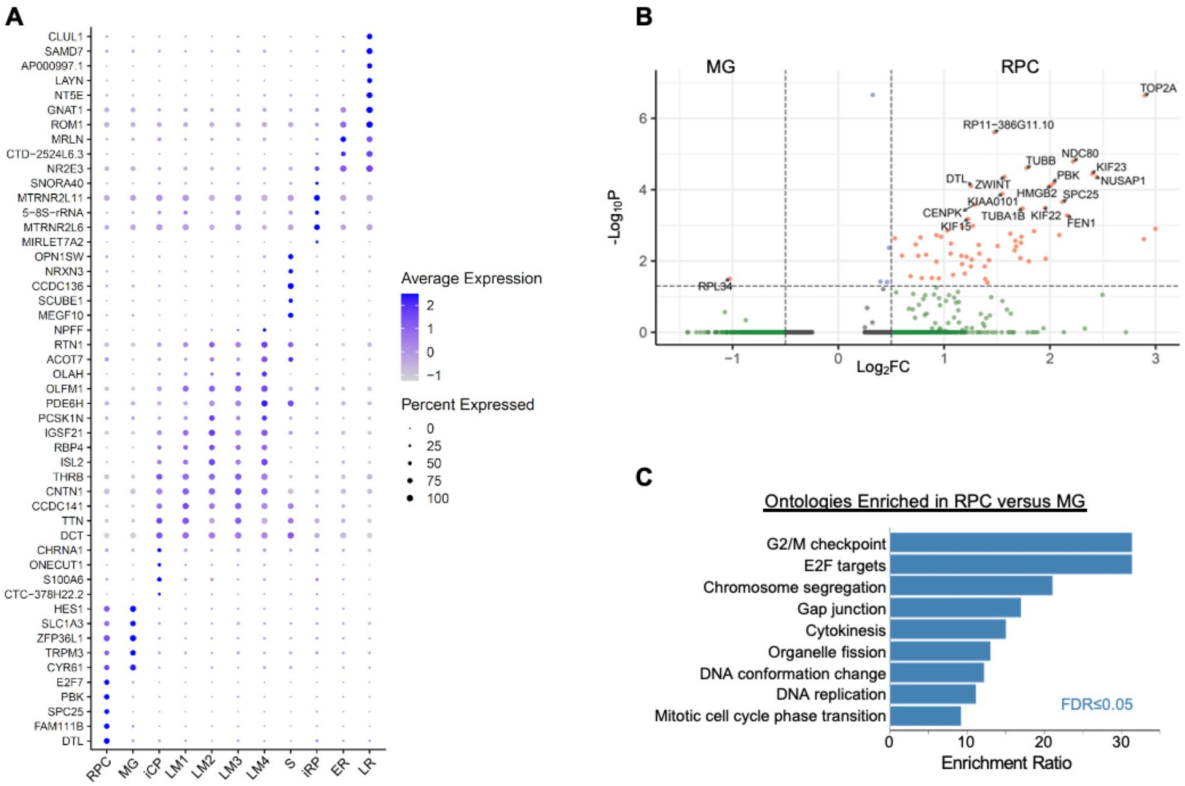

Figure S9

High resolution cluster marker genes and differential RPC versus MG gene expression.

A. Marker gene dot plot for high resolution Louvain clusters. Dot size: Percent of cells expressing gene. **B.** Volcano plot of differential expression (pAdj <0.05, log2FC >|0.5|) between MG and RPC clusters with genes labeled when p $<10^{-4}$ except for *RPL34*. **C.** Overrepresentation analysis for genes upregulated in RPC above pAdj and log2FC cutoff.

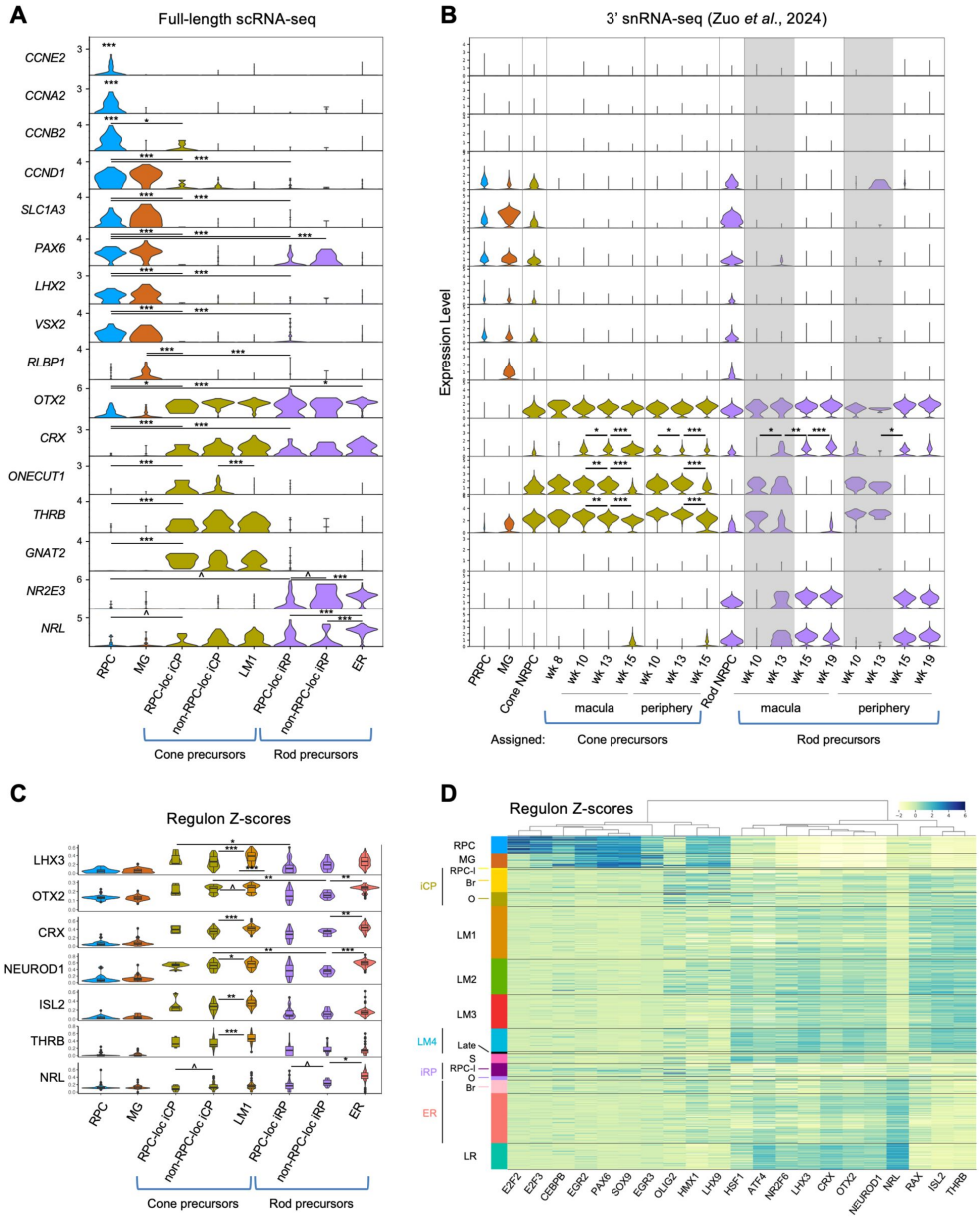

Figure S10

Immature photoreceptor precursor populations identified with deep full-length scRNA-seq and 3' snRNA-seq.

A. Violin plots based on full-length scRNA-seq depicting gene expression in RPCs, MG, RPC-localized and non-RPC-localized iCPs and iRPs, and the early maturing LM1 cone and ER clusters as designated in **Figure 5A,C**. **B.** Violin plots based on 3' snRNA-seq depicting expression of the same genes as in (A) in PRPCs, MG, cone- and rod-fated NRPCs, and cone and rod precursors at the indicated ages and macular versus peripheral retinal positions as designated in Zuo *et al,* [20]. Grey boxes = potential mixed cone plus rod precursor populations as shown in Figure S11. **C,D**. Regulon activities based on full-length scRNA-seq in high-resolution RPC and photoreceptor precursor states. **C.** Violin plot depicting selected Z-score normalized regulon activities in the indicated cell populations. Significant differences ($p<0.05$) between corresponding iCP and iRP states are indicated for pan-photoreceptor regulons LHX3, OTX2, CRX, and NEUROD1, and significant differences between successive iCP – LM1 and iRP – ER states are indicated for all regulons. Activities of all regulons except NRL also increased in RPC-localized iCPs and iRPs relative to RPCs ($p<0.05$ for all). **D.** Ward-clustered heatmap of the highest scoring SCENIC regulons in each high-resolution cluster, displaying Z-score normalized regulon activities. Subcluster labels: RPC-l = RPC-localized, Br = Bridge-localized, O = Other/remainder of original cluster, Late = late-maturing LM4 cones. ^<0.1; *, <0.05; **, <0.005; ***, <0.0005 (post-hoc Dunn test).

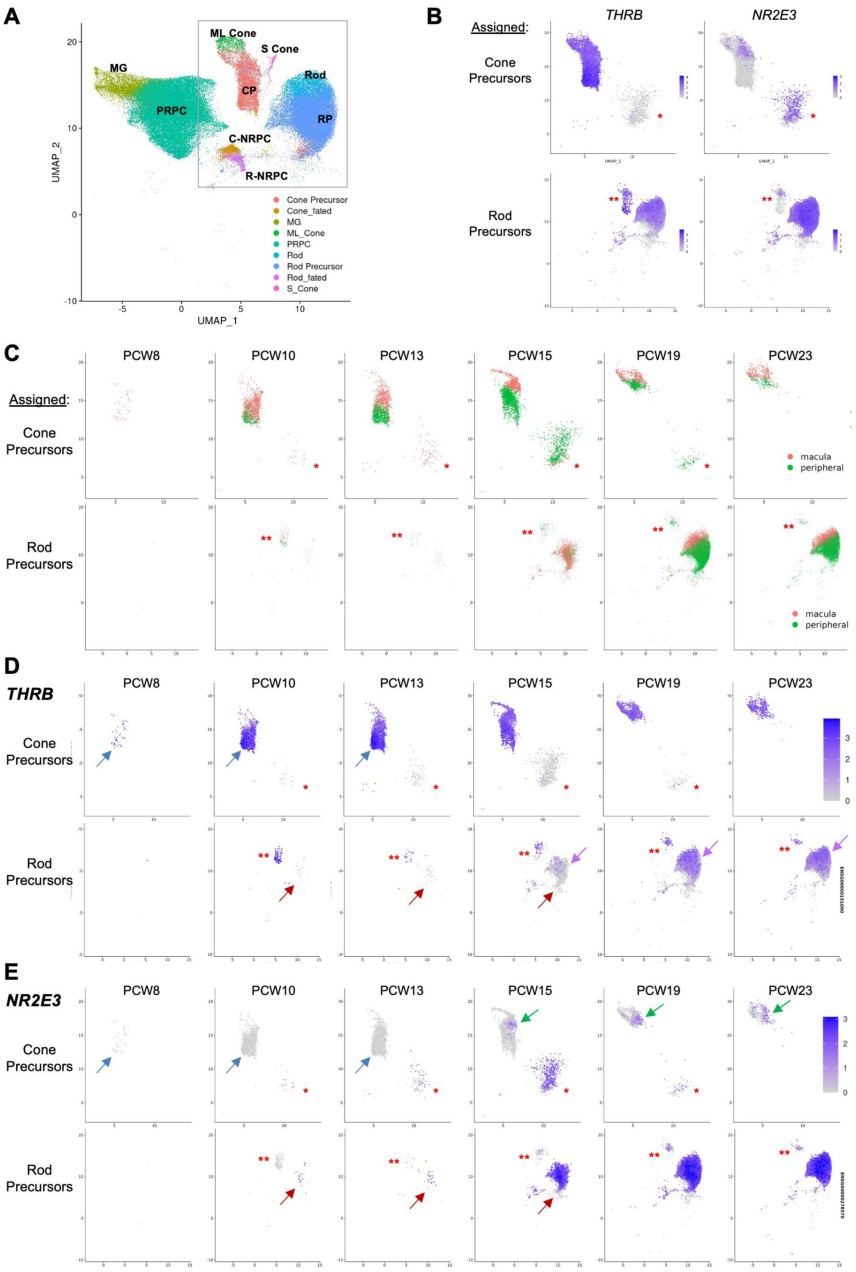

Figure S11

Cone and rod precursor cell type assignments, UMAP positions, and gene expression in a large 3' snRNA-seq analysis.

A. UMAP positions of cell populations as assigned in Zuo et al,[20]. MG = Muller glia; PRPC = primary retinal progenitor cells; C- and R-NRPC = cone and rod neurogenic retinal progenitor cells, CP = cone precursor, RP = rod precursor. Box = region enlarged in Cone Precursor UMAP plots in panels B-F. **B**. Expression of *THRB* and *NR2E3* overlaying UMAP plots of pcw 8-23 cone or rod precursors. ***** = possible rod precursors mis-assigned as cone precursors based on UMAP position, high *NR2E3*, and minimal *THRB*. ****** = possible cone precursors mis-assigned as rod precursors based on UMAP position, high *THRB*, and low *NR2E3*. **C**. UMAP plots of assigned cone and rod precursors in macula (orange) and peripheral retina (green) at each age. **D-F.** Expression of *THRB* (**D**), *NR2E3* (**E**), and *GNAT2* (**F**) overlaying UMAP plots of assigned cone or rod precursors at each age. Blue arrows = major cone precursor population at pcw 8, 10, 13 expressing *THRB* but not *NR2E3*. Red arrows = major rod precursor population at pcw 10, 13, 15 expressing *NR2E3* but not *THRB*. Purple arrows = later rod precursors with *THRB* co-expression at pcw 15, 19, 23. Green arrows = later cone precursors with *NR2E3* co-expression at pcw 15, 19, 23. Scale bars at right apply to all plots in each panel. Asterisks in **C-F** are as in panel **B**.

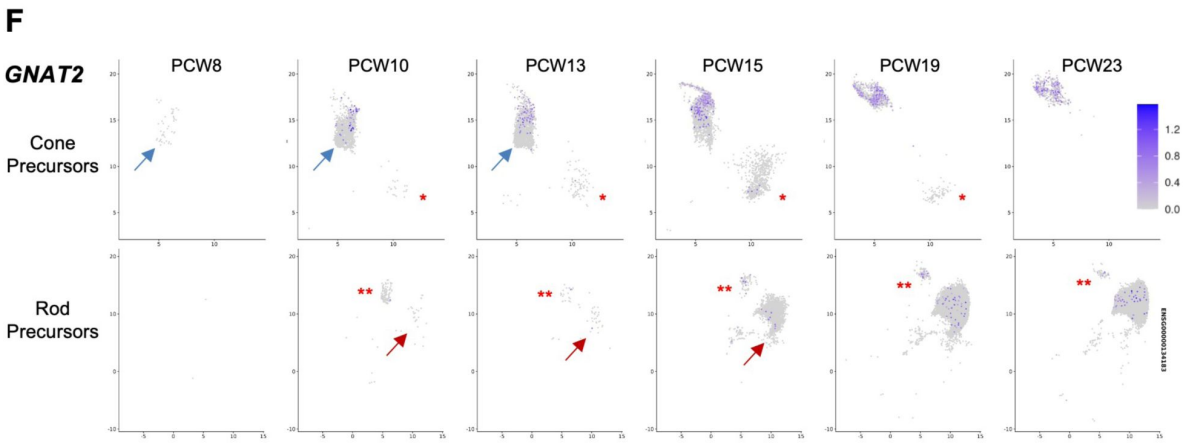

Figure S11 (continued)

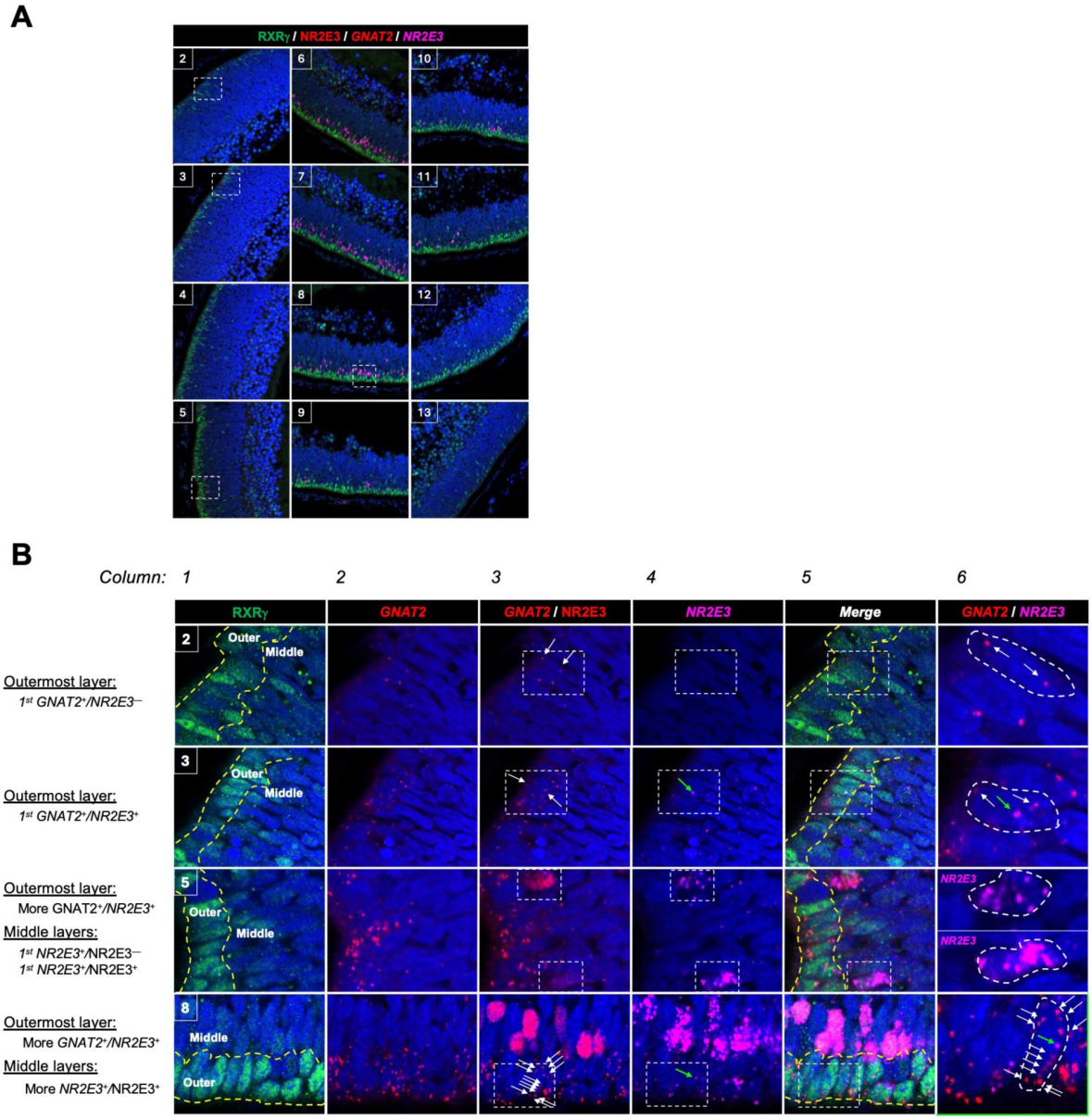

Figure S12

NR2E3 and *GNAT2* co-expression in photoreceptor precursors.

A. Composite images of combined RXRγ and NR2E3 immunofluorescence staining and *GNAT2* and *NR2E3* RNA FISH in boxed regions 2-13 of **Figure 7A**. **B.** Enlarged images of boxed regions in images 2, 3, 5, and 8 in panel A, as indicated at upper left of images in column 1. Dotted yellow lines demarcate the outermost and middle (sub-outermost) NBL cells analyzed separately in **Figure 7C,D**. White arrows = *GNAT2* puncta in boxed regions of interest. Green arrows = *NR2E3* puncta. Boxed regions in column 3 (*GNAT2* RNA plus NR2E3 protein) and column 4 (*NR2E3* RNA) are enlarged in column 6 (*GNAT2* RNA plus *NR2E3* RNA) and illustrate **region 2**) initial expression of *GNAT2* RNA without *NR2E3* RNA in outermost NBL nascent cones; **region 3**) initial co-expression of *GNAT2* and *NR2E3* RNA in early outermost NBL cones; **region 5**) initial expression of *NR2E3* RNA with or without co-expressed NR2E3 protein; and **region 8**) co-expression of high *GNAT2* and low *NR2E3* RNA without NR2E3 protein in RXRγ^{hi} outermost NBL cones.

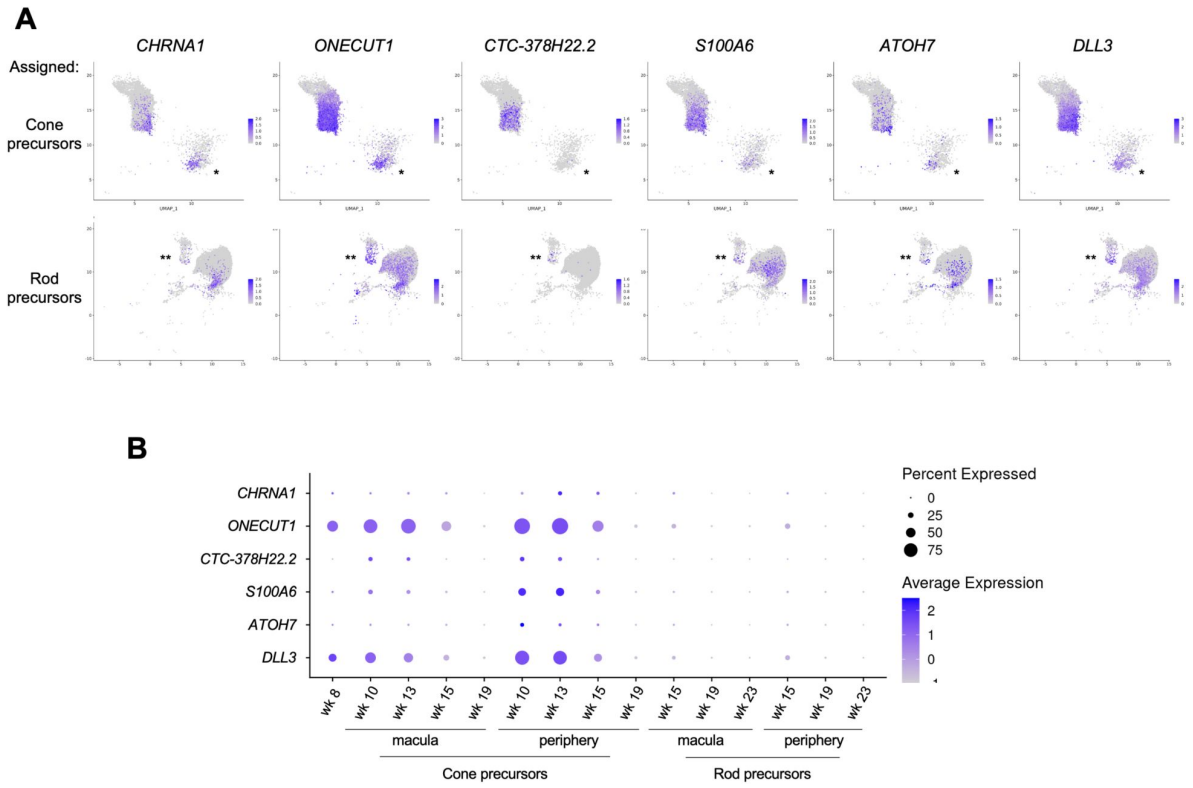

Figure S13

Developmental expression of photoreceptor precursor markers in a large 3' snRNA-seq dataset.

A. Expression of selected markers in pcw 8-23 cone precursors (*top*) and rod precursors (*bottom*), as assigned in Zuo *et al*[20]. ***** = possible rod precursors mis-assigned as cone precursors; ****** = possible cone precursors mis-assigned as rod precursors. **B.** Dot plot depicting the percentage of cells expressing each gene and average expression levels in assigned macular and peripheral cone and rod precursors at each age.

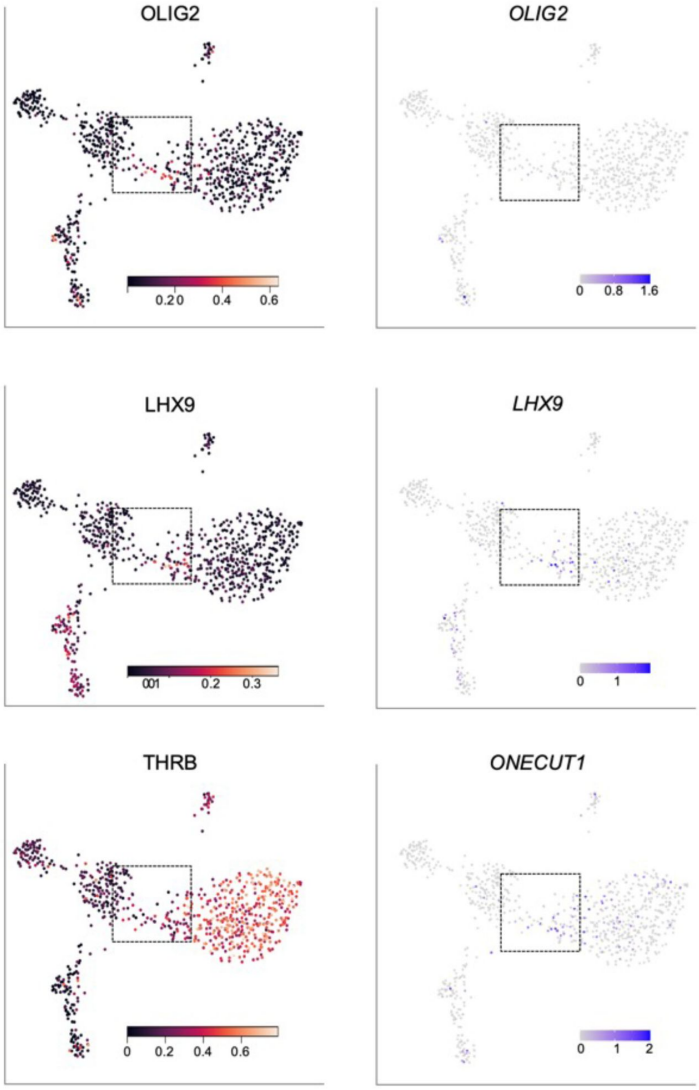

Figure S14

iCP-enriched regulon activities.

UMAP plots of OLIG2, LHX9, and THRB regulon activities (*left*) and *OLIG2*, *LHX9*, and *ONECUT1* gene expression (*right*), illustrating high OLIG2 regulon activity with minimal *OLIG2* gene expression, concurrent LHX9 regulon activity and *LHX9* gene expression, and *ONECUT1* gene expression in iCP cells preceding increased THRB regulon activity in early LM cones. Boxes indicate bridge region.

Figure S15

Heatmaps of coregulated gene modules across cone precursor pseudotime.

A. Heatmaps of individual genes in each module across the pseudotime trajectory shown in **Figure 6C**. lncRNA genes of interest are labeled. **B.** Heatmap of averaged gene module expression across pseudotime.

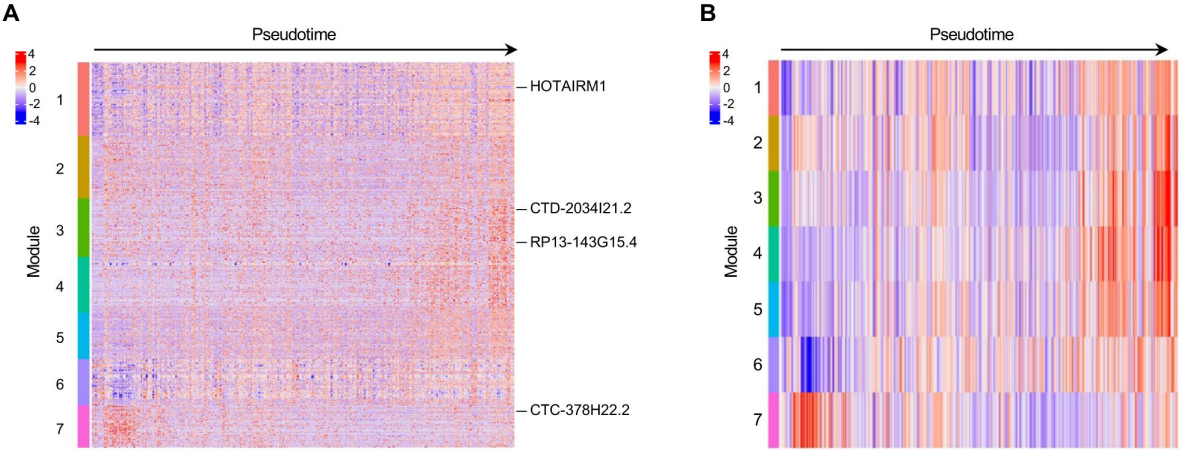

Figure S16

Differential gene expression in early cone and rod precursors.

A. Volcano plot of differential expression between early rod cluster ER and cone LM, excluding the 5-cell late-maturing population. pAdj cutoff = 0.05, log2FC cutoff = |0.4|. Labeled genes: pAdj <10e-32, except for *SYK* and *MYCN.* **B.** Overrepresentation analysis of cone-enriched genes pAdj <0.05, log2FC ≥ |0.4|.

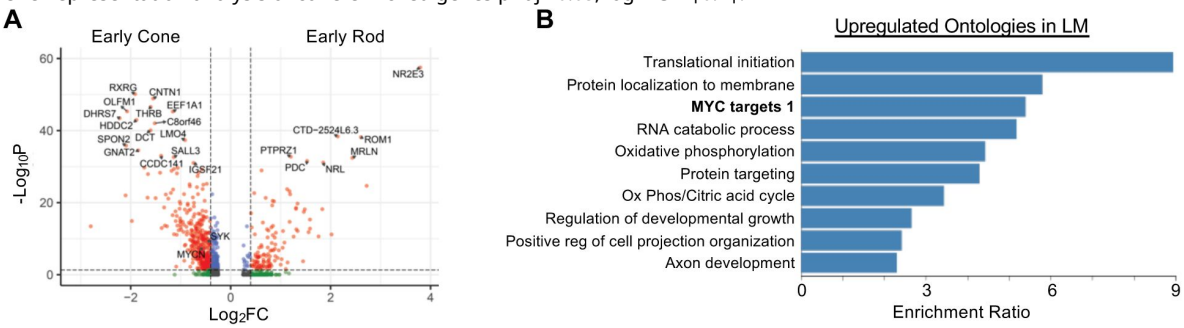

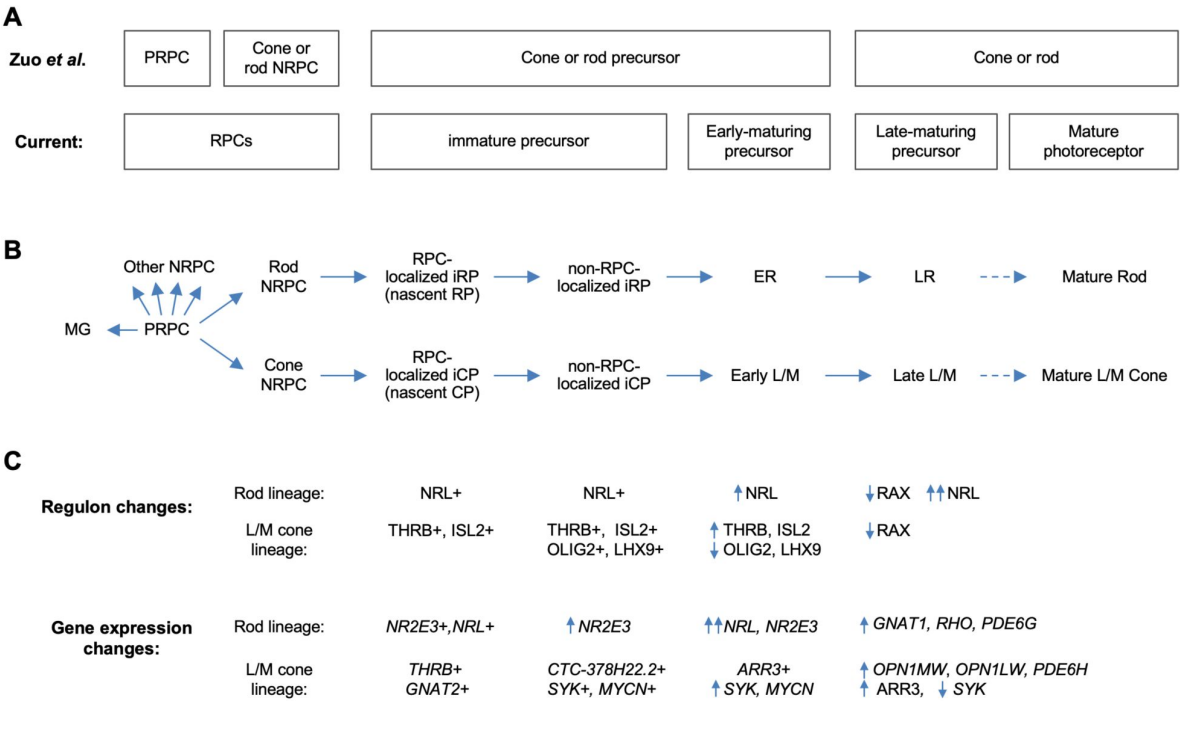

Figure S17

Proposed cell state trajectories in human L/M cone and rod development.

A. L/M cone and rod developmental stages discerned in the 3′ snRNA-seq analysis of Zuo *et al*. [20] (*top*) and in the current deep, full-length scRNA-seq study (*bottom*). Note discrimination of PRPC and NRPC populations in Zuo *et al.* and discrimination of immature and early-maturing precursors in the current work. Late maturing precursors in fetal retina are hypothesized to be distinguishable from fully mature photoreceptors in postnatal retina. **B**. RPC and L/M cone and rod developmental states referred to in the current study. **C.** Selected cell state features identified in the current work.

Key Resources Table

Information related to strains, cell lines, biological samples, antibodies, recombinant DNA reagents, sequence-based reagents, commercial assays or kits, and software.

Reagent type (species) or resource	Designation	Source or reference	Identifiers	Additional information
strain, strain background (*Escherichia coli*)	NEB 10-beta	New England Biolabs	C3019H	Competent cells
cell line (*Homo-sapiens*)	CHLA-VC-RB31	Stachelek *et al*., 2023 DOI: 10.1002/gcc.23120		
cell line (*Mus musculus*)	NIH-3T3	ATCC	CRL-1658.2	.
cell line (*Homo-sapiens*)	HEK-293T	ATCC	CRL-3216	
biological sample (*Human*)	Fetal eyes	Family Planning Associates, Los Angeles, CA		Freshly isolated from fetus
biological sample (*Human*)	Fetal eyes	Advanced Bioscience Resources, Alameda, CA		Freshly isolated from fetus
antibody	anti-NRL (Goat polyclonal)	R&D Systems	CAT# AF2945, RRID: AB_2155098	WB: 1:2000-4000)

antibody	anti-NRL (Mouse monoclonal)	Santa Cruz Biotechnology	CAT# SC-374277, RRID: AB_10991100	WB:1:250, IF:1:50
antibody	anti-RXRγ (Mouse monoclonal)	Santa Cruz Biotechnology	CAT# SC-514134, RRID: AB_2737293	IF: 1:200
antibody	anti-SYK (Mouse monoclonal)	Santa Cruz Biotechnology	CAT# SC1240, RRID: AB_628308	IF:(1:200)
antibody	anti-ARR3 (Rabbit polyclonal)	Li et al., 2003 DOI: 10.1167/iovs.02-0434 Zhang et al., 2001 DOI: 10.1007/978-1-4615-1355-1_33	LUMI-F - hCAR	IF: (1:5000) Cheryl Craft
antibody	anti-RXRγ (Rabbit polyclonal)	Santa Cruz Biotechnology	CAT# SC-555, RRID: AB_2269865	IF: (1:800)
antibody	anti-KI67 (Mouse monoclonal)	BD Bioscience	CAT# 550609, RRID: AB_393778	IF: (1:200)
antibody	anti-GFP and YFP (Goat polyclonal)	Abcam	CAT# ab6673, RRID: AB_305643	IF: (1:500)

antibody	anti-CD133-PE (Mouse monoclonal)	Miltenyi Biotec	CAT# 130-113-108, RRID: AB_2725937	FACS: (1:50)
antibody	Mouse monoclonal anti-CD44-FITC (1:50)	BD Biosciences	CAT# 555478, RRID: AB_395870	FACS: (1:50)
antibody	Mouse monoclonal anti-PNR/NR2E3 (1:50)	R&D Systems	CAT# PP-H7223-00, RRID: AB_2155481	IF: (1:50)
antibody	Mouse monoclonal anti-CD49b-FITC (1:10)	BD Biosciences	CAT# 555498, RRID: AB_395888	FACS: (1:10)
antibody	anti-goat IgG Alexa Fluor 488 (1:300)	Jackson Laboratories	CAT# 705-545-147, RRID: AB_2336933	IF: (1:300)
antibody	anti-mouse IgG Alexa Fluor 680 (Donkey polyclonal)	Life Technologies	CAT# A10038, RRID: AB_2534014	IF: (1:500)
antibody	Donkey polyclonal anti-mouse IgG Alexa Fluor 680 (Donkey polyclonal)	Invitrogen	CAT# A11057, RRID: AB_2534104	IF: (1:500)
recombinant DNA reagent	pLKO.1C-YFP	Lee and Cobrinik, 2020 DOI: 10.2144/btn-2019-0155		GFP version of pLKO.1-Puro

recombinant DNA reagent	pLKO.1C-YFP-shRB1-733	Lee and Cobrinik, 2020 DOI: 10.2144/btn-2019-0155	RRID :Addgene_10878	Pol III based shRNA backbone
recombinant DNA reagent	pcDNA4-His-Max-C-Nrl	Cheng et al., 2004 DOI: 10.1093/hmg/ddh173		Gift from A. Swaroop.
recombinant DNA reagent	pcDNA4-His-Max-C-EF1α-FL-NRL	This paper	Submitted to Addgene, RRID pending	See Materials and Methods NRL isoform analyses
recombinant DNA reagent	pcDNA4-C-EF1α-FL-NRL	This paper	Submitted to Addgene, RRID pending	See Materials and Methods NRL isoform analyses
recombinant DNA reagent	pcDNA4-C-EF1α-Tr-NRL	This paper	Submitted to Addgene, RRID pending	See Materials and Methods NRL isoform analyses
recombinant DNA reagent	pcDNA4-C-EF1α	This paper	Submitted to Addgene, RRID pending	See Materials and Methods NRL isoform analyses
recombinant DNA reagent	pGL3-SV40	Promega	AT# E1761, RRID:Addgene_173953	
recombinant DNA reagent	pGL3-PDE6B-146	This paper	Submitted to Addgene, RRID pending	See Materials and Methods NRL isoform analyses
recombinant DNA reagent	pGL3-empty	This paper	Submitted to Addgene, RRID pending	See Materials and Methods NRL isoform analyses

recombinant DNA reagent	pUltra-EGFP-P2A-Tr-NRL	This paper	Submitted to Addgene, RRID pending	See Materials and Methods NRL isoform analyses
recombinant DNA reagent	pUltra-EGFP	Lou et al., 2012 DOI: 10.1371/journal.pone.0033093	RRID: Addgene_24129	
sequence-based reagent	Gipc1_F	This paper	PCR primers	GGGAAAGGACAAAAGGAACCC
sequenced-based reagent	Gipc1_R	This paper	PCR primers	CAGGGCATTTGCACCCCATGCC
sequenced-based reagent	siRNA: nontargeting control	Thermo Fisher	4390843	Silencer Select
sequenced-based reagent	Subcloning PCR primer	Integrated DNA Technologies	1) Del-His F	5'-CCGAAACCATGGCCCTGCCCCCCAGC
sequenced-based reagent	Subcloning PCR primer	Integrated DNA Technologies	2) Del-His R	5'-GGGCCATGGTTTCGGAGGCCGTCCG
sequenced-based reagent	Subcloning PCR primer	Integrated DNA Technologies	3) NRL-no-His F	5'-CCGAAACCATGTCTGTGCGGGAGCTAAACC
sequenced-based reagent	Subcloning PCR primer	Integrated DNA Technologies	4) NRL-no-His R	5'-CAGACATGGTTTCGGAGGCCGTCCG

sequenced-based reagent	Subcloning PCR primer	Integrated DNA Technologies	5) pcDNA del NRL F	5'-CCGAAACC GCCGTTCA GAGCACCT TGTGG
sequenced-based reagent	Subcloning PCR primer	Integrated DNA Technologies	6) pcDNA del NRL R	5'-GAACGGCG GTTTCGGA GGCCGTCC G
sequenced-based reagent	Subcloning PCR primer	Integrated DNA Technologies	7) PDE -93 F IF	5'-TCTTACGC GTGCTAGA GCGCAGGC CCCCATTT G
sequenced-based reagent	Subcloning PCR primer	Integrated DNA Technologies	8) PDE +53 R IF	5'-CTTAGATC GCAGATCG GTGGCTGC CTGTCCCT G
sequenced-based reagent	Subcloning PCR primer	Integrated DNA Technologies	9) pGL3-sv40 SDM F	5'-CTGCGATC AAGCTTGG CATTCCGG TACTG
sequenced-based reagent	Subcloning PCR primer	Integrated DNA Technologies	10) pGL3-sv40 SDM R	5'-CAAGCTTG ATCGCAGA TCGGTGGC TG
sequenced-based reagent	Subcloning PCR primer	Integrated DNA Technologies	11) pGL3 del SV40 R	5'-CAAGCTTG ATCGCAGA TCTCGAGC CC
sequenced-based reagent	Subcloning PCR primer	Integrated DNA Technologies	12) Tr-NRL IF pU-G F	5'-GCCTTCTA GAGGATCC ATGTCTGT GCGGGAG CTAAACC

sequenced-based reagent	Subcloning PCR primer	Integrated DNA Technologies	13) Tr-NRL IF pU-G R	5'-CGCCGGAGCCGGATCCTCAGAGGAAGAGGTGGGAGGG
sequenced-based reagent	SmartSeq library amplification primer	Integrated DNA Technologies	5' PCR Primer II A	5'-AAGCAGTGGTATCAACGCAGAGT
sequenced-based reagent	RACE primer	Integrated DNA Technologies	5' RACE primer for SmartSeq cDNA	5'-AAGCAGTGGTATCAACGCAGAGTACGGG
sequenced-based reagent	NRL reverse primer for 5' RACE	Integrated DNA Technologies	Rev NRL-Full ex3	5'-GGTTTAGCTCCCGCACAGACATCGAGAC
sequenced-based reagent	RXRG reverse primer for 5' RACE	Integrated DNA Technologies	Rev RXR ex5	5'-GAAGAACCCTTTGCAGCCTTCACAACTG
sequenced-based reagent	RACE primer	Integrated DNA Technologies	3' RACE primer for SmartSeq cDNA	5'-AAGCAGTGGTATCAACGCAGAGTACTTTT
sequenced-based reagent	THRB1 forward primer for 3' RACE	Integrated DNA Technologies	Forw TRb1 ex4	5'-GCCTTACAGCCTGGGACAAACC
sequenced-based reagent	THRB2 forward primer for 3' RACE	Integrated DNA Technologies	Forw TRb2 ex1	5'-CCCTGGAAACATGTTTAAAAGCAAGGACT

sequenced-based reagent	*In situ* hybridization chain reaction probes	Molecular Instruments Inc.	FL-NRL exon 1, 2	Target sequence Ensembl ID: ENST00000619224.1
sequenced-based reagent	hybridization chain reaction probes	Molecular Instruments Inc.	*CHRNA1*	Target sequence NCBI accession number: NM_000079.4
sequenced-based reagent	hybridization chain reaction probes	Molecular Instruments Inc.	*RP13-143G15.4*	
sequenced-based reagent	hybridization chain reaction probes	Molecular Instruments Inc.	*CTC-378H22.2*	Target sequence Ensembl ID: ENST00000559786.1
sequenced-based reagent	hybridization chain reaction probes	Molecular Instruments Inc.	*HOTAIRM1*	Target sequence NCBI accession number: NR_038366.1
sequenced-based reagent	hybridization chain reaction probes	Molecular Instruments Inc.	*CTD-2034I21.2*	Target sequence NCBI accession number: XR_001752169.1
sequenced-based reagent	hybridization chain reaction probes	Molecular Instruments Inc.	*GNAT2*	Target sequence NCBI accession number: NM_005272.5

sequenced-based reagent	hybridization chain reaction probes	Molecular Instruments Inc.	*NR2E3*	Target sequence NCBI accession number: NM_01249.4
commercial assay or kit	In-Fusion HD Cloning	Clontech	Clontech:639647	
commercial assay or kit	SMARTer Ultra Low RNA Kit for the Fluidigm C1 System	Clontech (Takara Bio)	CAT# 634835/634935	
commercial assay or kit	SMART-Seq V4 Ultra Low Input RNA Kit	Takara Bio	CAT# 63891	
commercial assay or kit	Nextera XT DNA Library Preparation Kit	Illumina	CAT# FC-131-1096	
commercial assay or kit	CloneAmp HiFi PCR Premix	Clontech (Takara Bio)	Takara Bio #639298	
commercial assay or kit	Quant-iT PicoGreen dsDNA Assay Kit	Life Technologies	CAT# P11496	
commercial assay or kit	Nano-Glo Dual-Luciferase Reporter Assay System	Promega, Inc	CAT# N1610	
chemical compound, drug	GS-9876 (SYK inhibitor)	MedChemExpress	CAT# HY-109091	
software, algorithm	TrimGalore	Felix Krueger GitHub		https://github.com/FelixKr

				ueger/TrimGalore
software, algorithm	Cutadapt	Martin, 2011 DOI: 10.14806/ej.17.1.200		https://cutadapt.readthedocs.io/en/stable/
software, algorithm	HISAT2	Kim et al., 2019 DOI: 10.1038/s41587-019-0201-4		https://github.com/DaehwanKimLab/hisat2
software, algorithm	StringTie	Pertea et al., 2015 DOI: 10.1038/nbt.3122		minmmhttp://ccb.jhu.edu/software/stringtie/
software, algorithm	Snakemake/ARMOR	Orjuela et al., 2019 DOI: 10.1038/nbt.3122		https://github.com/whtns/ARMOR
software, algorithm	Minimap2	Li, 2018 DOI: 10.1093/bioinformatics/bty191		https://lh3.github.io/minimap2/
software, algorithm	WebGestalt	Liao et al., 2019 DOI: 10.1093/nar/gkz401		http://www.webgestalt.org/
software, algorithm	pySCENIC	Van de Sande et al., 2020 DOI: 10.1038/s41596-020-0336-2		https://github.com/aertslab/pySCENIC

software, algorithm	Tximport	Soneson et al., 2015 DOI: 10.12688/f1000research.7563.1		https://bioconductor.org/packages/release/bioc/html/tximport.html
software, algorithm	Seurat v3 (full-length scRNA-seq), Seurat v5 (3' snRNA-seq)	Stuart et al., 2019 DOI: 10.1016/j.cell.2019.05.031		https://satijalab.org/seurat/index.html
software, algorithm	EnhancedVolcano	Blighe et al., 2018 Github		https://github.com/kevinblighe/EnhancedVolcano
software, algorithm	genesorteR (v0.4.3)	Ibrahim and Kramann, 2019 DOI: 10.1101/676379		http://github.com/mahmoudibrahim/genesorteR
software, algorithm	Wiggleplotr (v1.13.1)	Alasoo, 2019 Bioconductor package		https://github.com/karalasoo/wiggleplotr
software, algorithm	DEXSeq	Anders et al., 2012 DOI: 10.1101/gr.133744.111		https://bioconductor.org/packages/release/bioc/html/DEXSeq.html
software, algorithm	velocytoR	La Manno et al., 2018 DOI: 10.1038/s41586-018-0414-6		https://velocyto.org/
software, algorithm	Monocle3	Cao et al., 2019 DOI: 10.1038/s415		https://cole-trapnell-lab.github.io/monocle3/

		86-019-0969-x		
software, algorithm	QuPath	Bankhead et al., 2017 DOI: 10.1038/s41586-019-0969-x		https://qupath.github.io/
software, algorithm	StarDist (QuPath implementation)	Schmidt et al., 2018 DOI: 10.1038/s41586-019-0969-x		https://qupath.readthedocs.io/en/stable/docs/advanced/stardist.html

Supplementary Tables

Source data Excel files for selected figures.

Table S1: Differentially expressed genes for low resolution rod clusters.

Table S2: Differentially expressed genes for low resolution cone clusters.

Table S3: Differentially expressed genes for low resolution late- vs early-maturing L/M cone populations.

Table S4: Differentially expressed genes in rods vs rod precursors in a 3' snRNA-seq dataset data of Zuo et al. PMID 39117640.

Table S5: Differentially expressed genes in cones vs cone precursors in a 3' snRNA-seq dataset (data of Zuo et al. PMID 39117640.

Table S6: SCENIC regulon specificity scores for low resolution clusters.

Table S7: Differentially expressed genes for high resolution MG and RPC clusters.

Table S8: SCENIC regulon specificity scores for high resolution clusters.

Table S9: Pseudotime-correlated genes and gene modules.

Table S10: Differentially expressed genes for low resolution early rod and L/M cone clusters.

Data and materials availability

All data needed to evaluate the conclusions in the paper are present in the paper and/or the Supplementary Materials. A web portal providing access to a Shiny app for manipulation of the presented full-length scRNA-seq data (including UMAP or tSNE display of clusters, gene or isoform expression, and sample metadata; cluster marker gene and violin plots; exon coverage plots; Ensembl isoform assignments) is available at *https://docker.saban.chla.usc.edu/cobrinik/app/seuratApp/*. The preprocessed Seurat Object for full-length scRNAseq (and for the above-linked Shiny app) is available at *https://doi.org/10.5281/zenodo.15231490*. The Seurat Object for 3'

snRNA-seq[20] was downloaded from CZ CELLxGENE Discover with accession code 5900dda8-2dc3-4770-b604084eac1c2c82. Single-cell RNA-sequencing files and processed final gene and transcript matrices are publicly available at the GEO database under accession number GSE207802.

Acknowledgements

We thank Melissa L. Wilson (USC Department of Preventive Medicine) and Family Planning Associates for assistance in obtaining fetal tissue, Tingting Yang and Rui Chen for sharing data, the Stem Cell Analytics Core Facility, FACS Core Facility, and Imaging Core Facility of The Saban Research Institute of Children's Hospital Los Angeles for technical support, and Biraj Mahato and Sumitha Bharathan for critical reading an earlier version of the manuscript.

Additional information

Funding

National Institutes of Health grant R01EY026661 (DC)

National Institutes of Health grant R01CA137124 (DC)

National Institutes of Health grant R01AG076956 (MAB)

National Institutes of Health grant 5T32HD060549 to USC Department of Development, Stem Cells, and Regenerative Medicine (DWHS)

USC Provost Fellowship (DWHS)

Saban Research Institute of Children's Hospital Los Angeles fellowship (JB)

Research to Prevent Blindness (unrestricted grant to USC Dept. of Ophthalmology)

Larry and Celia Moh Foundation (DC)

Neonatal Blindness Research Fund (DC)

A.B. Reins Foundation (DC)

Knights Templar Eye Foundation (DC)

Author contributions

Conceptualization: DWHS, DC

Methodology: DWHS, LC, DJW, HPS, DC

Investigation: DWHS, LC, SL, JB, DJW, JGA, YK, HPS, ZF

Computational analyses: KS, BB, MS

Statistical analyses: DWHS, MWR

Bioinformatic approaches: KS, MB, MAB

Computational infrastructure: ED, SGE

Tissue procurement: MT, BHG

Key reagent: CMC

Writing --- original draft: DWHS, DC

Writing --- review and editing: DWHS, KS, JGA, MAB, BHG, CMC, DC

Additional files

Shayler et al., Supplemental Tables S1-S10

References

1. Shiau F., Ruzycki P.A., Clark B.S (2021) **A single-cell guide to retinal development: Cell fate decisions of multipotent retinal progenitors in scRNA-seq** *Dev Biol* **478**:41–58 https://doi.org/10.1016/j.ydbio.2021.06.005 | Google Scholar

2. Brzezinski J.A., Reh T.A (2015) **Photoreceptor cell fate specification in vertebrates** *Development* **142**:3263–3273 https://doi.org/10.1242/dev.127043 | Google Scholar

3. Emerson M.M., Surzenko N., Goetz J.J., Trimarchi J., Cepko C.L (2013) **Otx2 and Onecut1 promote the fates of cone photoreceptors and horizontal cells and repress rod photoreceptors** *Dev Cell* **26**:59–72 https://doi.org/10.1016/j.devcel.2013.06.005 | Google Scholar

4. Ng L., Lu A., Swaroop A., Sharlin D.S., Swaroop A., Forrest D (2011) **Two Transcription Factors Can Direct Three Photoreceptor Outcomes from Rod Precursor Cells in Mouse Retinal Development** *The Journal of Neuroscience* **31**:11118–11125 https://doi.org/10.1523/JNEUROSCI.1709-11.2011 | Google Scholar

5. Hendrickson A., Possin D., Vajzovic L., Toth C.A (2012) **Histologic Development of the Human Fovea From Midgestation to Maturity** *Am J Ophthalmol* **154**:767–778 https://doi.org/10.1016/j.ajo.2012.05.007 | Google Scholar

6. Hoshino A., Ratnapriya R., Brooks M.J., Chaitankar V., Wilken M.S., Zhang C., Starostik M.R., Gieser L., La Torre A., Nishio M., et al. (2017) **Molecular Anatomy of the Developing Human Retina** *Dev Cell* **43**:763–779 https://doi.org/10.1016/j.devcel.2017.10.029 | Google Scholar

7. Georgiou M., Robson A.G., Fujinami K., de Guimarães T.A.C., Fujinami-Yokokawa Y., Daich Varela M., Pontikos N., Kalitzeos A., Mahroo O.A., Webster A.R., et al. (2024) **Phenotyping and genotyping inherited retinal diseases: Molecular genetics, clinical and imaging features, and therapeutics of macular dystrophies, cone and cone-rod dystrophies, rod-cone dystrophies, Leber congenital amaurosis, and cone dysfunction syndromes** *Prog Retin Eye Res* **100**:101244 https://doi.org/10.1016/j.preteyeres.2024.101244 | Google Scholar

8. Cobrinik D (2024) **Retinoblastoma Origins and Destinations** *New England Journal of Medicine* **390**:1408–1419 https://doi.org/10.1056/NEJMra1803083 | Google Scholar

9. Xu X.L., Fang Y., Lee T.C., Forrest D., Gregory-Evans C., Almeida D., Liu A., Jhanwar S.C., Abramson D.H., Cobrinik D (2009) **Retinoblastoma Has Properties of a Cone Precursor Tumor and Depends Upon Cone-Specific MDM2 Signaling** *Cell* **137**:1018–1031 https://doi.org/10.1016/j.cell.2009.03.051 | Google Scholar

10. Xu X.L., Singh H.P., Wang L., Qi D.L., Poulos B.K., Abramson D.H., Jhanwar S.C., Cobrinik D (2014) **Rb suppresses human cone-precursor-derived retinoblastoma tumours** *Nature* **514**:385–388 https://doi.org/10.1038/nature13813 | Google Scholar

11. Singh H.P., Wang S., Stachelek K., Lee S., Reid M.W., Thornton M.E., Craft C.M., Grubbs B.H., Cobrinik D (2018) **Developmental stage-specific proliferation and retinoblastoma genesis in RB-deficient human but not mouse cone precursors** *Proceedings of the National Academy of Sciences* **115**:E9391–E9400 https://doi.org/10.1073/pnas.1808903115 | Google Scholar

12. McEvoy J., Flores-Otero J., Zhang J., Nemeth K., Brennan R., Bradley C., Krafcik F., Rodriguez-Galindo C., Wilson M., Xiong S., et al. (2011) **Coexpression of Normally Incompatible Developmental Pathways in Retinoblastoma Genesis** *Cancer Cell* **20**:260–275 https://doi.org/10.1016/j.ccr.2011.07.005 | Google Scholar

13. Khanna H., Akimoto M., Siffroi-Fernandez S., Friedman J.S., Hicks D., Swaroop A (2006) **Retinoic Acid Regulates the Expression of Photoreceptor Transcription Factor NRL** *Journal of Biological Chemistry* **281**:27327–27334 https://doi.org/10.1074/jbc.M605500200 | Google Scholar

14. Clark B.S., Stein-O'Brien G.L., Shiau F., Cannon G.H., Davis-Marcisak E., Sherman T., Santiago C.P., Hoang T. V., Rajaii F., James-Esposito R.E., et al. (2019) **Single-Cell RNA-Seq Analysis of Retinal Development Identifies NFI Factors as Regulating Mitotic Exit and Late-Born Cell Specification** *Neuron* **102**:1111–1126 https://doi.org/10.1016/j.neuron.2019.04.010 | Google Scholar

15. Lu Y., Shiau F., Yi W., Lu S., Wu Q., Pearson J.D., Kallman A., Zhong S., Hoang T., Zuo Z., et al. (2020) **Single-Cell Analysis of Human Retina Identifies Evolutionarily Conserved and Species-Specific Mechanisms Controlling Development** *Dev Cell* **53**:473–491 https://doi.org/10.1016/j.devcel.2020.04.009 | Google Scholar

16. Sridhar A., Hoshino A., Finkbeiner C.R., Chitsazan A., Dai L., Haugan A.K., Eschenbacher K.M., Jackson D.L., Trapnell C., Bermingham-McDonogh O., et al. (2020) **Single-Cell Transcriptomic Comparison of Human Fetal Retina, hPSC-Derived Retinal Organoids, and Long-Term Retinal Cultures** *Cell Rep* **30**:1644–1659 https://doi.org/10.1016/j.celrep.2020.01.007 | Google Scholar

17. Buenaventura D.F., Corseri A., Emerson M.M (2019) **Identification of genes with enriched expression in early developing mouse cone photoreceptors** *Invest Ophthalmol Vis Sci* **60**:2787–2799 https://doi.org/10.1167/iovs.19-26951 | Google Scholar

18. Lo Giudice Q., Leleu M., La Manno G., Fabre P.J. (2019) **Single-cell transcriptional logic of cell-fate specification and axon guidance in early born retinal neurons** *Development* **146** https://doi.org/10.1242/dev.178103 | Google Scholar

19. Lyu P., Hoang T., Santiago C.P., Thomas E.D., Timms A.E., Appel H., Gimmen M., Le N., Jiang L., Kim D.W., et al. (2021) **Gene regulatory networks controlling temporal patterning, neurogenesis, and cell-fate specification in mammalian retina** *Cell Rep* **37**:109994 https://doi.org/10.1016/j.celrep.2021.109994 | Google Scholar

20. Zuo Z., Cheng X., Ferdous S., Shao J., Li J., Bao Y., Li J., Lu J., Jacobo Lopez A., Wohlschlegel J., et al. (2024) **Single cell dual-omic atlas of the human developing retina** *Nat Commun* **15**:1–21 https://doi.org/10.1038/s41467-024-50853-5 | Google Scholar

21. Omori Y., Kubo S., Kon T., Furuhashi M., Narita H., Kominami T., Ueno A., Tsutsumi R., Chaya T., Yamamoto H., et al. (2017) **Samd7 is a cell type-specific PRC1 component essential for establishing retinal rod photoreceptor identity** *Proceedings of the National Academy of Sciences* **114**:E8264–E8273 https://doi.org/10.1073/pnas.1707021114 | Google Scholar

22. Gagliardi G., Ben M'Barek K., Chaffiol A., Slembrouck-Brec A., Conart J.-B., Nanteau C., Rabesandratana O., Sahel J.-A., Duebel J., Orieux G., et al. (2018) **Characterization and Transplantation of CD73-Positive Photoreceptors Isolated from Human iPSC-Derived Retinal Organoids** *Stem Cell Reports* **11**:665–680 https://doi.org/10.1016/j.stemcr.2018.07.005 | Google Scholar

23. Chen T.W., Chen G., Funkhouser L.J., Nam S.-C (2009) **Membrane domain modulation by Spectrins in Drosophila photoreceptor morphogenesis** *genesis* **47**:744–750 https://doi.org/10.1002/dvg.20555 | Google Scholar

24. Burger C.A., Jiang D., Mackin R.D., Samuel M.A (2021) **Development and maintenance of vision's first synapse** *Dev Biol* **476**:218–239 https://doi.org/10.1016/j.ydbio.2021.04.001 | Google Scholar

25. Sokolov D., Sechrest E.R., Wang Y., Nevin C., Du J., Kolandaivelu S (2021) **Nuclear NAD+-biosynthetic enzyme NMNAT1 facilitates development and early survival of retinal neurons** *eLife* **10**:1–26 https://doi.org/10.7554/eLife.71185 | Google Scholar

26. Lukowski S.W., Lo C.Y., Sharov A.A., Nguyen Q., Fang L., Hung S.S., Zhu L., Zhang T., Grünert U., Nguyen T., et al. (2019) **A single-cell transcriptome atlas of the adult human retina** *EMBO J* **38**:1–15 https://doi.org/10.15252/embj.2018100811 | Google Scholar

27. Peng Y.R., Shekhar K., Yan W., Herrmann D., Sappington A., Bryman G.S., van Zyl T., Do M.T.H., Regev A., Sanes J.R. (2019) **Molecular Classification and Comparative Taxonomics of Foveal and Peripheral Cells in Primate Retina** *Cell* **176**:1222–1237 https://doi.org/10.1016/j.cell.2019.01.004 | Google Scholar

28. Kallman A., Capowski E.E., Wang J., Kaushik A.M., Jansen A.D., Edwards K.L., Chen L., Berlinicke C.A., Joseph Phillips M., Pierce E.A., et al. (2020) **Investigating cone photoreceptor development using patient-derived NRL null retinal organoids** *Commun Biol* **3**:82 https://doi.org/10.1038/s42003-020-0808-5 | Google Scholar

29. Voigt A.P., Whitmore S.S., Flamme-Wiese M.J., Riker M.J., Wiley L.A., Tucker B.A., Stone E.M., Mullins R.F., Scheetz T.E (2019) **Molecular characterization of foveal versus peripheral human retina by single-cell RNA sequencing** *Exp Eye Res* **184**:234–242 https://doi.org/10.1016/j.exer.2019.05.001 | Google Scholar

30. Van de Sande B., Flerin C., Davie K., De Waegeneer M., Hulselmans G., Aibar S., Seurinck R., Saelens W., Cannoodt R., Rouchon Q., et al. (2020) **A scalable SCENIC workflow for single-cell gene regulatory network analysis** *Nat Protoc* **15**:2247–2276 https://doi.org/10.1038/s41596-020-0336-2 | Google Scholar

31. Swaroop A., Kim D., Forrest D (2010) **Transcriptional regulation of photoreceptor development and homeostasis in the mammalian retina** *Nat Rev Neurosci* **11**:563–576 https://doi.org/10.1038/nrn2880 | Google Scholar

32. Ng L., Hurley J.B., Dierks B., Srinivas M., Saltó C., Vennström B., Reh T.A., Forrest D (2001) **A thyroid hormone receptor that is required for the development of green cone photoreceptors** *Nat Genet* **27**:94–98 https://doi.org/10.1038/83829 | Google Scholar

33. Roberts M.R., Hendrickson A., McGuire C.R., Reh T.A (2005) **Retinoid X Receptor γ Is Necessary to Establish the S-opsin Gradient in Cone Photoreceptors of the Developing Mouse Retina** *Investigative Opthalmology & Visual Science* **46**:2897 https://doi.org/10.1167/iovs.05-0093 | Google Scholar

34. Friedman J.S., Khanna H., Swain P.K., DeNicola R., Cheng H., Mitton K.P., Weber C.H., Hicks D., Swaroop A (2004) **The Minimal Transactivation Domain of the Basic Motif-Leucine Zipper**

Transcription Factor NRL Interacts with TATA-binding Protein *Journal of Biological Chemistry* **279**:47233–47241 https://doi.org/10.1074/jbc.M408298200 | Google Scholar

35. Rehemtulla A., Warwar R., Kumar R., Ji X., Zack D.J., Swaroop A (1996) **The basic motif-leucine zipper transcription factor Nrl can positively regulate rhodopsin gene expression** *Proceedings of the National Academy of Sciences* **93**:191–195 https://doi.org/10.1073/pnas.93.1.191 | Google Scholar

36. Swaroop A., Xu J.Z., Pawar H., Jackson A., Skolnick C., Agarwal N (1992) **A conserved retina-specific gene encodes a basic motif/leucine zipper domain** *Proceedings of the National Academy of Sciences* **89**:266–270 https://doi.org/10.1073/pnas.89.1.266 | Google Scholar

37. Stachelek K., Harutyunyan N., Lee S., Beck A., Kim J., Xu L., Berry J.L., Nagiel A., Reynolds C.P., Murphree A.L., et al. (2023) **Non-synonymous, synonymous, and non-coding nucleotide variants contribute to recurrently altered biological processes during retinoblastoma progression** *Genes Chromosomes Cancer* **62**:275–289 https://doi.org/10.1002/gcc.23120 | Google Scholar

38. Eldred K.C., Hadyniak S.E., Hussey K.A., Brenerman B., Zhang P.-W., Chamling X., Sluch V.M., Welsbie D.S., Hattar S., Taylor J., et al. (2018) **Thyroid hormone signaling specifies cone subtypes in human retinal organoids** *Science (1979)* **362**:eaau6348 https://doi.org/10.1126/science.aau6348 | Google Scholar

39. La Manno G., Soldatov R., Zeisel A., Braun E., Hochgerner H., Petukhov V., Lidschreiber K., Kastriti M.E., Lönnerberg P., Furlan A., et al. (2018) **RNA velocity of single cells** *Nature* **560**:494–498 https://doi.org/10.1038/s41586-018-0414-6 | Google Scholar

40. Roesch K., Jadhav A.P., Trimarchi J.M., Stadler M.B., Roska B., Sun B.B., Cepko C.L (2008) **The transcriptome of retinal Müller glial cells** *Journal of Comparative Neurology* **509**:225–238 https://doi.org/10.1002/cne.21730 | Google Scholar

41. Pereiro X., Miltner A.M., La Torre A., Vecino E. (2020) **Effects of Adult Müller Cells and Their Conditioned Media on the Survival of Stem Cell-Derived Retinal Ganglion Cells** *Cells* **9**:1759 https://doi.org/10.3390/cells9081759 | Google Scholar

42. Blackshaw S., Harpavat S., Trimarchi J., Cai L., Huang H., Kuo W.P., Weber G., Lee K., Fraioli R.E., Cho S.-H., et al. (2004) **Genomic Analysis of Mouse Retinal Development** *PLoS Biol* **2**:e247 https://doi.org/10.1371/journal.pbio.0020247 | Google Scholar

43. Walcott J.C., Provis J.M (2003) **Müller cells express the neuronal progenitor cell marker nestin in both differentiated and undifferentiated human foetal retina** *Clin Exp Ophthalmol* **31**:246–249 https://doi.org/10.1046/j.1442-9071.2003.00638.x | Google Scholar

44. Finkbeiner C., Ortuño-Lizarán I., Sridhar A., Hooper M., Petter S., Reh T.A (2022) **Single-cell ATAC-seq of fetal human retina and stem-cell-derived retinal organoids shows changing chromatin landscapes during cell fate acquisition** *Cell Rep* **38** https://doi.org/10.1016/j.celrep.2021.110294 | Google Scholar

45. Marquardt T., Ashery-Padan R., Andrejewski N., Scardigli R., Guillemot F., Gruss P (2001) **Pax6 Is Required for the Multipotent State of Retinal Progenitor Cells** *Cell* **105**:43–55 https://doi.org/10.1016/S0092-8674(01)00295-1 | Google Scholar

46. Poché R.A., Furuta Y., Chaboissier M.C., Schedl A., Behringer R.R (2008) **Sox9 is expressed in mouse multipotent retinal progenitor cells and functions in Müller Glial cell development**

Journal of Comparative Neurology **510**:237–250 https://doi.org/10.1002/cne.21746 | Google Scholar

47. Hafler B.P., Surzenko N., Beier K.T., Punzo C., Trimarchi J.M., Kong J.H., Cepko C.L (2012) **Transcription factor Olig2 defines subpopulations of retinal progenitor cells biased toward specific cell fates** *Proceedings of the National Academy of Sciences* **109**:7882–7887 https://doi.org/10.1073/pnas.1203138109 | Google Scholar

48. Zhang J., Benavente C.A., McEvoy J., Flores-Otero J., Ding L., Chen X., Ulyanov A., Wu G., Wilson M., Wang J., et al. (2012) **A novel retinoblastoma therapy from genomic and epigenetic analyses** *Nature* **481**:329–334 https://doi.org/10.1038/nature10733 | Google Scholar

49. Blomgren P., Chandrasekhar J., Di Paolo J.A., Fung W., Geng G., Ip C., Jones R., Kropf J.E., Lansdon E.B., Lee S., et al. (2020) **Discovery of Lanraplenib (GS-9876): A Once-Daily Spleen Tyrosine Kinase Inhibitor for Autoimmune Diseases** *ACS Med Chem Lett* **11**:506–513 https://doi.org/10.1021/acsmedchemlett.9b00621 | Google Scholar

50. Kamieniarz-Gdula K., Proudfoot N.J (2019) **Transcriptional Control by Premature Termination: A Forgotten Mechanism** *Trends in Genetics* **35**:553–564 https://doi.org/10.1016/j.tig.2019.05.005 | Google Scholar

51. Master A., Nauman A (2014) **THRB (Thyroid Hormone Receptor, Beta)** *Atlas Genet Cytogenet Oncol Haematol* **18**:400–433 https://doi.org/10.4267/2042/53769 | Google Scholar

52. Mercer T.R., Wilhelm D., Dinger M.E., Soldà G., Korbie D.J., Glazov E.A., Truong V., Schwenke M., Simons C., Matthaei K.I., et al. (2011) **Expression of distinct RNAs from 3' untranslated regions** *Nucleic Acids Res* **39**:2393–2403 https://doi.org/10.1093/nar/gkq1158 | Google Scholar

53. Fischer A.J., Foster S., Scott M.A., Sherwood P (2008) **Transient expression of LIM-domain transcription factors is coincident with delayed maturation of photoreceptors in the chicken retina** *J Comp Neurol* **506**:584–603 https://doi.org/10.1002/cne.21578 | Google Scholar

54. Irie S., Sanuki R., Muranishi Y., Kato K., Chaya T., Furukawa T (2015) **Rax Homeoprotein Regulates Photoreceptor Cell Maturation and Survival in Association with Crx in the Postnatal Mouse Retina** *Mol Cell Biol* **35**:2583–2596 https://doi.org/10.1128/MCB.00048-15 | Google Scholar

55. Chen C.-M.A., Cepko C.L (2002) **The chicken RaxL gene plays a role in the initiation of photoreceptor differentiation** *Development* **129**:5363–5375 https://doi.org/10.1242/dev.00114 | Google Scholar

56. Welby E., Lakowski J., Di Foggia V., Budinger D., Gonzalez-Cordero A., Lun A.T.L., Epstein M., Patel A., Cuevas E., Kruczek K., et al. (2017) **Isolation and Comparative Transcriptome Analysis of Human Fetal and iPSC-Derived Cone Photoreceptor Cells** *Stem Cell Reports* **9**:1898–1915 https://doi.org/10.1016/j.stemcr.2017.10.018 | Google Scholar

57. Chen J., Rattner A., Nathans J (2005) **The rod photoreceptor-specific nuclear receptor Nr2e3 represses transcription of multiple cone-specific genes** *Journal of Neuroscience* **25**:118–129 https://doi.org/10.1523/JNEUROSCI.3571-04.2005 | Google Scholar

58. Baluapuri A., Wolf E., Eilers M (2020) **Target gene-independent functions of MYC oncoproteins** *Nat Rev Mol Cell Biol* **21**:255–267 https://doi.org/10.1038/s41580-020-0215-2 | Google Scholar

59. Liu H., Zhang Y., Zhang Y.-Y., Li Y.-P., Hua Z.-Q., Zhang C.-J., Wu K.-C., Yu F., Zhang Y., Su J., et al. (2020) **Human embryonic stem cell-derived organoid retinoblastoma reveals a cancerous origin** *Proceedings of the National Academy of Sciences* **117**:33628–33638 https://doi.org/10.1073/pnas.2011780117 | Google Scholar

60. Pettker C.M., Goldberg J.D., El-Sayed Y.Y., Copel J.A., Committee on Obstetric Practice, the American Institute of Ultrasound in Medicine, and the Society for Maternal-Fetal Medicine, D (2017) **Committee Opinion No 700: Methods for Estimating the Due Date** *Obstetrics & Gynecology* **129** Google Scholar

61. Martin M (2011) **Cutadapt removes adapter sequences from high-throughput sequencing reads** *EMBnet J* **17**:10 https://doi.org/10.14806/ej.17.1.200 | Google Scholar

62. Kim D., Paggi J.M., Park C., Bennett C., Salzberg S.L (2019) **Graph-based genome alignment and genotyping with HISAT2 and HISAT-genotype** *Nat Biotechnol* **37**:907–915 https://doi.org/10.1038/s41587-019-0201-4 | Google Scholar

63. Pertea M., Pertea G.M., Antonescu C.M., Chang T.-C., Mendell J.T., Salzberg S.L (2015) **StringTie enables improved reconstruction of a transcriptome from RNA-seq reads** *Nat Biotechnol* **33**:290–295 https://doi.org/10.1038/nbt.3122 | Google Scholar

64. Soneson C., Love M.I., Robinson M.D (2015) **Differential analyses for RNA-seq: transcript-level estimates improve gene-level inferences** *F1000Res* **4**:1521 https://doi.org/10.12688/f1000research.7563.1 | Google Scholar

65. Orjuela S., Huang R., Hembach K.M., Robinson M.D., Soneson C (2019) **ARMOR: An A utomated R eproducible MO dular Workflow for Preprocessing and Differential Analysis of R NA-seq Data** *G3 Genes|Genomes|Genetics* **9**:2089–2096 https://doi.org/10.1534/g3.119.400185 | Google Scholar

66. Butler A., Hoffman P., Smibert P., Papalexi E., Satija R (2018) **Integrating single-cell transcriptomic data across different conditions, technologies, and species** *Nat Biotechnol* **36**:411–420 https://doi.org/10.1038/nbt.4096 | Google Scholar

67. Stuart T., Butler A., Hoffman P., Hafemeister C., Papalexi E., Mauck W.M., Hao Y., Stoeckius M., Smibert P., Satija R (2019) **Comprehensive Integration of Single-Cell Data** *Cell* **177**:1888–1902 https://doi.org/10.1016/j.cell.2019.05.031 | Google Scholar

68. McInnes L., Healy J., Melville J (2018) **UMAP: Uniform Manifold Approximation and Projection for Dimension Reduction** *ArXiv* https://doi.org/10.48550/ARXIV.1802.03426 | Google Scholar

69. Becht E., McInnes L., Healy J., Dutertre C.-A., Kwok I.W.H., Ng L.G., Ginhoux F., Newell E.W (2019) **Dimensionality reduction for visualizing single-cell data using UMAP** *Nat Biotechnol* **37**:38–44 https://doi.org/10.1038/nbt.4314 | Google Scholar

70. Blondel V.D., Guillaume J.-L., Lambiotte R., Lefebvre E (2008) **Fast unfolding of communities in large networks** *Journal of Statistical Mechanics: Theory and Experiment* **2008**:P10008 https://doi.org/10.1088/1742-5468/2008/10/P10008 | Google Scholar

71. Alasoo K (2019) **wiggleplotr: Make read coverage plots from BigWig files** *R package* version 1.8.0

72. Anders S., Reyes A., Huber W (2012) **Detecting differential usage of exons from RNA-seq data** *Genome Res* **22**:2008–2017 https://doi.org/10.1101/gr.133744.111 | Google Scholar

73. Ewels P.A., Peltzer A., Fillinger S., Patel H., Alneberg J., Wilm A., Garcia M.U., Di Tommaso P., Nahnsen S. (2020) **The nf-core framework for community-curated bioinformatics pipelines** *Nat Biotechnol* **38**:276–278 https://doi.org/10.1038/s41587-020-0439-x | Google Scholar

74. Li H (2018) **Minimap2: pairwise alignment for nucleotide sequences** *Bioinformatics* **34**:3094–3100 https://doi.org/10.1093/bioinformatics/bty191 | Google Scholar

75. Svoboda M., Frost H.R., Bosco G (2022) **Internal oligo(dT) priming introduces systematic bias in bulk and single-cell RNA sequencing count data** *NAR Genom Bioinform* **4**:lqac035 https://doi.org/10.1093/nargab/lqac035 | Google Scholar

76. Ibrahim M.M., Kramann R (2019) **genesorteR: Feature Ranking in Clustered Single Cell Data** *bioRxiv* https://doi.org/10.1101/676379 | Google Scholar

77. Blighe K., Rana S., Lewis M. (2018) **EnhancedVolcano: Publication-ready volcano plots with enhanced colouring and labeling** *R package*

78. Liao Y., Wang J., Jaehnig E.J., Shi Z., Zhang B (2019) **WebGestalt 2019: gene set analysis toolkit with revamped UIs and APIs** *Nucleic Acids Res* **47**:W199–W205 https://doi.org/10.1093/nar/gkz401 | Google Scholar

79. Aibar S., González-Blas C.B., Moerman T., Huynh-Thu V.A., Imrichova H., Hulselmans G., Rambow F., Marine J.-C., Geurts P., Aerts J., et al. (2017) **SCENIC: single-cell regulatory network inference and clustering** *Nat Methods* **14**:1083–1086 https://doi.org/10.1038/nmeth.4463 | Google Scholar

80. Cao J., Spielmann M., Qiu X., Huang X., Ibrahim D.M., Hill A.J., Zhang F., Mundlos S., Christiansen L., Steemers F.J., et al. (2019) **The single-cell transcriptional landscape of mammalian organogenesis** *Nature* **566**:496–502 https://doi.org/10.1038/s41586-019-0969-x | Google Scholar

81. Bankhead P., Loughrey M.B., Fernández J.A., Dombrowski Y., McArt D.G., Dunne P.D., McQuaid S., Gray R.T., Murray L.J., Coleman H.G., et al. (2017) **QuPath: Open source software for digital pathology image analysis** *Sci Rep* **7**:16878 https://doi.org/10.1038/s41598-017-17204-5 | Google Scholar

82. Schmidt U., Weigert M., Broaddus C., Myers G (2018) **Cell Detection with Star-Convex Polygons** In: *Medical Image Computing and Computer Assisted Intervention – MICCAI 2018* pp. 265–273 https://doi.org/10.1007/978-3-030-00934-2_30 | Google Scholar

83. Cheng H (2004) **Photoreceptor-specific nuclear receptor NR2E3 functions as a transcriptional activator in rod photoreceptors** *Hum Mol Genet* **13**:1563–1575 https://doi.org/10.1093/hmg/ddh173 | Google Scholar

84. Lerner L.E., Gribanova Y.E., Ji M., Knox B.E., Farber D.B (2001) **Nrl and Sp Nuclear Proteins Mediate Transcription of Rod-specific cGMP-phosphodiesterase β-Subunit Gene** *Journal of Biological Chemistry* **276**:34999–35007 https://doi.org/10.1074/jbc.M103301200 | Google Scholar

85. Lee S., Cobrinik D (2020) **Improved third-generation lentiviral packaging with pLKO.1C vectors** *Biotechniques* **68**:349–352 https://doi.org/10.2144/btn-2019-0155 | Google Scholar

Author information

Dominic WH Shayler
The Vision Center, Department of Surgery, and Saban Research Institute, Children's Hospital Los Angeles, Los Angeles, United States, Development, Stem Cell, and Regenerative Medicine Program, Keck School of Medicine, University of Southern California, Los Angeles, United States
ORCID iD: 0000-0003-1971-2617

Kevin Stachelek
The Vision Center, Department of Surgery, and Saban Research Institute, Children's Hospital Los Angeles, Los Angeles, United States, Cancer Biology and Genomics Program, Keck School of Medicine, University of Southern California, Los Angeles, United States

Linda Cambier
The Vision Center, Department of Surgery, and Saban Research Institute, Children's Hospital Los Angeles, Los Angeles, United States

Sunhye Lee
The Vision Center, Department of Surgery, and Saban Research Institute, Children's Hospital Los Angeles, Los Angeles, United States

Jinlun Bai
The Vision Center, Department of Surgery, and Saban Research Institute, Children's Hospital Los Angeles, Los Angeles, United States, Development, Stem Cell, and Regenerative Medicine Program, Keck School of Medicine, University of Southern California, Los Angeles, United States

Bhavana Bhat
The Vision Center, Department of Surgery, and Saban Research Institute, Children's Hospital Los Angeles, Los Angeles, United States

Mark W Reid
The Vision Center, Department of Surgery, and Saban Research Institute, Children's Hospital Los Angeles, Los Angeles, United States

Daniel J Weisenberger
Department of Cancer Biology, Keck School of Medicine, University of Southern California, Los Angeles, United States, Norris Comprehensive Cancer Center, Keck School of Medicine, University of Southern California, Los Angeles, United States

Jennifer G Aparicio
The Vision Center, Department of Surgery, and Saban Research Institute, Children's Hospital Los Angeles, Los Angeles, United States

Yeha Kim
The Vision Center, Department of Surgery, and Saban Research Institute, Children's Hospital Los Angeles, Los Angeles, United States

Mitali Singh
The Vision Center, Department of Surgery, and Saban Research Institute, Children's Hospital Los Angeles, Los Angeles, United States

Maxwell Bay
Development, Stem Cell, and Regenerative Medicine Program, Keck School of Medicine, University of Southern California, Los Angeles, United States

Matthew E Thornton
Maternal-Fetal Medicine Division of the Department of Obstetrics and Gynecology, Keck School of Medicine, University of Southern California, Los Angeles, United States

Eamon K Doyle
Department of Radiology and The Saban Research Institute, Children's Hospital Los Angeles, Los Angeles, United States, Department of Radiology, Keck School of Medicine, University of Southern California, Los Angeles, United States

Zachary Fouladian
The Vision Center, Department of Surgery, and Saban Research Institute, Children's Hospital Los Angeles, Los Angeles, United States, Development, Stem Cell, and Regenerative Medicine Program, Keck School of Medicine, University of Southern California, Los Angeles, United States

Stephan G Erberich
Department of Radiology and The Saban Research Institute, Children's Hospital Los Angeles, Los Angeles, United States, Department of Radiology, Keck School of Medicine, University of Southern California, Los Angeles, United States

Brendan H Grubbs
Maternal-Fetal Medicine Division of the Department of Obstetrics and Gynecology, Keck School of Medicine, University of Southern California, Los Angeles, United States

Michael A Bonaguidi
Department of Development, Stem Cell, and Regenerative Medicine, Keck School of Medicine, University of Southern California, Los Angeles, United States
ORCID iD: 0000-0002-9295-4762

Cheryl Mae Craft
Department of Integrative Anatomical Sciences, Keck School of Medicine, University of Southern California, Los Angeles, United States, USC Roski Eye Institute, Department of Ophthalmology, Keck School of Medicine, University of Southern California, Los Angeles, United States

Hardeep P Singh
The Vision Center, Department of Surgery, and Saban Research Institute, Children's Hospital Los Angeles, Los Angeles, United States, USC Roski Eye Institute, Department of Ophthalmology, Keck School of Medicine, University of Southern California, Los Angeles, United States

David Cobrinik
The Vision Center, Department of Surgery, and Saban Research Institute, Children's Hospital Los Angeles, Los Angeles, United States, Department of Cancer Biology, Keck School of Medicine, University of Southern California, Los Angeles, United States, Norris Comprehensive Cancer Center, Keck School of Medicine, University of Southern California, Los Angeles, United States, USC Roski Eye Institute, Department of Ophthalmology, Keck School of Medicine, University of Southern California, Los Angeles, United States
ORCID iD: 0000-0002-4478-2417

For correspondence: dcobrinik@chla.usc.edu

Editors

Reviewing Editor
Robert Johnston
Johns Hopkins University, Baltimore, United States of America

Senior Editor
Claude Desplan
New York University, New York, United States of America

Reviewer #1 (Public review):

Summary:

The authors have used full length single cell sequencing on a sorted population of human fetal retina to delineate expression patterns associated with the progression of progenitors to rod and cone photoreceptors. They find that rod.cone precursors contain a mix of rod/cone determinants, with a bias in both amounts and isoform balance likely deciding the ultimate cell fate. Markers of early rod/cone hybrids are clarified, and a gradient of lncRNAs is uncovered in maturing cones. Comparison of early rods and cones exposes an enriched MYCN regulon, as well as expression of SYK, which may contribute to tumor initiation in RB1 deficient cone precursors.

Strengths:

The insight into how cone and rod transcripts are mixed together at first is important and clarifies a long-standing notion in the field.

The discovery of distinct active vs inactive mRNA isoforms for rod and cone determinants is crucial to understand how cells make the decision to form one or the other cell type. This is only really possible with full length scRNAseq analysis.

New markers of subpopulations are also uncovered, such as CHRNA1 in rod/cone hybrids that seem to give rise to either rods or cones.

Regulon analyses provide insight into key transcription factor programs linked to rod or cone fates.

The gradient of lncRNAs in maturing cones is novel, and while the functional significance is unclear, it opens up a new line of questioning around photoreceptor maturation.

The finding that SYK mRNA is naturally expressed in cone precursors is novel, as previously it was assumed that SYK expression required epigenetic rewiring in tumors.

Weaknesses:

Functional data on many new hypothesis regarding potential players in cone genesis are not performed, but these are beyond the scope of the current work.

Validation of the SYK inhibitor data e.g. by genetic means, is not included, but the authors acknowledge this caveat throughout.

https://doi.org/10.7554/eLife.101918.2.sa3

Reviewer #2 (Public review):

Summary:

The authors used deep full-length single-cell sequencing to study the human photoreceptor development, with a particular emphasis on the characteristics of photoreceptors that may contribute to retinoblastoma.

Strengths:

This single-cell study captures gene regulation in photoreceptors across different developmental stages, defining post-mitotic cone and rod populations by highlighting their unique gene expression profiles through analyses such as RNA velocity and SCENIC. By leveraging full-length sequencing data, the study identifies differentially expressed isoforms of NRL and THRB in L/M cone and rod precursors, illustrating the dynamic gene regulation involved in photoreceptor fate commitment. Additionally, the authors performed high-resolution clustering to explore markers defining developing photoreceptors across the fovea and peripheral retina, particularly characterizing SYK's role in the proliferative response of cones in the RB loss background. The study provides an in-depth analysis of developing human photoreceptors, with the authors conducting thorough analyses using full-length single-cell RNA sequencing. The strength of the study lies in its design, which integrates single-cell full-length RNA-seq, long-read RNA-seq, and follow-up histological and functional experiments to provide compelling evidence supporting their conclusions. The model of cell type-dependent splicing for NRL and THRB is particularly intriguing. Moreover, the potential involvement of the SYK and MYC pathways with RB in cone progenitor cells aligns with previous literature, offering additional insights into RB development.

Weaknesses:

The manuscript feels somewhat unfocused, with a lack of a strong connection between the analysis of developing photoreceptors, which constitutes the bulk of the manuscript, and the discussion on retinoblastoma. Additionally, given the recent publication of several single-cell studies on developing human retina, it is important for the authors to cross-validate their findings and adjust their statements where appropriate.

Comments on revisions:

The authors have done quite thorough work addressing concerns raised by myself and other reviewers. The identification of unresolved developing state of rod/cone precursor cell is interesting and intriguing. I do not have much more to add.

https://doi.org/10.7554/eLife.101918.2.sa2

Reviewer #3 (Public review):

Summary:

The authors use high-depth, full-length scRNA-Seq analysis of fetal human retina to identify novel regulators of photoreceptor specification and retinoblastoma progression.

Strengths:

The use of high-depth, full-length scRNA-Seq to identify functionally important alternatively spliced variants of transcription factors controlling photoreceptor subtype specification, and identification of SYK as a potential mediator of RB1-dependent cell cycle reentry in immature cone photoreceptors.

Weaknesses:

Relatively minor. This is a technically strong and thorough study that is broadly useful to investigators studying retinal development and retinoblastoma.

Comments on revisions:

The authors have addressed all points raised in the review and considerably strengthened the manuscript. No additional changes are required.

https://doi.org/10.7554/eLife.101918.2.sa1

Author response:

The following is the authors' response to the original reviews

> ***Public Reviews:***
>
> ***Reviewer #1 (Public review):***
>
> *Summary:*
>
> *The authors have used full-length single-cell sequencing on a sorted population of human fetal retina to delineate expression patterns associated with the progression of progenitors to rod and cone photoreceptors. They find that rod and cone precursors contain a mix of rod/cone determinants, with a bias in both amounts and isoform balance likely deciding the ultimate cell fate. Markers of early rod/cone hybrids are clarified, and a gradient of lncRNAs is uncovered in maturing cones. Comparison of early rods and cones exposes an enriched MYCN regulon, as well as expression of SYK, which may contribute to tumor initiation in RB1 deficient cone precursors.*
>
> *Strengths:*

> *(1) The insight into how cone and rod transcripts are mixed together at first is important and clarifies a long-standing notion in the field.*
>
> *(2) The discovery of distinct active vs inactive mRNA isoforms for rod and cone determinants is crucial to understanding how cells make the decision to form one or the other cell type. This is only really possible with full-length scRNAseq analysis.*
>
> *(3) New markers of subpopulations are also uncovered, such as CHRNA1 in rod/cone hybrids that seem to give rise to either rods or cones.*
>
> *(4) Regulon analyses provide insight into key transcription factor programs linked to rod or cone fates.*
>
> *(5) The gradient of lncRNAs in maturing cones is novel, and while the functional significance is unclear, it opens up a new line of questioning around photoreceptor maturation.*
>
> *(6) The finding that SYK mRNA is naturally expressed in cone precursors is novel, as previously it was assumed that SYK expression required epigenetic rewiring in tumors.*

We thank the reviewer for describing the study's strengths, reflecting the major conclusions of the initially submitted manuscript. However, based on new analyses – including the requested analyses of other scRNA-seq datasets, our revision clarifies that:

- related to point (1), cone and rod transcripts do not appear to be mixed together at first (i.e., in immediately post-mitotic immature cone and rod precursors) but appear to be coexpressed in subsequent cone and rod precursor stages; and

- related to point (3), *CHRNA1* appears to mark immature cone precursors that are distinct from the maturing cone and rod precursors that co-express cone- and rod-related RNAs (despite the similar UMAP positions of the two populations in our dataset).

> *Weaknesses:*
>
> *(1) The writing is very difficult to follow. The nomenclature is confusing and there are contradictory statements that need to be clarified.*
>
> *(2) The drug data is not enough to conclude that SYK inhibition is sufficient to prevent the division of RB1 null cone precursors. Drugs are never completely specific so validation is critical to make the conclusion drawn in the paper.*

We thank the reviewer for noting these important issues. Accordingly, in the revised manuscript:

(1) We improve the writing and clarify the nomenclature and contradictory statements, particularly those noted in the Reviewer's Recommendations for Authors.

(2) We scale back claims related to the role of SYK in the cone precursor response to *RB1* loss, with wording changes in the Abstract, Results, and Discussion, which now recognize that the inhibitor studies only support the possibility that cone-intrinsic SYK expression contributes to retinoblastoma initiation, as detailed in our responses to Reviewer's Recommendations for Authors. We agree and now mention that genetic perturbation of *SYK* is required to prove its role.

> ***Reviewer #2 (Public review):***
>
> *Summary:*

> *The authors used deep full-length single-cell sequencing to study human photoreceptor development, with a particular emphasis on the characteristics of photoreceptors that may contribute to retinoblastoma.*
>
> *Strengths:*
>
> *This single-cell study captures gene regulation in photoreceptors across different developmental stages, defining post-mitotic cone and rod populations by highlighting their unique gene expression profiles through analyses such as RNA velocity and SCENIC. By leveraging fulllength sequencing data, the study identifies differentially expressed isoforms of NRL and THRB in L/M cone and rod precursors, illustrating the dynamic gene regulation involved in photoreceptor fate commitment. Additionally, the authors performed high-resolution clustering to explore markers defining developing photoreceptors across the fovea and peripheral retina, particularly characterizing SYK's role in the proliferative response of cones in the RB loss background. The study provides an in-depth analysis of developing human photoreceptors, with the authors conducting thorough analyses using full-length single-cell RNA sequencing. The strength of the study lies in its design, which integrates single-cell full-length RNA-seq, longread RNA-seq, and follow-up histological and functional experiments to provide compelling evidence supporting their conclusions. The model of cell type-dependent splicing for NRL and THRB is particularly intriguing. Moreover, the potential involvement of the SYK and MYC pathways with RB in cone progenitor cells aligns with previous literature, offering additional insights into RB development.*

We thank the reviewer for summarizing the main findings and noting the compelling support for the conclusions, the intriguing cell type-dependent splicing of rod and cone lineage factors, and the insights into retinoblastoma development.

> *Weaknesses:*
>
> *The manuscript feels somewhat unfocused, with a lack of a strong connection between the analysis of developing photoreceptors, which constitutes the bulk of the manuscript, and the discussion on retinoblastoma. Additionally, given the recent publication of several single-cell studies on the developing human retina, it is important for the authors to cross-validate their findings and adjust their statements where appropriate.*

We agree that the manuscript covers a range of topics resulting from the full-length scRNAseq analyses and concur that some studies of developing photoreceptors were not well connected to retinoblastoma. However, we also note that the connection to retinoblastoma is emphasized in several places in the Introduction and throughout the manuscript and was a significant motivation for pursuing the analyses. We suggest that it was valuable to highlight how deep, fulllength scRNA-seq of developing retina provides insights into retinoblastoma, including i) the similar biased expression of NRL transcript isoforms in cone precursors and RB tumors, ii) the cone precursors' co-expression of rod- and cone-related genes such as *NR2E3* and *GNAT2*, which may explain similar co-expression in RB cells, and iii) the expression of *SYK* in early cones and RB cells. While the earlier version had mainly highlighted point (iii), the revised Discussion further refers to points (i) and (ii) as described further in the response to the Reviewer's Recommendations for Authors.

We address the Reviewer's request to cross-validate our findings with those of other single-cell studies of developing human retina by relating the different photoreceptor-related cell populations identified in our study to those characterized by Zuo et al (PMID 39117640), which was specifically highlighted by the reviewer and is especially useful for such cross-validation given the extraordinarily large ~ 220,000 cell dataset covering a wide range of retinal ages (pcw 8–23) and spatiotemporally stratified by macular or peripheral retina

location. Relevant analyses of the Zuo et al dataset are shown in Supplementary Figures S3G-H, S10B, S11A-F, and S13A,B.

> ***Reviewer #3 (Public review):***
>
> *Summary:*
>
> *The authors use high-depth, full-length scRNA-Seq analysis of fetal human retina to identify novel regulators of photoreceptor specification and retinoblastoma progression.*
>
> *Strengths:*
>
> *The use of high-depth, full-length scRNA-Seq to identify functionally important alternatively spliced variants of transcription factors controlling photoreceptor subtype specification, and identification of SYK as a potential mediator of RB1-dependent cell cycle reentry in immature cone photoreceptors.*
>
> *Human developing fetal retinal tissue samples were collected between 13-19 gestational weeks and this provides a substantially higher depth of sequencing coverage, thereby identifying both rare transcripts and alternative splice forms, and thereby representing an important advance over previous droplet-based scRNA-Seq studies of human retinal development.*
>
> *Weaknesses:*
>
> *The weaknesses identified are relatively minor. This is a technically strong and thorough study, that is broadly useful to investigators studying retinal development and retinoblastoma.*

We thank the reviewer for describing the strengths of the study. Our revision addresses the concerns raised separately in the Reviewer's Recommendations for Authors, as detailed in the responses below.

> ***Recommendations for the authors:***
>
> ***Reviewing Editor Comments:***
>
> *The reviewers have completed their reviews. Generally, they note that your work is important and that the evidence is generally convincing. The reviewers are in general agreement that the paper adds to the field. The findings of rod/cone fate determination at a very early stage are intriguing. Generally, the paper would benefit from clarifications in the writing and figures. Experimentally, the paper would benefit from validation of the drug data, for example using RNAi or another assay. Alternatively, the authors could note the caveats of the drug experiments and describe how they could be improved. In terms of analysis, the paper would be improved by additional comparisons of the authors' data to previously published datasets.*

We thank the reviewing editor for this summary. As described in the individual reviewer responses, we clarify the writing and figures and provide comparisons to previously published datasets (in particular, the large snRNA-seq dataset of Zuo et al., 2024 (PMID 39117640). With regard to the drug (i.e., SYK inhibitor) studies, we opted to provide caveats and describe the need for genetic approaches to validate the role of SYK, owing to the infeasibility of completing genetic perturbation experiments in the appropriate timeframe. We are grateful for the opportunity to present our findings with appropriate caveats.

Reviewer #1 (Recommendations for the authors):

Shayler cell sort human progenitor/rod/cone populations then full-length single cell RNAseq to expose features that distinguish paths towards rods or cones. They initially distinguish progenitors (RPCs), immature photoreceptor precursors (iPRPs), long/medium wavelength (LM) cones, late-LM cones, short wavelength (S) cones, early rods (ER) and late rods (LR), which exhibit distinct transcription factor regulons (Figures 1, 2). These data expose expected and novel enriched genes, and support the notion that S cones are a default state lacking expression of rod (NRL) or cone (THRB) determinants but retaining expression of generic photoreceptor drivers (CRX/OTX2/NEUROD1 regulons). They identify changes in regulon activity, such as increasing NRL activity from iPRP to ER to LR, but decreasing from iPRP to cones, or increasing RAX/ISL2/THRB regulon activity from iPRP to LM cones, but decreasing from iPRP to S cones or rods.

They report co-expression of rod/cone determinants in LM and ER clusters, and the ratios are in the expected directions (NRLTHRB or RXRG in ER). A novel insight from the FL seq is that there are differing variants generated in each cell population. Full-length NRL (FL-NRL) predominates in the rod path, whereas truncated NRL (Tr-NRL) does so in the cone path, then similar (but opposite) findings are presented for THRB (Fig 3, 4), whereas isoforms are not a feature of RXRG expression, just the higher expression in cones.

The authors then further subcluster and perform RNA velocity to uncover decision points in the tree (Figure 5). They identify two photoreceptor precursor streams, the Transitional Rods (TRs) that provide one source for rod maturation and (reusing the name from the initial clustering) iPRPs that form cones, but also provide a second route to rods. TR cells closest to RPCs (immediately post-mitotic) have higher levels of the rod determinant NR2E3 and NRL, whereas the higher resolution iPRPs near RPCs lack NR2E3 and have higher levels of ONECUT1, THRB, and GNAT2, a cone bias. These distinct rod-biased TR and cone-biased high-resolution iPRPs were not evident in published scRNAseq with 3' end-counting (i.e. not FL seq). Regulon analysis confirmed higher NRL activity in TR cells, with higher THRB activity in highresolution iPRP cells.

Many of the more mature high-resolution iPRPs show combinations of rod (GNAT1, NR2E3) and cone (GNAT2, THRB) paths as well as both NRL and THRB regulons, but with a bias towards cone-ness (Figure 6). Combined FISH/immunofluorescence in fetal retina uncovers cone-biased RXRG-protein-high/NR2E3-protein-absent cone-fated cells that nevertheless expressed NR2E3 mRNA. Thus early cone-biased iPRP cells express rod gene mRNA, implying a rod-cone hybrid in early photoreceptor development. The authors refer to these as "bridge region iPRP cells".

In Figure 7, they identify CHRNA1 as the most specific marker of these bridge cells (overlapping with ATOH7 and DLL3, previously linked to cone-biased precursors), and FISH shows it is expressed in rod-biased NRL protein-positive and cone-biased RXRG proteinpositive cones at fetal week 12.

Figure 8 outlines the graded expression of various lncRNAs during cone maturation, a novel pattern.

Finally (Figure 9), the authors identify differential genes expressed in early rods (ER cluster from Figure 1) vs early cones (LM cluster, excluding the most mature opsin+ cells), revealing high levels of MYCN targets in cones. They also find SYK expression in cones. SYK was previously linked to retinoblastoma, so intrinsic expression may predispose cone precursors to transformation upon RB loss. They finish by showing that a SYK inhibitor blocks the proliferation of dividing RB1 knockdown cone precursors in the human fetal retina.

> *Overall, the authors have uncovered interesting patterns of biased expression in cone/rod developmental paths, especially relating to the isoform differences for NRL and THRB which add a new layer to our understanding of this fate choice. The analyses also imply that very soon after RPCs exit the cell cycle, they generate post-mitotic precursors biased towards a rod or cone fate, that carry varying proportions of mixed rod/cone determinants and other rod/cone marker genes. They also introduce new markers that may tag key populations of cells that precede the final rod/cone choice (e.g. CHRNA1), catalogue a new lncRNA gradient in cone maturation, and provide insight into potential genes that may contribute to retinoblastoma initiation, like SYK, due to intrinsic expression in cone precursors. However, as detailed below, the text needs to be improved considerably, and overinterpretations need to be moderated, removed, or tested more rigorously with extra data.*
>
> *Major Comments*
>
> *The manuscript is very difficult to follow. The nomenclature is at times torturous, and the description of hybrid rod/cone hybrid cells is confusing in many aspects.*
>
> *(1) A single term, iPRP, is used to refer to an initial low-resolution cluster, and then to a subset of that cluster later in the paper.*

We agree that using immature photoreceptor precursor (iPRP) for both high-resolution and lowresolution clusters was confusing. We kept this name for the low-resolution cluster (which includes both immature cone and immature rod precursors), renamed the high-resolution iPRP cluster immature cone precursors (iCPs). and renamed their transitional rod (TR) counterparts immature rod precursors (iRPs). These designations are based on

- the biased expression of *THRB*, *ONECUT1*, and the THRB regulon in iCPs (Fig. 5D,E);

- the biased expression of *NRL*, *NR2E3*, and NRL regulon iRPs (Fig. 5D,E);

- the partially distinct iCP and iRP UMAP positions (Figure 5C); and

- the evidence of similar immature cone versus rod precursor populations in the Zuo et al 3' snRNA-seq dataset, as noted below and described in two new paragraphs starting at the bottom of p. 12.

> *(2) To complicate matters further, the reader needs to understand the subset within the iPRP referred to as bridge cells, and we are told at one point that the earliest iPRPs lack NR2E3, then that they later co-express NR2E3, and while the authors may be referring to protein and RNA, it serves to further confuse an already difficult to follow distinction. I had to read and re-read the iPRP data many times, but it never really became totally clear.*

We agree that the description of the high-resolution iPRP (now "iCP") subsets was unclear, although our further analyses of a large 3' snRNA-seq dataset in Figure S11 support the impression given in the original manuscript that the earliest iCPs lack *NR2E3* and then later coexpress *NR2E3* while the earliest iRPs lack *THRB* and then later express *THRB*. As described in new text in the Two post-mitotic immature photoreceptor precursor populations section (starting on line 7 of p. 13):

When considering only the main cone and rod precursor UMAP regions, early (pcw 8 – 13) cone precursors expressed *THRB* and lacked *NR2E3* (Figure S11D,E, blue arrows), while early (pcw 10 – 15) rod precursors expressed NR2E3 and lacked THRB (Figure S11D,E, red arrows), similar to RPC-localized iCPs and iRPs in our study (Figure 5D).

Next, as summarized in new text in the Early cone and rod precursors with rod- and conerelated RNA co-expression section (new paragraph at top of p. 16):

Thus, a 3' snRNA-seq analysis confirmed the initial production of immature photoreceptor precursors with either L/M cone-precursor-specific *THRB* or rod-precursor-specific *NR2E3* expression, followed by lower-level co-expression of their counterparts, *NR2E3* in cone precursors and *THRB* in rod precursors. However, in the Zuo et al. analyses, the co-expression was first observed in well-separated UMAP regions, as opposed to a region that bridges the early cone and early rod populations in our UMAP plots. These findings are consistent with the notion that cone- and rod-related RNA co-expression begins in already fate-determined cone and rod precursors, and that such precursors aberrantly intermixed in our UMAP bridge region due to their insufficient representation in our dataset.

Importantly, and as noted in our 'Public response' to Reviewer 1, "*CHRNA1* appears to mark immature cone precursors that are distinct from the maturing cone and rod precursors that coexpress cone- and rod-related RNAs (despite the similar UMAP positions of the two populations in our dataset)." In support of this notion, the immature cone precursors expressing *CHRNA1* and other populations did not overlap in UMAP space in the Zuo et al dataset. We hope the new text cited above along with other changes will significantly clarify the observations.

> *(3) The term "cone/rod precursor" shows up late in the paper (page 12), but it was clear (was it not?) much earlier in this manuscript that cone and rod genes are co-expressed because of the coexpressed NRL and THRB isoforms in Figures 3/4.*

We thank the reviewer for noting that the differential *NRL* and *THRB* isoform expression already implies that cone and rod genes are co-expressed. However, as we now state, the co-expression of RNAs encoding an additional cone marker (*GNAT2*) and rod markers (*GNAT1*, *NR2E3*) was

"suggestive of a proposed hybrid cone/rod precursor state more extensive than implied by the coexpression of different *THRB* and *NRL* isoforms" (first paragraph of "Early cone and rod …" section on p. 14; new text underlined).

> *(4) The (incorrect) impression given later in the manuscript is that the rod/cone transcript mixture applies to just a subset of the iPRP cells, or maybe just the bridge cells (writing is not clear), but actually, neither of those is correct as the more abundant and more mature LM and ER populations analyzed earlier coexpress NRL and THRB mRNAs (Figures 2, 3). Overall, the authors need to vastly improve the writing, simplify/clarify the nomenclature, and better label figures to match the text and help the reader follow more easily and clearly. As it stands, it is, at best, obtuse, and at worst, totally confusing.*

We thank the reviewer for bringing the extent of the confusing terminology and wording to our attention. We revised the terminology (as in our response to point 1) and extensively revised the text. We also performed similar analyses of the Zuo et al. data (as described in more detail in our response to Reviewer 2), which clarifies the distinct status of cells with the "rod/cone transcript mixture" and cells co-expressing early cone and rod precursor markers.

To more clearly describe data related to cells with rod- and cone-related RNA co-expression, we divided the former Figure 6 into two figures, with Figure 6 now showing the cone- and rodrelated RNA co-expression inferred from scRNA-seq and Figure 7 showing *GNAT2* and *NR2E3* co-expression in FISH analyses of human retina plus a new schematic in the new panel 7E.

To separate the conceptually distinct analyses of cone and rod related RNA co-expression and the expression of early photoreceptor precursor markers (which were both found in the so-called bridge region – yet now recognized to be different subpopulations), we separated the analyses of the early photoreceptor precursor markers to form a new section, "Developmental expression of photoreceptor precursor markers and fate determinants," starting on p. 16.

Additionally, we further review the findings and their implications in four revised Discussion paragraphs starting at the bottom of p. 23).

> *(5) The data showing that overexpressing Tr-NRL in murine NIH3T3 fibroblasts blocks FL-NRL function is presented at the end of page 7 and in Figure 3G. Subsequent analysis two paragraphs and two figures later (end page 8, Figure 5C + supp figs) reveal that Tr-NRL protein is not detectable in retinoblastoma cells which derive from cone precursors cells and express Tr-NRL mRNA, and the protein is also not detected upon lentiviral expression of Tr-NRL in human fetal retinal explants, suggesting it is unstable or not translated. It would be preferable to have the 3T3 data and retinoblastoma/explant data juxtaposed. E.g. they could present the latter, then show the 3T3 that even if it were expressed (e.g. briefly) it would interfere with FL-NRL. The current order and spacing are somewhat confusing.*

We thank the reviewer for this suggestion and moved the description of the luciferase assays to follow the retinoblastoma and explant data and switched the order of Figure panels 3G and 3H.

> *(6) On page 15, regarding early rod vs early cone gene expression, the authors state: "although MYCN mRNA was not detected....", yet on the volcano plot in Figure S14A MYCN is one of the marked genes that is higher in cones than rods, meaning it was detected, and a couple of sentences later: "Concordantly, the LM cluster had increased MYCN RNA". The text is thus confusing.*

With respect, we note that the original text read, "although *MYC* RNA was not detected," which related to a statement in the previous sentence that the gene ontology analysis identified "MYC targets." However, given that this distinction is subtle and may be difficult for readers to recognize, we revised the text (now on p. 19) to more clearly describe expression of *MYCN* (but not *MYC*) as follows:

"The upregulation of MYC target genes was of interest given that many MYC target genes are also targets of MYCN, that MYCN protein is highly expressed in maturing (ARR3+) cone precursors but not in NRL+ rods (Figure 10A), and that MYCN is critical to the cone precursor proliferative response to pRB loss8–10. Indeed, whereas *MYC* RNA was not detected, the LM cone cluster had increased *MYCN* RNA …"

> *(7) The authors state that the SYK drug is "highly specific". They provide no evidence, but no drug is 100% specific, and it is possible that off-target hits are important for the drug phenotype. This data should be removed or validated by co-targeting the SYK gene along with RB1.*

We agree that our data only show *the potential* for SYK to contribute to the cone proliferative response; however, we believe the inhibitor study retains value in that a negative result (no effect of the SYK inhibitor) would disprove its potential involvement. To reflect this, we changed wording related to this experiment as follows:

In the Abstract, we changed:

(1) "*SYK*, which contributed to the early cone precursors' proliferative response to *RB1* loss" To: "*SYK*, which was implicated in the early cone precursors' proliferative response to *RB1* loss."

(2) "These findings reveal … and a role for early cone-precursor-intrinsic *SYK* expression." To: "These findings reveal … and suggest a role for early cone-precursor-intrinsic *SYK* expression."

In the last paragraph of the Results, we changed:

(1) "To determine if SYK contributes…" To: "To determine if SYK might contribute…"

(2) "the highly specific SYK inhibitor" To: "the selective SYK inhibitor"

(3) "indicating that cone precursor intrinsic SYK activity is critical to the proliferative response" To: "consistent with the notion that cone precursor intrinsic SYK activity contributes to the proliferative response."

In the Results, we added a final sentence:

"However, given potential SYK inhibitor off-target effects, validation of the role of SYK in retinoblastoma initiation will require genetic ablation studies."

In the Discussion (2nd-to-last paragraph), we changed:

"SYK inhibition impaired pRB-depleted cone precursor cell cycle entry, implying that native SYK expression rather than *de novo* induction contributes to the cone precursors' initial proliferation." To: "…the pRB-depleted cone precursors' sensitivity to a SYK inhibitor suggests that native SYK expression rather than *de novo* induction contributes to the cone precursors' initial proliferation, although genetic ablation of *SYK* is needed to confirm this notion." In the Discussion last sentence, we changed:

"enabled the identification of developmental stage-specific cone precursor features that underlie retinoblastoma predisposition." To: "enabled the identification of developmental stage-specific cone precursor features that are associated with the cone precursors' predisposition to form retinoblastoma tumors."

> *Minor/Typos*
>
> *Figure 7 legend, H should be D.*

We corrected the figure legend (now related to Figure 8).

> ***Reviewer #2 (Recommendations for the authors):***
>
> *(1) The author should take advantage of recently published human fetal retina data, such as PMID:39117640, which includes a larger dataset of cells that could help validate the findings. Consequently, statements like "To our knowledge, this is the first indication of two immediately post-mitotic photoreceptor precursor populations with cone versus rod-biased gene expression" may need to be revised.*

We thank the reviewer for noting the evidence of distinct immediately post-mitotic rod and cone populations published by others after we submitted our manuscript. In response, we omitted the sentence mentioned and extensively cross-checked our results including:

- comparison of our early versus late cone and rod maturation states to the cone and rod precursor versus cone and rod states identified by Zuo et al (new paragraph on the top half of

p. 6 and new figure panels S3G,H);

- detection of distinct immediately post-mitotic versus later cone and rod precursor populations (two new paragraphs on pp. 12-13 and new Figures S10B and S11A-E);

- identification of cone and rod precursor populations that co-express cone and rod marker genes (two new paragraphs starting at the bottom of p. 15 and new Figures S11D-F);

- comparison of expression patterns of immature cone precursor (iCP) marker genes in our and the Zuo et al dataset (new paragraph on top half of p. 17 and new Figure S13).

We also compare the cell states discerned in our study and the Zuo et al. study in a new Discussion paragraph (bottom of p. 23) and new Figure S17.

> *(2) The data generated comes from dissociated cells, which inherently lack spatial context. Additionally, it is unclear whether the dataset represents a pool of retinas from multiple developmental stages, and if so, whether the developmental stage is known for each cell profiled. If this information is available, the authors should examine the distribution of developmental stages on the UMAP and trajectory analysis as part of the quality control process.*

We thank the reviewer for highlighting the importance of spatial context and developmental stage.

Related to whether the dataset represents a pool of retinae from multiple developmental stages, the different cell numbers examined at each time point are indicated in Figure S1A. To draw the readers' attention to this detail, Figure S1A is now cited in the first sentence of the Results.

Related to the age-related cell distributions in UMAP plots, the distribution of cells from each retina and age was (and is) shown in Fig. S1F. In addition, we now highlight the age distributions by segregating the FW13, FW15-17, and FW17-18-19 UMAP positions in the new Figure 1C. We describe the rod temporal changes in a new sentence at the top of p. 5:

"Few rods were detected at FW13, whereas both early and late rods were detected from FW15-19 (Figure 1C), corroborating prior reports [15,20]."

We describe the cone temporal changes and note the likely greater discrimination of cell state changes that would be afforded by separately analyzing macula versus peripheral retina at each age in a new sentence at the bottom of p. 5:

"L/M cone precursors from different age retinae occupied different UMAP regions, suggesting age-related differences in L/M cone precursor maturation (Figure 1C)."

> *Moreover, they should assess whether different developmental stages impact gene expression and isoform ratios. It is well established that cone and rod progenitors typically emerge at different developmental times and in distinct regions of the retina, with minimal physical overlap. Grouping progenitor cells based solely on their UMAP positioning may lead to an oversimplified interpretation of the data.*

(2a) We agree that different developmental stages may impact gene expression and isoform ratios, and evaluated stages primarily based on established Louvain clustering rather than UMAP position. However, we also used UMAP position to segregate so-called RPC-localized and nonRPC-localized iCPs and iRPs, as well as to characterize the bridge region iCP sub-populations. In the revision, we examine whether cell groups defined by UMAP positions helped to identify transcriptomically distinct populations and further examine the

spatiotemporal gene expression patterns of the same genes in the Zuo et al. 3' snRNA-seq dataset.

(2b) Related to analyses of immediately post-mitotic iRPs and iCPs, the new Figure S10A expanded the violin plots first shown in Figure 5D to compare gene expression in RPC-localized versus non-RPC-localized iCPs and iRPs and subsequent cone and rod precursor clusters (also presented in response to Reviewer 3). The new Figure S10C, shows a similar analysis of UMAP region-specific regulon activities. These figures support the idea that there are only subtle UMAP region-related differences in the expression of the selected gene and regulons.

To further evaluate early cone and rod precursors, we compared expression patterns in our cluster- and UMAP-defined cell groups to those of the spatiotemporally defined cell groups in the Zuo et al. 3' snRNA-seq study. The results revealed similar expression timing of the genes examined, although the cluster assignments of a subset of cells were brought into question, especially the assigned rod precursors at pcw 10 and 13, as shown in new Figures S10B (grey columns) and S11, and as described in two new paragraphs starting near the bottom of p.12.

(2c) Related to analyses of iCPs in the so-called bridge region, our analyses of the Zuo et al dataset helped distinguish early cone and rod precursor populations (expressing early markers such as *ATOH7* and *CHRNA1*) from the later stages exhibiting rod- and cone-related gene coexpression, which had intermixed in the UMAP bridge region in our dataset. Further parsing of early cone precursor marker spatiotemporal expression revealed intriguing differences as now described in the second half of a new paragraph at the top of p. 17, as follows:

"Also, different iCP markers had different spatiotemporal expression: *CHRNA1* and *ATOH7* were most prominent in peripheral retina with *ATOH7* strongest at pcw 10 and *CHRNA1* strongest at pcw 13; *CTC-378H22.2* was prominently expressed from pcw 10-13 in both the macula and the periphery; and *DLL3* and *ONECUT1* showed the earliest, strongest, and broadest expression (Figure S13B). The distinct patterns suggest spatiotemporally distinct roles for these factors in cone precursor differentiation."

> *(3) I would commend the authors for performing a validation experiment via RNA in situ to validate some of the findings. However, drawing conclusions from analyzing a small number of cells can still be dangerous. Furthermore, it is not entirely clear how the subclustering is done. Some cells change cell type identities in the high-resolution plot. For example, some iPRP cells from the low-resolution plots in Figure 1 are assigned as TR in high-resolution plots in Figure 5.*
>
> *The authors should provide justification on the identifies of RPC localized iPRP and TR.*
>
> *Comparison of their data with other publicly available data should strengthen their annotation*

We agree that drawing conclusions from scRNA-seq or *in situ* hybridization analysis of a small number of cells can be dangerous and have followed the reviewer's suggestion to compare our data with other publicly available data, focusing on the 3' snRNA-seq of Zuo et al. given its large size and extensive annotation. Our analysis of the Zuo et al. dataset helped clarify cell identities by segregating cone and rod precursors with similar gene expression properties in distinct UMAP regions. However, we noted that the clustering of early cone and rod precursors likely gave numerous mis-assigned cells (as noted in response 2b above and shown in the new Figure S11). It would appear that insights may be derived from the combination of relatively shallow sequencing of a high number of cells *and* deep sequencing of substantially fewer cells.

Related to how subclustering was done, the Methods state, “A nearest-neighbors graph was constructed from the PCA embedding and clusters were identified using a Louvain algorithm at low and high resolutions (0.4 and 1.6)[70],” citing the Blondel et al reference for the Louvain clustering algorithm used in the Seurat package. To clarify this, the results text was revised such that it now indicates the levels used to cluster at low resolution (0.4, p. 4, 2nd paragraph) and at high resolution (1.6, top of p. 11) .

Related to the assignment of some iPRP cells from the low-resolution plots in Figure 1 to the TR cluster (now called the ‘iRP’ ‘cluster) in the high-resolution plots in Figure 5, we suggest that this is consistent with Louvain clustering, which does not follow a single dendrogram hierarchy.

The justification for referring to these groups as RPC-localized iCPs and iRPs relates to their biased gene and regulon expression in Fig. 5D and 5E, as stated on p. 12:

“In the RPC-localized region, iCPs had higher *ONECUT1*, *THRB*, and *GNAT2*, whereas iRPs trended towards higher NRL and NR2E3 (p= 0.19, p=0.054, respectively).”

> *(4) Late-stage LM5 cluster Figure 9 is not defined anywhere in previous figures, in which LM clusters only range from 1 to 4. The inconsistency in cluster identification should be addressed.*

We revised the text related to this as follows:

“Indeed, our scRNA-seq analyses revealed that *SYK* RNA expression increased from the iCP stage through cluster LM4, in contrast to its minimal expression in rods (Figure 10E). Moreover, *SYK* expression was abolished in the five-cell group with properties of late maturing cones (characterized in Figure 1E), here displayed separately from the other LM4 cells and designated LM5 (Figure 10E).” (p. 19-20)

> *(5) Syk inhibitor has been shown to be involved in RB cell survival in previous studies. The manuscript seems to abruptly make the connection between the single-cell data to RB in the last figure. The title and abstract should not distract from the bulk of the manuscript focusing on the rod and cone development, or the manuscript should make more connection to retinoblastoma.*

We appreciate the reviewer’s concern that the title may seem to over-emphasize the connection to retinoblastoma based solely on the SYK inhibitor studies. However, we suggest the title also emphasizes the identification and characterization of early human photoreceptor states, *per se*, and that there are a number of important connections beyond the SYK studies that could warrant the mention of cell-state-specific retinoblastoma-related features in the title.

Most importantly, a prior concern with the cone cell-of-origin theory was that retinoblastoma cells express RNAs thought to mark retinal cell types other than cones, especially rods. The evidence presented here, that cone precursors also express the rod-related genes helps resolve this issue. The issue is noted numerous times in the manuscript, as follows:

In the Introduction, we write:

“However, retinoblastoma cells also express rod lineage factor *NRL* RNAs, which – along with other evidence – suggested a heretofore unexplained connection between rod gene expression and retinoblastoma development[12,13]. Improved discrimination of early photoreceptor states is needed to determine if co-expression of rod- and cone-related genes is adopted during tumorigenesis or reflects the co-expression of such genes in the retinoblastoma cell of origin.” (bottom, p. 2) And:

"In this study, we sought to further define the transcriptomic underpinnings of human photoreceptor development and their relationship to retinoblastoma tumorigenesis." (last paragraph, p. 3)

The Discussion also alluded to this issue and in the revised Discussion, we aimed to make the connection clearer. We previously ended the 3rd-to-last paragraph with,

"iPRP [now iCP] and early LM cone precursors' expression of *NR2E3* and *NRL* RNAs suggest that their presence in retinoblastomas[12,13] reflects their normal expression in the L/M cone precursor cells of origin."

We now separate and elaborate on this point in a new paragraph as follows:

"Our characterization of cone and rod-related RNA co-expression may help resolve questions about the retinoblastoma cell of origin. Past studies suggested that retinoblastoma cells co-express RNAs associated with rods, cones, or other retinal cells due to a loss of lineage fidelity[12]. However, the early L/M cone precursors' expression of NR2E3 and NRL RNAs suggest that their presence in retinoblastomas[12,13] reflects their normal expression in the L/M cone precursor cells of origin. This idea is further supported by the retinoblastoma cells' preferential expression of cone-enriched NRL transcript isoforms (Figure S5B)." (middle of p. 24) Based on the above, we elected to retain the title.

> *Minor comments:*
>
> *(1) It is difficult to see the orange and magenta colors in the Fig 3E RNA-FISH image. The colors should be changed, or the contrast threshold needs to be adjusted to make the puncta stand out more.*

We re-assigned colors, with red for *FL-NRL* puncta and green for *Tr-NRL* puncta.

> *(2) Figure 5C on page 8 should be corrected to Supplementary Figure 5C.*

We thank the reviewer for noting this error and changed the figure citation.

> ***Reviewer #3 (Recommendations for the authors):***
>
> *(1) Minor concerns*
>
> *a. Abbreviation of some words needs to be included, example: FW.*

We now provide abbreviation definitions for FW and others throughout the manuscript.

> *b. Cat # does not matches with the 'key resource table' for many reagents/kits. Some examples are: CD133-PE mentioned on Page # 22 on # 71, SMART-Seq V4 Ultra Low Input RNA Kit and SMARTer Ultra Low RNA Kit for the Fluidigm C1 Sytem on Page # 22 on # 77, Nextera XT DNA Library preparation kit on Page # 23 on # 77.*

We thank the reviewer for noting these discrepancies. We have now checked all catalog numbers and made corrections as needed.

> *c. Cat # and brand name of few reagents & kits is missing and not mentioned either in methods or in key resource table or both. Eg: FBS, Insulin, Glutamine, Penicillin, Streptomycin, HBSS, Quant-iT PicoGreen dsDNA assay, Nextera XT DNA LibraryPreparation Kit, 5' PCR Primer II A with CloneAmp HiFi PCR Premix.*

Catalog numbers and brand names are now provided for the tissue culture and related reagents within the methods text and for kits in the Key Resources Table. Additional descriptions of the primers used for re-amplification and RACE were added to the Methods (p. 28-29).

> *d. Spell and grammar check is needed throughout the manuscript is needed. Example. In Page # 46 RXRylo is misspelled as RXRlo.*

Spelling and grammar checks were reviewed.

> *(2) Methods & Key Resource table.*
>
> *a. In Page # 21, IRB# needs to be stated.*

The IRB protocols have been added, now at top of p. 26.

> *b. In Page # 21, Did the authors dissociate retinae in ice-cold phosphate-buffered saline or papain?*

The relevant sentence was corrected to “dissected while submerged in ice-cold phosphatebuffered saline (PBS) and dissociated as described10.” (p. 26)

> *c. In Page # 21, How did the authors count or enumerate the cell count? Provide the details.*

We now state, “… a 10 µl volume was combined with 10 µl trypan blue and counted using a hemocytometer” (top of p. 27)

> *d. Why did the authors choose to specifically use only 8 cells for cDNA preparation in Page # 22? State the reason and provide the details.*

The reasons for using 8 cells (to prevent evaporation and to manually transfer one slide-worth of droplets to one strip of PCR tubes) and additional single cell collection details are now provided as follows (new text underlined):

“Single cells were sorted on a BD FACSAria I at 4°C using 100 µm nozzle in single-cell mode into each of eight 1.2 µl lysis buffer droplets on parafilm-covered glass slides, with droplets positioned over pre-defined marks … . Upon collection of eight cells per slide, droplets were transferred to individual low-retention PCR tubes (eight tubes per strip) (Bioplastics K69901, B57801) pre-cooled on ice to minimize evaporation. The process was repeated with a fresh piece of parafilm for up to 12 rounds to collect 96 cells). (p. 27, new text underlined)

> *e. Key resource table does not include several resources used in this study. Example - NR2E3 antibody.*

We added the NR2E3 antibody and checked for other omissions.

> *(3) Results & Figures & Figure Legends*
>
> *a. Regulon-defined RPC and photoreceptor precursor states*
>
> *i. On page # 4, 1 paragraph - Clarify the sentence 'Exclusion of all cells with <100,000 cells read and 18 cells.....Emsembl transcripts inferred'. Did the authors use 18 cells or 18FW retinae?*

The sentence was changed to:

“After sequencing, we excluded all cells with <100,000 read counts and 18 cells expressing one or more markers of retinal ganglion, amacrine, and/or horizontal cells (*POU4F1, POU4F2, POU4F3, TFAP2A, TFAP2B, ISL1*) and concurrently lacking photoreceptor lineage marker *OTX2*. This yielded 794 single cells with averages of 3,750,417 uniquely aligned reads, 8,278 genes detected, and 20,343 Ensembl transcripts inferred (Figure S1A-C).” (p. 4, new words underlined)

To clarify that 18 retinae were used, the first sentence of the Results was revised as follows:

“To interrogate transcriptomic changes during human photoreceptor development, dissociated RPCs and photoreceptor precursors were FACS-enriched from 18 retinae, ages FW13-19 …” (p. 4).

Why did the authors 'exclude cells lacking photoreceptor lineage marker OTX2' from analysis especially when the purpose here was to choose photoreceptor precursor states & further results in the next paragraph clearly state that 5 clusters were comprised of cells with OTX2 and CRX expression. This is confusing.

We apologize for the imprecise diction. We divided the evidently confusing sentence into two sentences to more clearly indicate that we removed cells that did not express *OTX2*, as in the first response to the previous question.

> *ii. In Page # 5, the authors reported the number of cell populations (363 large and 5 distal) identified in the THRB+ L/M-cone cluster. What were the # of cell populations identified in the remaining 5 clusters of the UMAP space?*

We added the cell numbers in each group to Fig. 1B. We corrected the large LM group to 366 cells (p. 5) and note 371 LM cells , which includes the five distal cells, in Figure 1B.

> *b. Differential expression of NRL and THRB isoforms in rod and cone precursors*
>
> *i. In Figure 3B, the authors compare and show the presence of 5 different NRL isoforms for all the 6 clusters that were defined in 3A. However, in the results, the ENST# of just 2 highly assigned transcript isoforms is given. What are the annotated names of the three other isoforms which are shown in 3B? Please explain in the Results.*

As requested, we now annotate the remaining isoforms as encoding full-length or truncated NRL in Fig. 3B and show isoform structures in new Supplementary Figure S4B. We also refer to each transcript isoform in the Results (p. 7, last paragraph) and similarly evaluate all isoforms in RB31 cells (Fig. S5B).

> *ii. What does the Mean FPM in the y-axis of Fig 3C refer to?*

Mean FPM represents mean read counts (fragments per million, FPM) for each position across Ensembl NRL exons for each cluster, as now stated in the 6th line of the Fig. 3 legend.

> *iii. A clear explanation of the results for Figures 3E-3F is missing.*

We revised the text to more clearly describe the experiment as follows:

“The cone cells’ higher proportional expression of Tr-NRL first exon sequences was validated by RNA fluorescence *in situ* hybridization (FISH) of FW16 fetal retina in which NRL immunofluorescence was used to identify rod precursors, RXRg immunofluorescence was used to identify cone precursors, and FISH probes specific to truncated Tr-NRL exon 1T or FL-

NRL exons 1 and 2 were used to assess Tr-NRL and FL-NRL expression (Figure 3E,F)." (p. 8, new text underlined).

> *c. Two post-mitotic photoreceptor precursor populations*
>
> *i. Although deep-sequencing and SCENIC analysis clarified the identities of four RPC-localized clusters as MG, RPC, and iPRP indicative of cone-bias and TR indicative of rod-bias. It would be interesting to see the discriminating determinant between the TR and ER by SCENIC and deep-sequencing gene expression violin/box plots.*

We agree it is of interest to see the discriminating determinant between the TR [now termed *iRP*] and ER clusters by SCENIC and deep-sequencing gene expression violin/box plots. We now provide this information for selected genes and regulons of interest in the new Supplementary Figures S10A and S10C, along with a similar comparison between the prior high-resolution iPRP (now termed *iCP*) cluster and the first high-resolution LM cluster, LM1, as described for gene expression on p. 12:

"Notably, *THRB* and *GNAT2* expression did not significantly change while *ONECUT1* declined in the subsequent non-RPC-localized iCP and LM1 stages, whereas *NR2E3* and *NRL* dramatically increased on transitioning to the ER state (Figure S10A)."

And as described for regulon activities on pp. 13-14:

"Finally, activities of the cone-specific THRB and ISL2 regulons, the rod-specific NRL regulon, and the pan-photoreceptor LHX3, OTX2, CRX, and NEUROD1 regulons increased to varying extents on transitioning from the immature iCP or iRP states to the early-maturing LM1 or ER states (Figure 10C)."

We also show expression of the same genes for spatiotemporally grouped cells from the Zuo et al. dataset in the new Figure S10B, which displays a similar pattern (apart from the possibly mixed pcw 10 and pcw13 designated rod precursors).

> *d. Early cone precursors with cone- and rod-related RNA expression*
>
> *i. On page #12, the last paragraph where the authors explain the multiplex RNA FISH results of RXRγ and NR2E3 by citing Figure S8E. However, in Fig S8E, the authors used NRL to identify the rods. Please clarify which one of the rod markers was used to perform RNA FISH?*

Figure S8E (where NRL was used as a rod marker) was cited to remind readers that RXRg has low expression in rods and high expression in cones, rather than to describe the results of this multiplex FISH section. To avoid confusion on this point, Figure S8E is now cited using "(as earlier shown in Figure S8E)." With this issue clarified, we expect the markers used in the FISH + IF analysis will be clear from the revised explanation,

"… we examined *GNAT2* and *NR2E3* RNA co-expression in RXRg+ cone precursors in the outermost NBL and in RXRg+ rod precursors in the middle NBL … ." (p. 14-15).

To provide further clarity, we provide a diagram of the FISH probes, protein markers, and expression patterns in the new Figure 7E.

> *ii. The Y-axis of Fig 6G-6H needs to be labelled.*

The axes have been re-labeled from "Nb of cells" to "Number of RXRg+ outermost NBL cells in each region" (original Fig. 6G, now Fig. 7C) and "Number of RXRg+ middle NBL cells in each region" (original Fig. 6H, now Fig. 7D).

> *iii. The legends of Figures 6G and 6H are unclear. In the Figure 6G legend, the authors indicate 'all cells are NR2E3 protein-'. Does that imply the yellow and green bars alone? Similarly, clarify the Figure 6H legend, what does the dark and light magenta refer to? What does the light magenta color referring to NR2E3+/ NR2E3- and the dark magenta color referring to NR2E3+/ NR2E3+ indicate?*

We regret the insufficient clarity. We revised the Fig. 6G (now Fig. 7C) key, which now reads

"All outermost NBL cells are NR2E3 protein-negative." We added to the figure legend for panel 7C,D "(*n.b.*, italics are used for RNAs, non-italics for proteins)." The new scheme in Figure 7E shows the RNAs in italics proteins in non-italics. We hope these changes will clarify when RNA or protein are represented in each histogram category.

Overall, the results (on page # 13) reflecting Figures 6E-6H & Figure S11 are confusing and difficult to understand. Clear descriptions and explanations are needed.

We revised this results section described in the paragraph now spanning p. 14:

- We now refer to the bar colors in Figures 7C and 7D that support each statement.

- We provide an illustration of the findings in Figure 7E.

> *iv. Previously published literature has shown that cells of the inner NBL are RXRγ+ ganglion cells. So, how were these RXRγ+ ganglion cells in the inner NBL discriminated during multiplex RNA FISH (in Fig 6E-6H and in Fig S11)?*

We thank the reviewer for requesting this clarification. We agree that "inner NBL" is the incorrect term for the region in which we examined RXRg+ photoreceptor precursors, as this could include RXRγ+ nascent RGCs. We now clarify that

"we examined *GNAT2* and *NR2E3* RNA co-expression in RXRg+ cone precursors in the outermost NBL and in RXRg+ rod precursors in the middle NBL … ." (p. 14-15) We further state,

"Limiting our analysis to the outer and middle NBL allowed us to disregard RXRγ+ retinal ganglion cells in the retinal ganglion cell layer or inner NBL (top of p. 15)"

Figure 7E is provided to further aid the reader in understanding the positions examined, and the legend states "RXRg+ retinal ganglion cells in the inner NBL and ganglion cell layer not shown.

> *v. In Figure 6E, what marker does each color cell correspond to?*

In this figure (now panel 7A), we declined to provide the color key since the image is not sufficiently enlarged to visualize the IF and FISH signals. The figure is provided solely to document the regions analyzed and readers are now referred to "see Figure S12 for IF + FISH images" (2nd line, p. 15), where the marker colors are indicated.

> *vi. In Figure S11 & 6E, Protein and RNA transcript color of NR2E3, GNAT2 are hard to distinguish. Usage of other colors is recommended.*

We appreciate the reviewer's concern related to the colors (in the now redesignated Figure S12 and 7A); however, we feel this issue is largely mitigated by our use of arrows to point to the cells needed to illustrate the proposed concepts in Figure S12B. All quantitation was performed by examining each color channel separately to ensure correct attribution, which is now mentioned in the Methods (2nd-to-last line of Quantitation of FISH section, p. 35).

> *vii.*

With due respect, we suggest that labeling each box (now in Figure 8B) makes the figure rather busy and difficult to infer the main point, which is that boxed regions were examined at various distanced from the center (denoted by the “C” and “0 mm”) with distances periodically indicated. We suggest the addition of such markers would not improve and might worsen the figure for most readers.

> *e. An early L/M cone trajectory marked by successive lncRNA expression*
>
> *i. In Figure 8C - color-coded labelling of LM1-4 clusters is recommended.*

We note Fig. 8C (now 9C) is intended to use color to display the pseudotemporal positions of each cell. We recognize that an additional plot with the pseudotime line imposed on LM subcluster colors could provide some insights, yet we are unaware of available software for this and are unable to develop such software at present. To enable readers to obtain a visual impression of the pseudotime vs subcluster positions, we now refer the reader to Figure 5A in the revised figure legend, as follows: (“The pseudotime trajectory may be related to LM1-LM4 subcluster distributions in Figure 5A.”).

> *ii. In Figure 8G - what does the horizontal color-coded bar below the lncRNAs name refer to? These bars are similar in all four graphs of the 8G figure.*

As stated in the Fig. 8G (now 9G) legend, “Colored bars mark lncRNA expression regions as described in the text.” We revised the text to more clearly identify the color code. (p. 18-19)

> *f. Cone intrinsic SYK contributions to the proliferative response to pRB loss*
>
> *i. In Fig 9F - The expression of ARR3+ cells (indicated by the green arrow in FW18) is poorly or rarely seen in the peripheral retina.*

We thank the reviewer for finding this oversight. In panel 9F (now 10F), we removed the green arrows from the cells in the periphery, which are ARR3- due to the immaturity of cones in this region.

> *ii. In Figure 9F - Did the authors stain the FW16 retina with ARR3?*

Unfortunately, we did not stain the FW16 retina for ARR3 in this instance.

> *iii. Inclusion of DAPI staining for Fig 9F is recommended to justify the ONL & INL in the images.*

We regret that we are unable to merge the DAPI in this instance due to the way in which the original staining was imaged. A more detailed analysis corroborating and extending the current results is in progress.

> *iv. Immunostaining images for Figure 9G are missing & are required to be included. What does shSCR in Fig 9G refer to?*

We now provide representative immunostaining images below the panel (now 10G). The legend was updated: “Bottom: Example of Ki67, YFP, and RXRg co-immunostaining with DAPI+ nuclei (yellow outlines). Arrows: Ki67+, YFP+, RXRg+ nuclei.” The revised legend now notes that shSCR refers to the scrambled control shRNA.

> *v. For Figure 9H - Is the presence and loss of SYK activity consistent with all the subpopulations (S & LM) of early maturing and matured cones?*

We appreciate the reviewer's question and interest (relating to the redesignated Figure 10H); however, we have not yet completed a comprehensive evaluation of SYK expression in all the subpopulations (S & LM) of early maturing and matured cones and will reserve such data for a subsequent study. We suggest that this information is not critical to the study's major conclusions.

> *vi. Figure 9A is not explained in the results. Why were MYCN proteins assessed along with ARR3 and NRL? What does this imply?*

We thank the reviewer for noting that this figure (now Figure 10A) was not clearly described.

As per the response to Reviewer 1, point 6 , the text now states,

"The upregulation of MYC target genes was of interest given that many MYC target genes are also MYCN targets, that MYCN protein is highly expressed in maturing (ARR3+) cone precursors but not in NRL+ rods (Figure 10A), and that MYCN is critical to the cone precursor proliferative response to pRB loss [8–10]." (middle, p. 19, new text underlined).

Hence, the figure demonstrates the cone cell specificity of high MYCN protein. This is further noted in the Fig. 10a legend: "A. Immunofluorescent staining shows high MYCN in ARR3+ cones but not in NRL+ rods in FW18 retina."

https://doi.org/10.7554/eLife.101918.2.sa0